Triangular-n Postmaster: From the Triangular Primitive to the Completed Source Frontier

Volume I — The Reading Volume – v4.7

TRIANGULAR ROOT TO COMPLETED SOURCE FRONTIER

1 · TRIANGULAR ROOT

$T_n, \quad j_n = 2n+1$

Odd layers, midpoint tails, reciprocals

2 · ANALYTIC COORDINATE

$x = 2T_{s-1}, \quad D_x = R^{-1}D_s$

Sine, Gamma, Bessel derivatives

3 · COMPLETED FOLD

$q = s(1-s), \quad S_\xi, \quad h = xS_\xi$

Reflection with both sheets retained

4 · RUNGS AND MATRICES

$W_k \longleftrightarrow B_{2k-1,\,k-1}$

Exact entries; full matrix quantifiers

5 · EXACT SOURCE ENERGY

$\mathscr{E}_N = \sum_j B_{N,j}^2$

Circle and Laguerre norms agree

6 · OPEN FULL-PRIME CAP

$\mathscr{E}_N[P](2) \le (1+\log 2+\pi/6)^2$

Every degree; cutoff obstructions in Dossier 166C

The connecting identities are proved; the final source estimate remains open

Jeffery Huckstead ORCID 0009-0007-0234-2177 Cerebral Graphix

15 September 2026

RH STATUS: OPEN

Contents

Start here

A triangle you already know

Stack bowling pins. Count handshakes in a room. Add up $1 + 2 + \cdots + n$. The same numbers appear:

$$1,\ 3,\ 6,\ 10,\ 15,\ 21,\ 28,\ 36,\ 45,\ 55,\ \ldots \qquad \boxed{T_n = \frac{n(n+1)}{2}} \tag{R.1}$$

Two facts about them are usually met once and then walked past.

The triangular numbers are a column of Pascal's triangle. Not a resemblance — an identity:

$$\binom{k}{2} = \frac{k(k-1)}{2} = T_{k-1} \tag{R.1a}$$

Read Pascal's triangle down its third column and you are reading $1, 3, 6, 10, 15, \ldots$ exactly. The next column over is the running sum of *those*: $\binom{k}{3} = T_1 + T_2 + \cdots + T_{k-2}$.

And they collide with the rest of the triangle in a way nobody can fully explain. The number $3003 = T_{77}$ occupies four distinct positions $\binom{3003}{1} = \binom{78}{2} = \binom{15}{5} = \binom{14}{6} = 3003$. Each of those four positions has a mirror copy, so 3003 occurs **eight** times in all. No integer is known to occur more often, and whether any does is open (Singmaster's problem). Figure 12 of this volume prints the row where that happens.

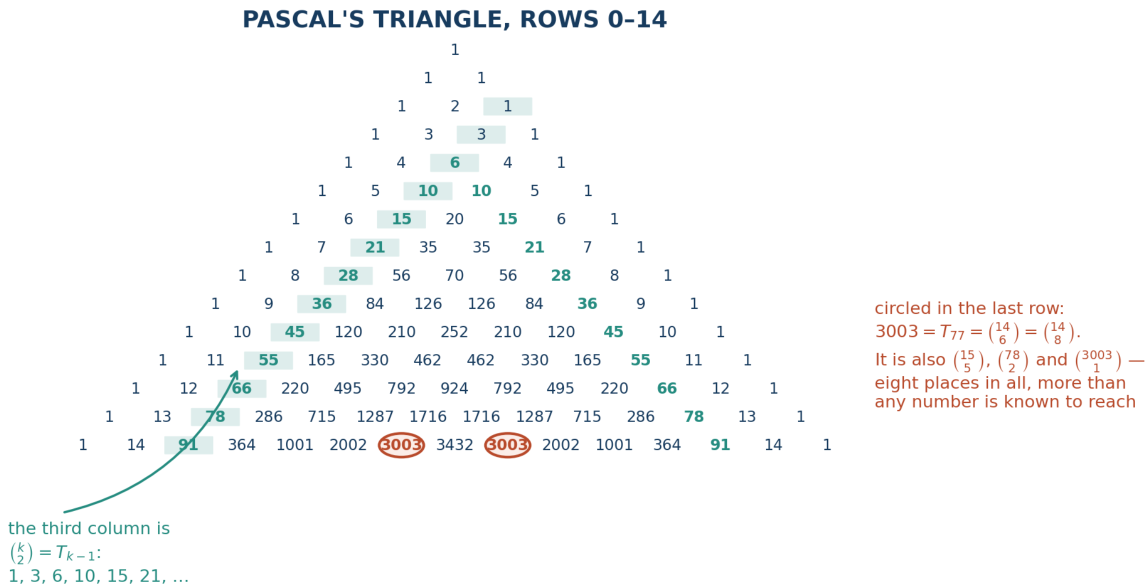

Figure 1: The familiar triangle, before any sign is attached. The tinted column is the triangular numbers themselves; the circled row is the one that makes 3003 famous. Both features survive into the signed grid this volume actually uses.

These are not decorations. This volume is about what one signed version of that same triangle does when it is pointed at the Riemann zeta function.

Put a sign on it

Alternate the signs along each row:

$$\boxed{c_{k,j} = (-1)^j \binom{k}{j}}, \qquad \sum_{j=0}^{k} c_{k,j} z^j = (1-z)^k \tag{R.1b}$$

Row k is nothing more exotic than the coefficient list of $(1-z)^k$. Row 6 reads $1, -6, 15, -20, 15, -6, 1$. Every row is generated from the one above it by a single subtraction, $c_{k+1,j} = c_{k,j} - c_{k,j-1}$, from the seed $c_{0,0} = +1$. You can write row 17 without computing rows 1 through 16. Nothing in this grid is hard, and nothing in it is approximate.

What each row is for

Zeta's zeros are hard to look at directly. Fold them. With $q = s(1-s)$ — the same reflection $n \mapsto -n-1$ that centres T_n, now on the complex plane — every zero ρ of the completed function ξ becomes a single point q_ρ, and its mirror partner $1-\rho$ lands on top of it. Build the resolvent of that folded set,

$$S_\xi(x) = \sum_{[\rho]} \frac{m_\rho}{x + q_\rho}, \qquad Z_r(x) = \sum_{[\rho]} \frac{m_\rho}{(x + q_\rho)^r} \tag{R.1c}$$

so $Z_1 = S_\xi$ and each Z_r is one more derivative of it; the sum runs over folded zero orbits $[\rho]$ with multiplicity m_ρ (§R10).

Now the point of the grid. Define the k-th **rung**

$$\boxed{W_k(x) = (-1)^{k-1} D_x^{2k-1}\left[x^k S_\xi(x)\right] = (2k-1)! \sum_{[\rho]} m_\rho \left(\frac{q_\rho}{(x + q_\rho)^2}\right)^k} \tag{R.3}$$

and row k of the signed triangle is exactly its recipe, the identity (SW.4b) established in §R12A:

CLOSED FORM *Every rung is a finite row of the grid*

$$\frac{W_k(x)}{(2k-1)!} = \sum_{j=0}^{k} c_{k,j}\, x^j Z_{k+j}(x) = Z_k - kxZ_{k+1} + \binom{k}{2} x^2 Z_{k+2} - \cdots$$

This is an identity, not an approximation and not a truncation. The rung W_k is a $(k+1)$-term combination of consecutive derivatives of one function, and the coefficients are read straight off row k. The grid is not computationally irreducible, and no simulation is hiding in it.

Why zeta cares

Look at the right-hand side of (R.3). It is a sum of k-th powers of one quantity, the **carrier** (11.1) of §R11,

$$u_x(q) = \frac{q}{(x + q)^2}$$

On the critical line $\Re s = 1/2$ the carrier is a squared modulus, so $u_x \geq 0$ and every power of it is nonnegative. Off the critical line it need not be, and its powers can rotate. Widder's characterization of Stieltjes functions converts the whole family into an exact statement with nothing left over:

RH-EQUIVALENT *Exact criterion*

$$\boxed{\text{RH} \iff W_k(x) \geq 0 \ \text{ for every } k \geq 1 \text{ and every } x > 0} \tag{R.4}$$

So the Riemann hypothesis, in this volume's coordinates, reads:

Does every row of a signed Pascal triangle, applied to the derivatives of one explicit function, come out nonnegative?

Both quantifiers are load-bearing. **No finite collection of rungs is an RH statement.** Nothing in this volume promotes one, and every place a finite result could be mistaken for the full one is marked.

Master status key — where this volume actually stands

This is the **single status key for the Reading Volume and Dossier**. Later PROVED, CERTIFIED, RH-EQUIVALENT, EVIDENCE and OPEN tags stand on their own and refer back here; the legend is not repeated elsewhere.

PROVED	proved here or cited as proved: an unconditional theorem or an exact identity.
CERTIFIED	rigorous but computer-assisted, or dependent on verified zero heights; the finite region it certifies is stated with it.
RH-EQUIVALENT	logically equivalent to the Riemann hypothesis. An equivalence is not a proof in either direction.
OPEN	not proved anywhere in this work, and not implied by any finite result in it.
EVIDENCE	numerical or empirical support only. It never upgrades a status.

the claim	status
Every rung is a finite row of the grid, (SW.4b)	PROVED closed form
RH $\iff$ $W_k \geq 0$ for all $k \geq 1, x > 0$, (R.4)	RH-EQUIVALENT
$W_1 > 0$ for all $x > 0$, from the source	PROVED analytic
$W_2, \ldots, W_6 > 0$ for all $x > 0$, from the source	CERTIFIED A-CAT through $F^{(12)}$
$W_k > 0$ for all $x > 0$, every $k \leq 4{,}712{,}664{,}392{,}502$	CERTIFIED verified-height channel
$4x - 1 < R_x$ at every fixed scale, (13A.2); $\Delta < 1$ is *not* proved	PROVED analytic, pointwise in x
$W_7 \rightsquigarrow F^{(14)}$ from the independent source	OPEN
$W_k > 0$ for all $x > 0$, every $k \geq 1$	OPEN
$L_\Gamma - L_P \succeq 0$ on every finite node set, (23.1)	RH-EQUIVALENT OPEN
$\mathscr{E}_N[P](2) \leq 5$ for every degree N, (166B.12a)	RH-EQUIVALENT OPEN

Certificate provenance. W_2–W_4: PP85/§74 MPFR, last-run date not retained in this slim edition, named receipt not bundled. W_5–W_6: supplied Green run, 14 Sep 2026, python-flint/Arb at 256 and 384 bits using the same backend, not rerun for v4.7. The verified-height row uses the external input named in §R13. A retained CERTIFIED grade is never a fresh replay.

How far the criterion has been checked — and why that is not progress. The K_H row is not a sample. Section R13 proves that if every zero up to a height H lies on the critical line, then every rung with index at most $\lfloor \pi/(2 \arctan(1/H)) \rfloor$ is positive at every $x > 0$. Platt and Trudgian's verified height puts the lowest 12,363,153,437,138 zeros on the line, and the resulting index, exact at (13.6), is

$$\boxed{K_H = 4{,}712{,}664{,}392{,}502}.$$

Thus (R.4) holds for the first four and a half trillion rungs, and the first **six** also have an independent source certificate. It is still not evidence for RH: (R.4) quantifies over every k, and a larger verified height only makes a finite prefix larger. The live pair is

$$\boxed{W_7 \rightsquigarrow F^{(14)} \qquad \text{and} \qquad L_\Gamma - L_P \succeq 0 \text{ on every finite positive node set.}} \tag{R.2}$$

The first is the next scalar source rung; the second is RH-equivalent.

The live frontier: one line per route

What remains is **one line per route, and no reduction between the routes is known**. Section R23 lists the live targets and marks each one as equivalent, sufficient, or necessary. The principal matrix route asks for

$$\boxed{L_\Gamma - L_P \succeq 0 \quad \text{for every finite positive node set.}}$$

Here L_Γ and L_P are the Gamma and prime Löwner blocks built in §§R16–R17E. That inequality is RH-equivalent, but it is not proved to subsume the distinct curvature, fixed-scale energy, or exact-divisor routes. The unconditional implications actually known between targets are recorded in the lattice at §R12; Part VIII collects the routes that have been closed by NO-GO theorems.

Reader's study spine

Why read this. Triangular coordinates lead to the completed source of the Riemann zeta function, to exact criteria stated in that coordinate, and to the proof obligations that remain. The Riemann hypothesis remains open.

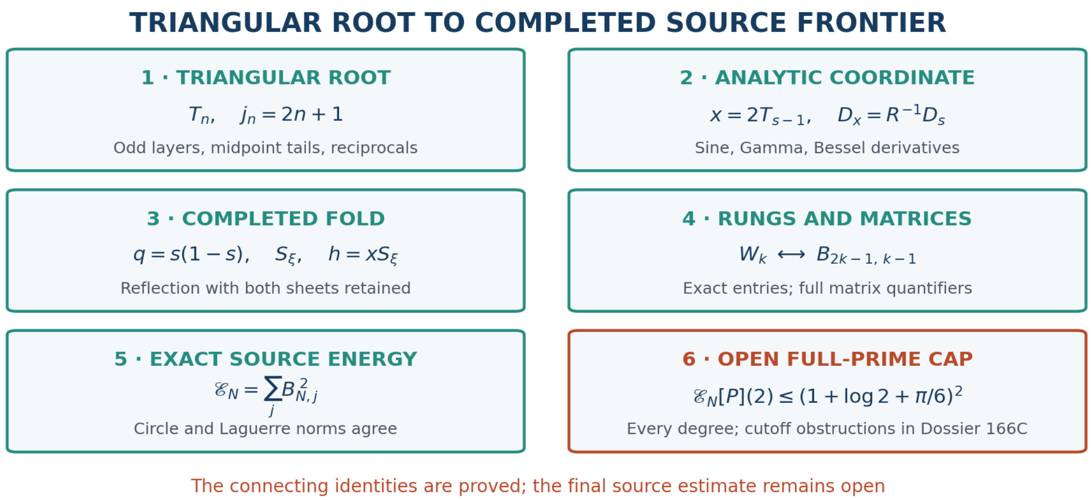

Figure 2: The reading map for this volume. Arrows give the reading order, not an implication from a finite certificate to RH. Section R12 controls the rung status; §R23 states the all-node frontier.

How to read this volume

The work is published in two documents: this **Reading Volume**, the continuous argument in reader sections §R1–§R25 across Parts I–VIII, and the **Technical Dossier**, the proofs, certificates and empirical context in plain numbered sections with lettered insertions; see §R24. **A number without an R is in the Dossier.** Equation tags are global, so (SW.4b) and (166C.25) name the same equations in both. Every reader section states its own quantifiers, and this volume can be read straight through before the Dossier is opened.

The dependency route is root to frontier: triangular coordinate → fold and completion → Widder/Hausdorff rungs → Li/Löwner source split → source energy and exact-divisor residual → reflection defects → the live targets of §R23 and the NO-GO ledger of §R25. The section-level map is printed once, in §R24.

Notation visible at every analytic interface

The Riemann variable will never be allowed to hide its two real axes:

role	notation	exact reading
point	s	$s = \sigma + it$
reflection	$1 - s$	$(1-\sigma) - it$
conjugate	$\bar{s}$	$\sigma - it$
reflected conjugate	$1 - \bar{s}$	$(1-\sigma) + it$
folded coordinate	$q = s(1-s)$	$\sigma(1-\sigma) + t^2 + i\,t(1-2\sigma)$
analytic triangular coordinate	$T_{s-1} = s(s-1)/2$	$(\sigma^2 - \sigma - t^2)/2 + i\,t(\sigma - 1/2)$
safe real source branch	s_x	$(1 + \sqrt{1+4x})/2 > 1$
source Jacobian	R	$R = 2s_x - 1 = \sqrt{1+4x}$

role	notation	exact reading
integer odd coordinate	j_n	$j_n = 2n + 1$
rung odd coordinate	j_k	$j_k = 2k + 1$

The symbols s, ρ, and s_x distinguish an arbitrary point, a zero, and the safe source branch by mathematical role. Reflection $s \mapsto 1 - s$ and conjugation $s \mapsto \bar{s}$ coincide exactly on $\sigma = 1/2$; identifying the two off that line is the positivity problem of §R20.

Part I. The triangular coordinate

The triangular coordinate, its half-step reflection and its Pascal column supply the arithmetic vocabulary for the analytic constructions that follow. All identities in this Part stand independently of zeta zeros.

R1. Discrete primitive and centered square

Triangular numbers integrate the integer sequence by one forward difference:

$$T_n - T_{n-1} = n \qquad T_n = 1 + 2 + \cdots + n \tag{1.1}$$

A square displays both triangular copies at once. Split an $(n+1) \times (n+1)$ grid into the entries above the diagonal, the entries below it, and the diagonal itself:

$$\boxed{2T_n + (n+1) = (n+1)^2 \qquad T_n + T_{n+1} = (n+1)^2} \tag{SQ.1}$$

The two strict triangular halves each contain T_n cells, and the shared diagonal contains $n + 1$. The border ending at n^2 and the border beginning there are consecutive members of one odd sequence:

$$\boxed{n^2 - (n-1)^2 = 2n - 1, \qquad (n+1)^2 - n^2 = 2n + 1} \tag{SQ.2}$$

Summing the first identity gives $n^2 = \sum_{k=1}^{n}(2k - 1)$. Equivalently $n^2 = T_{n-1} + T_n$; taking successive differences of this adjacent-triangle identity gives the same borders. Thus $2n - 1$ and $2n + 1$ describe the incoming and outgoing layers at the same square, with the index shift stated explicitly.

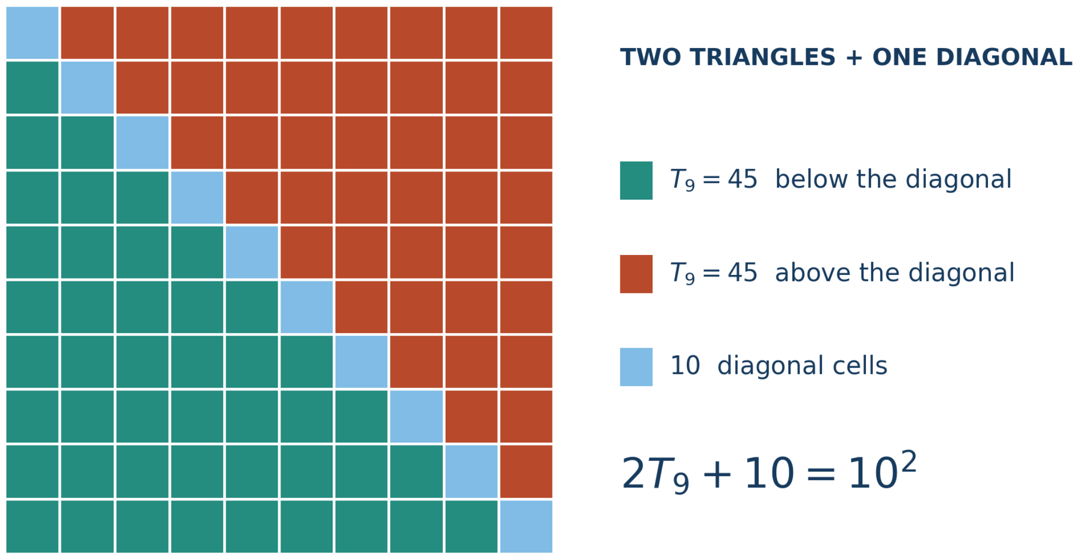

Figure 3: A 10 by 10 square splits into two 45-cell triangles and a 10-cell diagonal: $2T_9 + 10 = 100$. The diagonal is counted once. This exact counting diagram also prepares the reflected index pairs used later in matrices.

Introduce the centered odd coordinate

$$j_n := 2n + 1 \tag{1.2}$$

Then

$$\boxed{8T_n + 1 = j_n^2, \qquad T_n = \frac{j_n^2 - 1}{8} = \frac{1}{2}\left(n + \frac{1}{2}\right)^2 - \frac{1}{8}} \tag{1.3}$$

The reflection $n \mapsto -n-1$ becomes $j_n \mapsto -j_n$ while T_n is fixed. Thus T_n is the invariant coordinate and j_n is its signed sheet coordinate. This is the elementary model for the analytic fold used later. In particular the two border counts in (SQ.2) are j_{n-1} and j_n. Their squared difference recovers the primitive exactly: $j_n^2 - j_{n-1}^2 = 8(T_n - T_{n-1}) = 8n$.

The paper will keep three exact readings beside one another whenever doing so exposes structure rather than adding notation:

mainstream form	triangular form	centered form
$n(n+1)$	$2T_n$	$(j_n^2 - 1)/4$
$n + (n+1)$	$T_{n+1} - T_{n-1}$	j_n
$n \mapsto -n-1$	$T_n \mapsto T_n$	$j_n \mapsto -j_n$

This "three-language line" is an editorial convention, not a claim that every formula becomes simpler after triangularization.

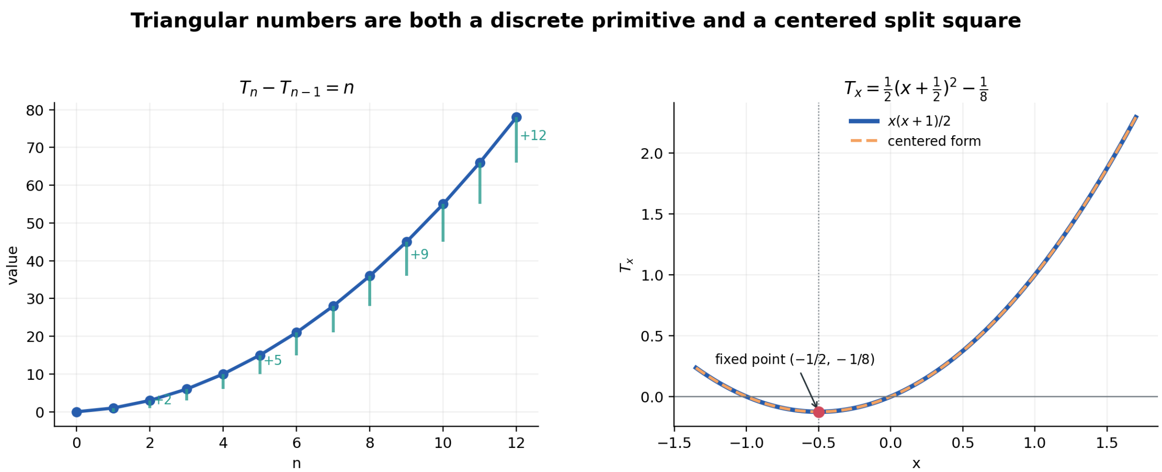

Figure 4: Triangular numbers are the discrete primitive; centering at the half-step turns reflection into a sign change.

R1A. The general discrete primitive and its reflection

The same polynomial identities hold for real or complex inputs. Define

$$T_x = \frac{x(x+1)}{2}, \qquad j_x = 2x+1$$

Then

$$T_x - T_{x-1} = x, \qquad T_{x+1} - T_x = x+1, \qquad \Delta^2 T_x = 1$$

while the adjacent sum is

$$\boxed{T_x + T_{x-1} = x^2} \tag{TDP.1}$$

Factoring through the primitive difference gives the cubic identity

$$\boxed{T_x^2 - T_{x-1}^2 = (T_x - T_{x-1})(T_x + T_{x-1}) = x^3} \tag{TDP.2}$$

The same adjacent pair also resolves the square index:

$$\boxed{T_{x^2} = T_{x-1}^2 + T_x^2} \tag{TDP.3}$$

Indeed, the right side is $x^2((x-1)^2 + (x+1)^2)/4 = x^2(x^2+1)/2$.
The forward adjacent product and its reflection can be kept on one line:

$$\boxed{2T_x = (T_x - T_{x-1})(T_{x+1} - T_x), \qquad T_{-x-1} = T_x} \tag{TDP.4}$$

With $j_x = 2x+1$, the centered sheet coordinate is visible without a new symbol collision:

$$\boxed{T_x = \frac{j_x^2 - 1}{8} = \frac{1}{2}\left(x + \frac{1}{2}\right)^2 - \frac{1}{8}} \tag{TDP.5}$$

Thus the half-shift and the value $-1/8$ are not numerical coincidences. They are the split-norm coordinates of two consecutive counting legs.

More generally, for a fixed gap $D \geq 0$,

$$x(x+D) = \left(x + \frac{D}{2}\right)^2 - \left(\frac{D}{2}\right)^2$$

This is the common null-coordinate grammar behind the Casimir square, complementary phase states, and reciprocal uniformization. It is a scalar grammar; a shared operator must still be proved separately in each family.

The square-index recurrence and the two Pell constructions are proved in Dossier §5 (Theorems TDP-A–TDP-C); the identities above are the algebraic reference used below.

R2. Odd and even power sums

Let $S_p(n) = \sum_{k=1}^{n} k^p$. Reflection about $n = -1/2$ forces the Faulhaber parity split

$$\boxed{S_{2m+1}(n) = P_m(T_n), \qquad S_{2m}(n) = j_n Q_m(T_n), \qquad j_n = 2n+1} \tag{2.1}$$

for polynomials P_m, Q_m, with $m \geq 0$ in the odd formula and $m \geq 1$ in the even formula. The case $S_0(n) = n$ is excluded from the even formula. The first examples are

$$\begin{aligned} S_1 &= T_n & S_2 &= \frac{j_n T_n}{3} = \frac{(2n+1)T_n}{3} \\ S_3 &= T_n^2 & S_4 &= \frac{j_n T_n(6T_n - 1)}{15} \\ S_5 &= \frac{T_n^2(4T_n - 1)}{3} & S_6 &= \frac{j_n T_n(12T_n^2 - 6T_n + 1)}{21} \end{aligned} \tag{2.2}$$

The square-sum formula follows from these same adjacent quantities, without a separate counting hypothesis. Set $A(n) = j_n T_n$. Then

$$A(n) - A(n-1) = (2n+1)T_n - (2n-1)T_{n-1} = 3n^2 \tag{2.2a}$$

Since $A(0) = 0$, summation proves $3S_2(n) = j_n T_n$. Factoring $T_n^2 - T_{n-1}^2$ uses the same primitive difference n and adjacent sum n^2, giving (2.3). The square and cube branches therefore follow from one adjacent-triangle calculation.

In the half-step variable $u = n + 1/2$, odd power sums are polynomials in u^2 while even sums are u times polynomials in u^2. The factor $j_n = 2n+1$ is therefore not an accessory: it records the odd sheet of the same centered geometry.

The cubic identity is the cleanest instance:

$$\boxed{T_n^2 - T_{n-1}^2 = n^3, \qquad 1^3 + \cdots + n^3 = T_n^2} \tag{2.3}$$

The same adjacent pair resolves a square-index triangular number:

$$\boxed{T_{n^2} = T_{n-1}^2 + T_n^2} \tag{2.4}$$

R3. Factorial switch and diagonal defect

The factorial form makes the triangular polynomial appear by exact cancellation:

$$\boxed{\frac{(n+1)!}{2(n-1)!} = \left(\frac{n!}{2}\right)\left(\frac{n+1}{(n-1)!}\right) = \frac{n(n+1)}{2} = T_n} \tag{3.1}$$

The two-variable continuation

$$F_\triangle(x,y) = \frac{\Gamma(y+2)}{2\Gamma(x)} \tag{3.2}$$

restricts to T_x on the diagonal. At regular points with $T_x \neq 0$, its exact relative defect is

$$\boxed{\frac{F_\triangle(x,y)}{T_x} = \frac{\Gamma(y+2)}{\Gamma(x+2)}, \qquad \frac{F_\triangle(x,x+\varepsilon) - T_x}{T_x} = \varepsilon\psi(x+2) + O(\varepsilon^2)} \tag{3.3}$$

The reduced factor $(n+1)/(2(n-1)!)$ still carries the successor-prime numerator gate before multiplication. After the factorial cancellation, the whole expression is the integer T_n; the reduced-numerator signal is not a separate invariant of the product.

R4. Reciprocal triangular numbers as moments

The reciprocal triangle starts with a complete telescope,

$$\frac{1}{T_n} = \frac{2}{n(n+1)} = 2\left(\frac{1}{n} - \frac{1}{n+1}\right), \qquad \sum_{n\geq 1} \frac{1}{T_n} = 2. \tag{4.1}$$

The adjacent pair retains the centered coordinate $j_n = 2n+1$:

$$\frac{1}{n} - \frac{1}{n+1} = \frac{1}{2T_n}, \qquad \frac{1}{n} + \frac{1}{n+1} = \frac{j_n}{2T_n}. \tag{4.2}$$

Squaring and summing gives the exact Basel bridge

$$\boxed{\sum_{n\geq 1}\frac{1}{T_n^2}=8\zeta(2)-12,\qquad \zeta(2)=\frac{3}{2}+\frac{1}{8}\sum_{n\geq 1}\frac{1}{T_n^2}.} \tag{4.4}$$

The cubic reciprocal identity needed later is

$$\boxed{\sum_{n\geq 1}\frac{1}{T_n^3}=8-6\sum_{n\geq 1}\frac{1}{T_n^2}=80-48\zeta(2).} \tag{4.4f}$$

More generally, with $R_m(n)=n^{-m}+(n+1)^{-m}$, the adjacent roots $1/n$ and $1/(n+1)$ give

$$R_m(n)=\frac{j_n}{2T_n}R_{m-1}(n)-\frac{1}{2T_n}R_{m-2}(n),\qquad R_0=2,\quad R_1=\frac{j_n}{2T_n}. \tag{4.4b}$$

Thus the higher reciprocal identities are one recurrence, not isolated simplifications. The distinction between reciprocating each term and reciprocating a completed sum is retained throughout the volume.

Finally the reciprocal triangle is already a compact moment sequence:

$$\boxed{\frac{1}{T_{k+1}}=\int_0^1 u^k\,2(1-u)\,du.} \tag{4.5}$$

This positive Hausdorff measure later supplies Hankel and Gram models. It is an auxiliary triangular owner and must not be identified with the signed Gamma or completed-zero measures.

R5. The triangular coordinate as a real analytic chart

Replace the integer index by a real source variable $s>1$ and define

$$x=s(s-1)=2T_{s-1}\qquad R=2s-1=\sqrt{1+4x} \tag{5.1}$$

At $s=n+1$ this reads

$$\boxed{x=2T_n,\qquad R=2n+1} \tag{5.2}$$

Thus the repeatedly occurring $2n+1$ is the Jacobian dx/ds of the folded safe-axis coordinate. The integer centered coordinate and the analytic source Jacobian are the same object on this lattice. Writing $R(x)=\sqrt{1+4x}$ makes both neighboring values visible, for $n\geq 2$ on the open source half-line:

$$R(2T_{n-1})=2n-1,\qquad R(2T_n)=2n+1,\qquad D_x=\frac{1}{R}D_s \tag{5.2a}$$

This is the route by which the elementary odd coordinate enters the source derivatives. Dossier §34 uses this differential operator to obtain the rung denominators, and §146 derives its Bessel polynomials.

A noninteger example makes the interpolation visible:

$$\boxed{T_3 = 6 < T_\pi = \frac{\pi(\pi+1)}{2} < 7, \qquad T_\pi \approx 6.5055985273} \tag{5.3}$$

Indeed, T_z is increasing for real $z > -1/2$, and $3 < \pi < 22/7$ gives $6 < T_\pi < T_{22/7} = 319/49 < 7$. The value lies close to, but above, the midpoint 6.5. At $s = \pi + 1$, the source chart has $x = 2T_\pi$; the same reflection identity holds exactly: $T_\pi = T_{-\pi-1}$.

Value scaling and horizontal-coordinate scaling must be separated. The polynomial T_x has zeros at $-1, 0$; its reciprocal has poles there. Multiplying its value by 2 leaves those locations fixed. Replacing the horizontal coordinate by $u = 2x$ changes the displayed locations:

expression	symmetry center	zeros; poles of its reciprocal
$T_x = x(x+1)/2$	$x = -1/2$	$x = -1, 0$
$2T_x = x(x+1)$	$x = -1/2$	$x = -1, 0$
$2T_{u/2} = u(u+2)/4$	$u = -1$	$u = -2, 0$

The general coordinate rule, for $c > 0$, is

$$T_{u/c} = \frac{u(u+c)}{2c^2}, \qquad \frac{1}{T_{u/c}} = \frac{2c^2}{u(u+c)}, \qquad u_{\text{center}} = -\frac{c}{2} \tag{SC.1}$$

The centered coordinate carries the same change explicitly. In the shifted input s used by the completed function,

$$j_{s-1} = 2s - 1, \qquad 8T_{s-1} + 1 = (2s-1)^2 \qquad T_{s-1} = T_{-s} \tag{SC.2}$$

The symmetry center is now $s = 1/2$, with reciprocal poles at $s = 0, 1$. For the particular squared-root condition $(2s-1)^2 = 2$, the two branches are $s = (1 \pm \sqrt{2})/2$ and $T_{s-1} = 1/8$. Squaring removes the sign of the centered coordinate; keeping j_{s-1} retains the branch. This is why the integer $2n + 1$, its shifted real version, and the imaginary $2it$ will continue to be printed beside the triangular fold.

Equations (5.1)–(5.2) are the safe-axis specialization of the full discrete primitive and centered split recorded in §R1A, especially (TDP.4)–(TDP.5).

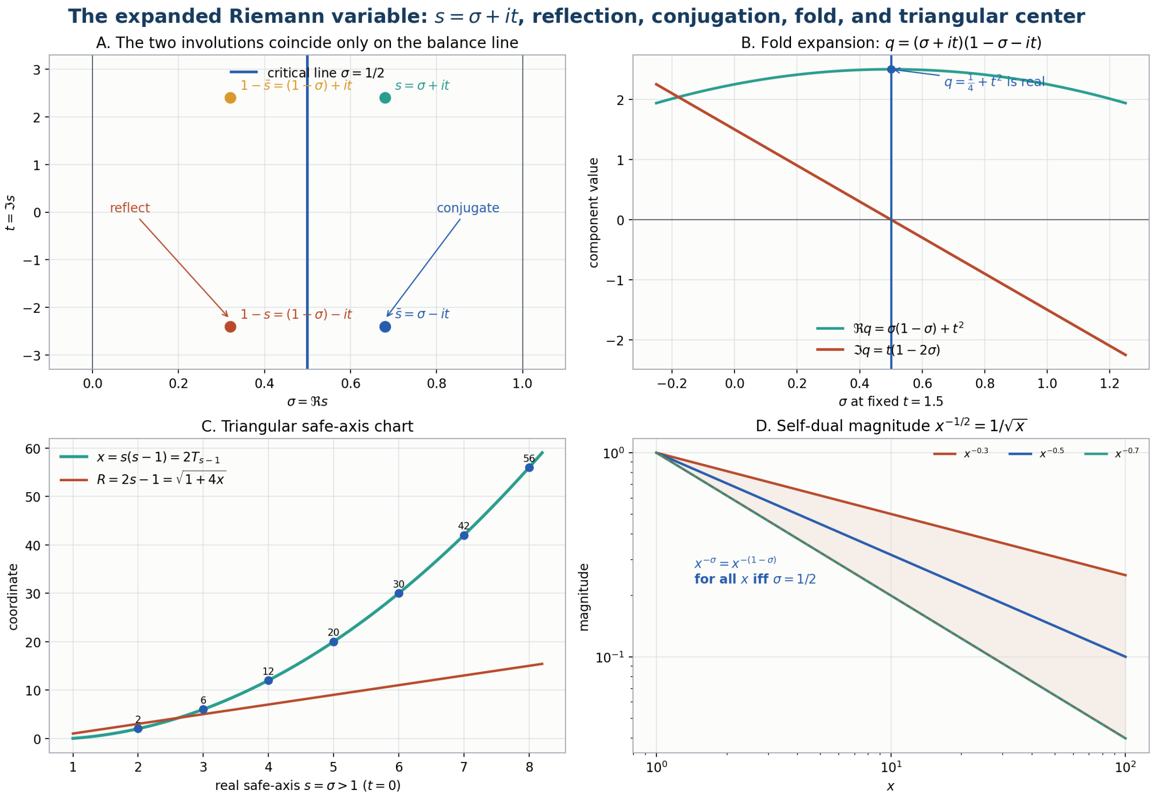

Figure 5: The expanded variable, its involutions, the folded coordinate, and the real triangular safe axis.

R5C. The even-triangular rail and the half-step sequence

The even-index subsequence deserves its own visible line. For $n \geq 1$, put

$$\boxed{a_n = 2n + \frac{1}{2} = \frac{j_{2n}}{2}, \qquad a_n^2 - \frac{1}{4} = 2n(2n+1) = 2T_{2n}} \tag{TR.1}$$

Geometrically, $2T_{2n}$ is the $2n$ by $(2n+1)$ rectangle formed by two equal triangles. Centering the two side lengths at a_n writes its area as $a_n^2 - (1/2)^2$. This is why the quarter-square and odd coordinate occur together. The even indices also pair successive factors in the odd factorial, as (PR.6) will show. Its reciprocal sequence is

$$\boxed{A_n := \frac{1}{2T_{2n}} = \frac{1}{2n} - \frac{1}{2n+1} = \frac{1}{a_n^2 - 1/4}} \tag{TR.2}$$

n	even triangle T_{2n}	adjacent product $2T_{2n}$	reciprocal A_n	centered root a_n
1	3	6	1/6	5/2
2	10	20	1/20	9/2
3	21	42	1/42	13/2
4	36	72	1/72	17/2
5	55	110	1/110	21/2

The same fractions have two useful sums:

$$\boxed{\log 2 = 1 - \sum_{n\geq 1} A_n, \qquad \zeta(2) = 3 - 2\log 2 + \sum_{n\geq 1} A_n^2} \tag{TR.3}$$

The first follows from the alternating harmonic series. For the second, square the adjacent reciprocal difference and use $\sum_{n\geq 1}[(2n)^{-2} + (2n+1)^{-2}] = \zeta(2) - 1$. These are ordinary convergent sums of positive terms.

This selection by even index is distinct from the gcd selection in Dossier §170. The latter groups rational rays and their multiplicities; here we select a specific adjacent-product sequence. Both remain rooted in T_x. In the later real source chart the same entry is $x = 2T_{2n}$, $s = 2n+1$, and $R = 2s - 1 = 4n + 1 = 2a_n$.

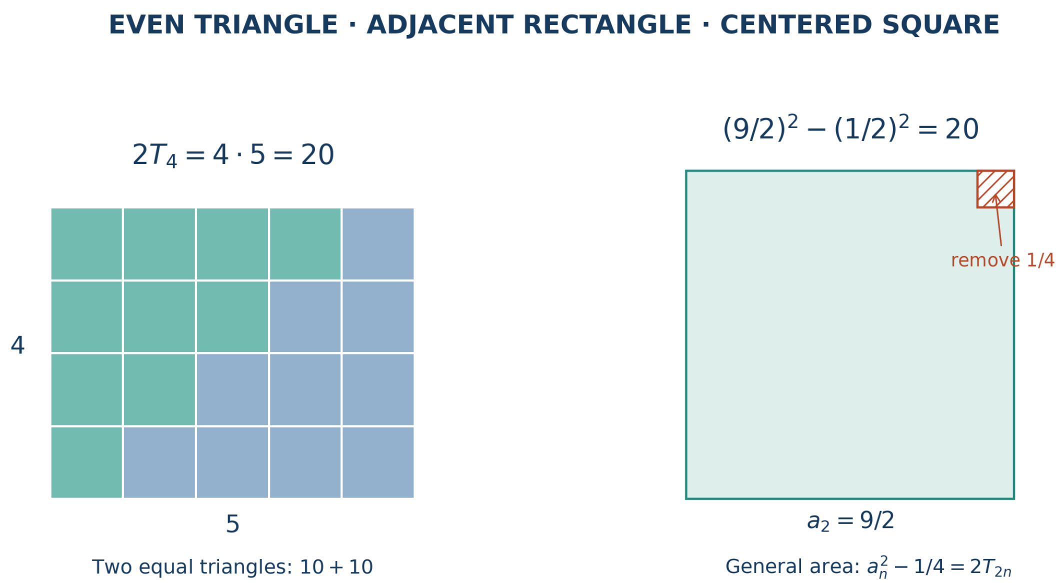

Figure 6: Two triangles form an adjacent-side rectangle. Centering its side lengths gives the same area as a square minus one quarter. The even index is the one used by the odd-factorial product.

Later, the Gamma scaffold has poles at $-2T_{2n}$ (§R17). Voros's auxiliary half-step sequence is precisely a_n [56, equation (59)]. Equation (TR.1) therefore supplies an exact triangular dictionary for that sequence. The analytic continuation built from A_n will be introduced only after the completed source has been defined (§R17A). Its regularized values are a different operation from the convergent sums in (TR.3).

R5D. One real coordinate, several roles for π

The polynomial chart accepts real input without inventing a new interpolation:

$$\boxed{T_x = \frac{x(x+1)}{2} = \frac{\Gamma(x+2)}{2\Gamma(x)} = \frac{(2x+1)^2-1}{8}.} \tag{PR.1}$$

At $x=\pi$, the adjacent reflected values satisfy $T_\pi - T_{-\pi} = \pi$ and $T_\pi + T_{-\pi} = \pi^2$; these identities describe the input rather than evaluate it. An evaluation from integer triangular numbers follows instead from (4.4) and Euler's Basel identity:

$$\boxed{\pi = 3\sqrt{1+\frac{1}{12}\sum_{n\geq 1}\frac{1}{T_n^2}} = \sqrt{10-\frac{1}{8}\sum_{n\geq 1}\frac{1}{T_n^3}}.} \tag{PR.4a}$$

The square root acts on the whole expression. This is the only reading used later when the same constant enters the source-energy cap.

Euler's sine product gives the analytic bridge from ordinary integers to the even triangular subfamily:

$$\frac{\sin(\pi x)}{\pi x} = \sum_{m\geq 0}\frac{(-1)^m(\pi x)^{2m}}{(2m+1)!} = \prod_{n\geq 1}\left(1-\frac{x^2}{n^2}\right), \tag{PR.5}$$

and

$$\boxed{(2m+1)! = \prod_{r=1}^{m}(2r)(2r+1) = \prod_{r=1}^{m} 2T_{2r}.} \tag{PR.6}$$

The same normalization gives

$$(2m+1)! = T_{2m+1}(m!)^2 C_m, \qquad \frac{4^m(m!)^2}{(2m+1)!}\frac{C_m}{4^m} = \frac{1}{T_{2m+1}}, \tag{PR.7a}$$

where C_m is the mth Catalan number. These coefficient identities are comparison structure; no completed-source sign follows from them.

Gamma reflection supplies the normalized sine directly,

$$\frac{\sin(\pi x)}{\pi x} = \frac{1}{\Gamma(1+x)\Gamma(1-x)}. \tag{PR.8}$$

The half-step constants that recur in the later determinant and pole calculations are

$$\boxed{\Gamma(1/2)=\sqrt{\pi}, \qquad \Gamma(3/2)=\frac{\sqrt{\pi}}{2},} \tag{PR.10a}$$

and

$$\boxed{\frac{\Gamma(m+3/2)}{\Gamma(m+1/2)}=m+\frac{1}{2}=\frac{j_m}{2}, \qquad \frac{\Gamma(m+1/2)}{m!\Gamma(1/2)}=\frac{\binom{2m}{m}}{4^m}.} \tag{PR.10b}$$

The first pair is used in the triangular determinant calculation (PC.7) of §R17C; the normalized ratio supplies the pole coefficients (PC.1) of the same section. The central-binomial row is also the local inverse-Jacobian series

$$R(x)^{-1}=(1+4x)^{-1/2}=\sum_{m\geq 0}(-1)^m\binom{2m}{m}x^m, \qquad |x|<\frac{1}{4}. \tag{PR.10c}$$

A final centered product closes the elementary loop:

$$\boxed{\pi=4\prod_{n\geq 1}\frac{8T_n}{8T_n+1}=4\prod_{n\geq 1}\frac{(2n)(2n+2)}{(2n+1)^2}.} \tag{PR.10d}$$

Changing logarithmic scale does not alter the Mellin phase if its Jacobian is retained. For $v=\log_{10} n$,

$$n^{-s}=10^{-\sigma v}e^{-it(\ln 10)v}, \qquad \overline{n^{-s}}=10^{-\sigma v}e^{+it(\ln 10)v}. \tag{PR.11}$$

The full earlier catalog of angle and decimal examples is preserved in the v4.5 source provenance. The current Reading Volume keeps only the identities that re-enter the analytic argument.

R5E. The half-step and the reflected pair

The finite odd-factorial product has an integer upper limit. Its analytic continuation is supplied separately by Gamma duplication:

$$\mathcal{C}(m):=\frac{1}{\Gamma(2m+2)}=\frac{\sqrt{\pi}}{2^{2m+1}\Gamma(m+1)\Gamma(m+3/2)}. \tag{HS.1}$$

Now make the shift explicit, $m=s-1$. On the critical line,

$$s=\frac{1}{2}+it \Longrightarrow m=-\frac{1}{2}+it, \quad T_m=-\frac{1}{8}-\frac{t^2}{2}, \quad q(s)=-2T_m=\frac{1}{4}+t^2. \tag{HS.2}$$

The conjugate pair has the exact positive Gamma owner

$$\boxed{\mathcal{C}(-\tfrac{1}{2}+it)\mathcal{C}(-\tfrac{1}{2}-it) = \frac{\sinh(2\pi t)}{2\pi t} = \prod_{n\geq 1}\left(1+\frac{4t^2}{n^2}\right).} \tag{HS.3}$$

This is a Gamma identity, not the completed zeta source: the Euler-prime term has not disappeared.

Three involutions recur later and should not be conflated: conjugation $z \mapsto \bar{z}$, inversion $z \mapsto 1/z$, and reflection $z \mapsto 1-z$. Conjugation and reflection agree on $\Re s = 1/2$; the Cayley coordinate of §R7 converts reflection into inversion. Away from those loci they remain different operations.

For the fold $q = s(1-s)$,

$$(2s-1)^2 = 1-4q = 1+8T_{s-1}, \qquad s = \frac{1\pm\sqrt{1-4q}}{2}. \tag{HS.8}$$

Reflection exchanges the two inverse branches. If $q > 1/4$ is real they are the conjugate pair $1/2 \pm i\sqrt{q-1/4}$; for complex q, conjugation also moves q to $\bar{q}$. This branch distinction is the only part of the former power-tower comparison needed downstream; the longer fixed-point discussion is retained in the v4.5 provenance.

Part II. From the half-step to the complex fold

The fold $q = s(1-s)$ identifies the reflection pair, the Cayley chart expresses it as inversion, and the Mellin factor fixes the weight $1/\sqrt{n}$. Equation (6.4) is the key conclusion: a folded zero is real exactly when its zero lies on the critical line.

R6. Folding the two axes of $s = \sigma + it$

Define

$$q = q(s) = s(1-s) = \sigma(1-\sigma) + t^2 + i\,t(1-2\sigma) \tag{6.1}$$

The centered identity is

$$\boxed{q = \frac{1}{4} - \left(s-\frac{1}{2}\right)^2} \tag{6.2}$$

This is the analytic continuation of the centered split in (TDP.5): the signed coordinate $2s-1$ is squared and the two sheets s and $1-s$ fold to the same q.

Three specializations should be kept side by side:

locus in the s-plane	condition	folded image
critical line	$s = 1/2 + it$	$q = 1/4 + t^2 \in \mathbb{R}_{>0}$
real safe sheet	$s > 1$, $t = 0$	$q = -s(s-1) = -x < 0$
general point	$s = \sigma + it$	$\Im q = t(1-2\sigma)$

There is no omitted real-zero branch. For $0 < \sigma < 1$, the alternating Dirichlet eta function satisfies

$$\eta(\sigma) = (1 - 2^{1-\sigma})\zeta(\sigma) > 0 \tag{6.3}$$

Since $1 - 2^{1-\sigma} < 0$, one has $\zeta(\sigma) < 0$. Thus every nontrivial zero $\rho = \beta + i\gamma$ has $\gamma \neq 0$, and

$$q_\rho \in \mathbb{R} \iff \gamma(1-2\beta) = 0 \iff \beta = \frac{1}{2} \tag{6.4}$$

Therefore RH is exactly the assertion that all folded zero orbits land on the positive real q-axis.

R6A. Sum to product, and the model in which the hypothesis is true

Equation (6.4) says RH is the assertion that every folded orbit q_ρ is real and positive. Before six Parts are spent on it, it is worth writing down the assertion's **model**: a node set for which it holds, whose product is closed in elementary terms, and which the volume has been carrying since Part I without saying what it was for.

One dictionary. Let $A = \{a_j\}$ be positive with multiplicities m_j and $\sum_j m_j/a_j < \infty$. Put

$$E_A(x) = \prod_j \Bigl(1 + \frac{x}{a_j}\Bigr)^{m_j}, \qquad S_A(x) = \frac{E_A'}{E_A}(x) = \sum_j \frac{m_j}{x + a_j}, \qquad \exp\Bigl(-\int_0^x S_A\Bigr) = \frac{1}{E_A(x)} \tag{6A.1}$$

Sum becomes product here by one operation: integrate the resolvent and exponentiate. Three objects are compared through it.

instance	nodes a_j	resolvent	product
triangular ladder	$2T_n = n(n+1)$	(6A.3)	(6A.2), closed
folded zeros	$q_\rho = \rho(1-\rho)$	S_ξ, (9.5)	$X(-x)/X(0)$, §48B
primes	*not a node product*	P, §R16	$\zeta(s_x)/\zeta(2)$, Euler

The prime row is the odd one, and the distinction is not cosmetic: its passage from sum to product is unique factorization, a product over primes rather than over the nodes of a resolvent, absolutely convergent only for $\Re s > 1$. Dossier §48B keeps its three cutoffs apart — the prime-power cutoff, the truncated Euler product and the finite Dirichlet sum are three different objects, equal at $X = 2$ to $\exp(2^{-s})$, $(1 - 2^{-s})^{-1}$ and $1 + 2^{-s}$. The two node rows are what this section compares.

The triangular instance is closed, and it is already proved. Dossier §11 evaluates $\Pi_\triangle(u) = \prod_n (1 - u/T_n) = 1/[\Gamma(1+s)\Gamma(2-s)]$ under $u = s(s-1)/2$. That substitution is the fold: $x = -2u = s(1-s) = q(s)$. In the fold coordinate, with $\nu = \sqrt{x - \frac{1}{4}}$ (imaginary for $x < \frac{1}{4}$), the same identity reads

CLOSED FORM *the triangular model*

$$\boxed{\prod_{n\geq 1}\Big(1 + \frac{x}{2T_n}\Big) = \frac{\sin \pi s}{\pi\, q(s)} = \frac{\cosh \pi\nu}{\pi x}}, \qquad \boxed{\sum_{n\geq 1} \frac{1}{x + 2T_n} = \frac{\pi \tanh \pi\nu}{2\nu} - \frac{1}{x}} \tag{6A.2–6A.3}$$

the second being the logarithmic derivative of the first, and Γ reflection carrying one form to the other. The removable values are 1 at $x = 0$ and $4/\pi$ at $x = \frac{1}{4}$.

Keep the parameter signs visible. The numerator $\cosh \pi\nu$ is entire of order one-half in this model parameter; its zeros are exactly $x = -2T_n$ for $n \geq 0$. Division by πx removes the zero mode. The model's reflection variable gives $z = q(s)$ and $E_\triangle(q(1/2)) = 4/\pi$. The completed source instead uses $x = -q(s)$, so its centered value is $E_\xi(-1/4) = X(1/4)/X(0)$. At the common positive comparison parameter $x = 1/4$, its value is $X(-1/4)/X(0)$. These are distinct evaluations, not an identification of spectral measures.

The completed determinant $E_\xi(x) = X(-x)/X(0)$ also has order one-half, but the property shared with the triangular model is a zero-set condition:

$$\boxed{\text{RH} \iff E_\xi(x) = X(-x)/X(0) \text{ has all its zeros on the negative real axis.}} \tag{6A.4}$$

Equal order does not mean equal type. Dossier Section 12B proves, unconditionally, $\log E_\triangle(x) \sim \pi\sqrt{x}$ whereas $\log E_\xi(x) \sim \sqrt{x}\log x/4$. The model has finite type π; the completed determinant has infinite type at order one-half. An independent positive realization of the completed product remains missing.

A multiplicity-one operator. Dossier Section 12A realizes the product by $A_\triangle = -d^2/d\theta^2 - 1/4$ on $(0, \pi)$, with $f(0) = 0$, $f'(\pi) = 0$. Its normalized half-integer sine eigenfunctions have eigenvalues $2T_m$; removing $m = 0$ gives $\det(I + xA_+^{-1})$ equal to (6A.2). Unlike the full spherical Laplacian, this realization uses each positive degree once.

The same modes are unitary images of the reflected polynomials in Section R15. With $n = 2m + 1$ they satisfy

$$\frac{1}{n}\mathcal{P}_m\left(4\sin^2\frac{\pi u}{n}\right) = \frac{\operatorname{sinc}_\pi(u)}{\operatorname{sinc}_\pi(u/n)} \longrightarrow \operatorname{sinc}_\pi(u). \tag{6A.5}$$

Their squares are finite Fejer kernels: the pair counts give $n + 2T_{n-1} = n^2$. The finite sine projection has an interior sine-kernel limit; at the boundary its reflected-sum term survives. Section 61A matches its bandwidth to $N \sim T^2 \log(T/(2\pi))/2$. This is a proved comparison limit, not a completed-source kernel limit or a theorem about zeta pair correlation. The latter prediction uses $1 - \operatorname{sinc}_\pi(u)^2$, not the nearest-neighbor gap density [79].

Three entries, with their status.

quantity	triangular model	folded zeros
$\sum_j m_j/a_j$	$\sum_n 1/(2T_n) = 1$ exactly	$S_\xi(0) = \lambda_1 = 0.0230957\ldots$ (9.8)
at comparison parameter 1/4	$E_\triangle(1/4) = 4/\pi$	$E_\xi(1/4) = X(-1/4)/X(0)$
odd-factorial layer	$(2m+1)! = \prod_r 2T_{2r}$ (PR.6)	rung weight $(2k-1)!$ (13A.3)

The model nodes start at 2, while the zeta nodes start near 200. The shared odd-factorial and hyperbolic identities therefore identify constructions, not their measures: nothing transfers without a source theorem, and no bound on Δ of (13A.2) follows from the model. An operator with spectrum q_ρ has not been supplied. That is precisely the input this volume cannot supply for ζ.

R7. Reflection, conjugation, and the Cayley circle

Use the global Cayley coordinate

$$z_C(s) = \frac{s}{1-s} \qquad s = \frac{z_C}{1+z_C} \qquad q = \frac{z_C}{(1+z_C)^2} \tag{7.1}$$

Then

$$\boxed{\frac{1}{q} = 2 + z_C + \frac{1}{z_C}} \tag{7.2}$$

This is the reciprocal coordinate of Dossier §171: $y_C = z_C + z_C^{-1}$. The same Pascal recurrence now has coefficients expressed through $q(s)$, so the arithmetic reciprocal fold returns here as an exact analytic identity, with its inverse branches retained.

Reflection becomes inversion $z_C \mapsto 1/z_C$, while conjugation becomes $z_C \mapsto \bar{z}_C$. They agree on the unit circle. Hence

$$\Re s = \frac{1}{2} \iff |z_C| = 1 \iff 1 - s = \bar{s} \tag{7.3}$$

The subscript C distinguishes this global s-plane coordinate from the scale-dependent Cayley complement $c_x(q) = (q-x)/(q+x)$ used in §R11.

This is a useful uniformization, not a proof engine. Differentiating a self-inversive reformulation does not import the Cohn or Speiser one-sided conditions: the derivative zeros of the completed symmetric function inherit inversion symmetry. The point $z_C = -1$ is an isolated essential singularity of $\xi(z_C/(1+z_C))$, with transformed zeros accumulating there.

R8. The self-dual Mellin magnitude

For $n > 0$,

$$n^{-s} = n^{-\sigma} e^{-it\log n} \qquad n^{-\bar{s}} = n^{-\sigma} e^{+it\log n} = \overline{n^{-s}} \qquad \left|n^{-s}\right| = n^{-\sigma} \tag{8.1}$$

Every negative-frequency factor is therefore carried together with its positive-frequency conjugate. Their sum and product are

$$n^{-s} + n^{-\bar{s}} = 2n^{-\sigma}\cos(t\log n) \qquad n^{-s} n^{-\bar{s}} = n^{-2\sigma} \tag{8.1a}$$

Reflection and conjugation give two products:

$$n^{-s} n^{-(1-s)} = \frac{1}{n} \qquad n^{-s}\overline{n^{-s}} = \frac{1}{n^{2\sigma}} \tag{8.2}$$

They agree for every n exactly at $\sigma = 1/2$. The common factor per side is

$$\boxed{n^{-1/2} = \frac{1}{\sqrt{n}}} \tag{8.3}$$

The conjugate pair $e^{\mp it\log n}$ changes phase but not length. This explains the self-dual $\Lambda(n)/\sqrt{n}$ normalization in the completed explicit formula. It does not identify the Gauss circle error term with the zeta zero problem; the shared square-root scale is geometric, while the arithmetic coefficients and summation problems are different.

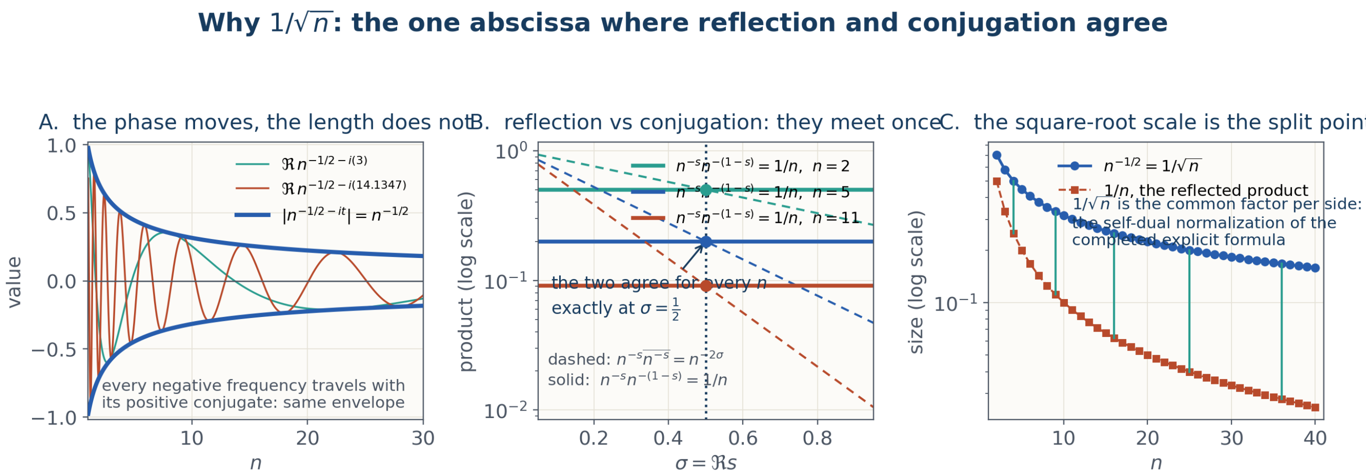

Figure 7: Why $1/\sqrt{n}$. The modulus of n^{-s} does not see the imaginary part; reflection and conjugation give two different products of a term with its partner; and those two products agree, for every n, at exactly one abscissa. The shared square-root scale is geometric, and does not identify two different problems.

Part III. Completion and the folded zero resolvent

Completion removes the pole and trivial zeros of ζ, leaving the entire function ξ with symmetry $s \mapsto 1-s$. Folding halves its order and gives one point per orbit $\{\rho, 1-\rho\}$. Its logarithmic derivative is the absolutely convergent simple-pole sum S_ξ in (9.7). Section R9 gives the Gamma–prime source formula; Sections R10–R10B give the zero-side criteria, positive realizations and off-line heat trace. Part IV differentiates this same resolvent.

R9. The completed function

The completed Riemann function is

$$\xi(s) = \frac{1}{2}s(s-1)\pi^{-s/2}\Gamma(s/2)\zeta(s) \qquad \xi(s) = \xi(1-s) \tag{9.1}$$

Here the half-Gamma value in (PR.10a) fixes a normalization: $\pi^{-1/2}\Gamma(1/2) = 1$ and $\lim_{s\to 1}(s-1)\zeta(s) = 1$ give $\xi(1) = 1/2$. On the critical line, however, the argument of this Gamma factor is $s/2 = 1/4 + it/2$. The distinction between the source variable and the Gamma argument matters when using a half-integer identity.

Because it is invariant under reflection, it factors through the fold:

$$\boxed{\xi(s) = X(q), \qquad q = s(1-s) = -2T_{s-1}, \qquad 4q = 1-(2s-1)^2} \tag{9.2}$$

for an entire function X. Define

$$M_\xi(q) = -\frac{X'(q)}{X(q)} \qquad S_\xi(x) = M_\xi(-x), \quad x > 0 \tag{9.3}$$

On the safe real sheet

$$s_x = \frac{1+\sqrt{1+4x}}{2} = \sigma_x + i0 > 1 \tag{9.4}$$

one has the absolutely convergent source formula

$$\boxed{S_\xi(x) = \frac{1}{R}\left[\frac{1}{s_x} + \frac{1}{s_x - 1} - \frac{1}{2}\log\pi + \frac{1}{2}\psi(s_x/2) - \sum_{n\geq 2}\frac{\Lambda_{\mathrm{vM}}(n)}{n^{s_x}}\right]} \tag{9.5}$$

This formula is the source-side entry: Gamma and primes are evaluated where their defining expansions converge.

Where the zeros enter. Write $[\rho]$ for one functional-equation orbit $\{\rho, 1-\rho\}$ and m_ρ for its multiplicity; an off-line quartet contributes two conjugate folded values, each counted once. This convention is used in every folded sum in the volume.

ξ is entire of order one. Since $q = s(1-s)$ is quadratic in s, the entire function X of (9.2) has order one **half** in q, so it has genus zero: its Hadamard product needs no exponential factors and converges absolutely [5],

$$X(q) = X(0)\prod_{[\rho]}\left(1 - \frac{q}{q_\rho}\right)^{m_\rho} \tag{9.6}$$

Taking $-X'/X$ and evaluating at $q = -x$ turns that product into the identity every later Part differentiates:

$$\boxed{S_\xi(x) = \sum_{[\rho]}\frac{m_\rho}{x+q_\rho}, \qquad Z_r(x) = \sum_{[\rho]}\frac{m_\rho}{(x+q_\rho)^r}} \tag{9.7}$$

This is what the fold buys, and it is worth being explicit about it. In the s-plane ξ has order one and genus one: the Hadamard product carries a factor $e^{s/\rho}$ at every zero, and $\sum_\rho \rho^{-1}$ needs a symmetric grouping to converge; pairing ρ with $1-\rho$ supplies one. The fold performs that pairing in the variable itself. The order halves, the exponential factors disappear, and $\sum_{[\rho]} m_\rho q_\rho^{-1}$ converges absolutely on its own. The underlying resolvent is an absolutely convergent sum of simple poles at $x = -q_\rho$, all in the open left half-plane. They lie

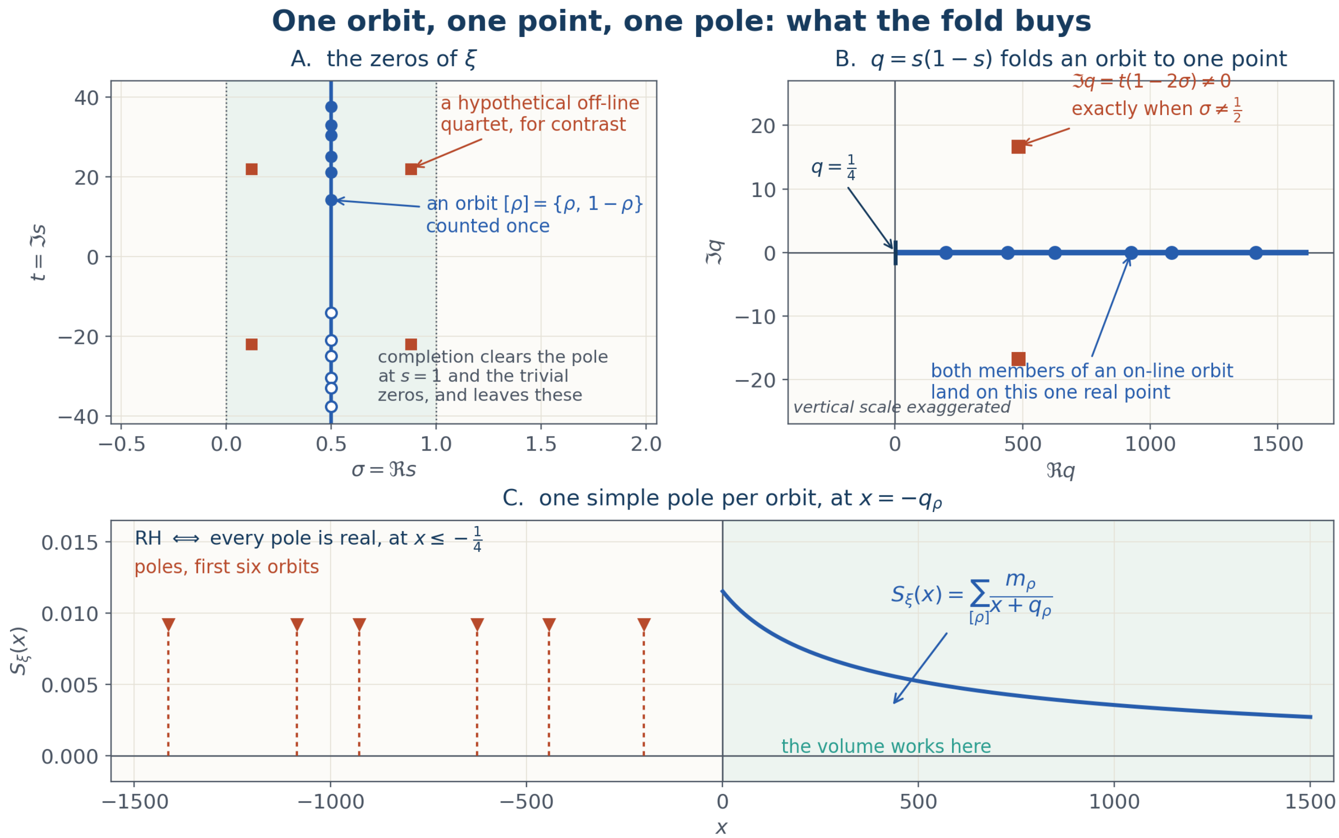

Figure 8: One orbit, one point, one pole. The zeros of ξ come in orbits $\{\rho, 1-\rho\}$; $q = s(1-s)$ sends both members of an orbit to a single point, real exactly when the orbit lies on the critical line; and S_ξ has one simple pole per orbit, at $x = -q_\rho$. Every argument in this volume is made to the right of all of them.

on the negative real axis exactly under RH. Higher resolvents and derivatives have higher pole orders on the same set; the safe-axis source formulas use $x > 0$.

One number, for orientation. At $x = 0$,

$$S_\xi(0) = \sum_{[\rho]} \frac{m_\rho}{q_\rho} = 1 + \frac{\gamma_{\mathrm{E}}}{2} - \log(2\sqrt{\pi}) = 0.0230957089661\ldots \tag{9.8}$$

with γ_{E} Euler's constant. The middle expression is the classical value of $\sum_\rho \rho^{-1}$, and the pairing $\rho^{-1} + (1-\rho)^{-1} = q_\rho^{-1}$ is why the folded sum reproduces it. This same number returns as the boundary moment μ_0 in §R12 and as Li's λ_1 in §R15. **Three names, one number, and it is the value at $x = 0$ of the function in (9.7).**

R9A. The first zero, in these coordinates

The volume is written in q and x and never evaluates them. One worked orbit fixes the scale of everything that follows, and the natural one is the lowest.

The first zero of ζ on the critical line sits at $\gamma_1 = 14.134725141734693790\ldots$, so by (9.2) its folded coordinate is

$$\boxed{q_1 = \tfrac{1}{4} + \gamma_1^2 = 200.0404548323868594\ldots = -2T_{\rho_1 - 1}} \tag{9.9}$$

The second equality is (9.2) read at $s = \rho_1$: **the folded image of a zero is -2 times the triangular number at its centered index.** For a critical-line zero that index is $-\frac{1}{2} + i\gamma$, and $(-\frac{1}{2} + i\gamma)(\frac{1}{2} + i\gamma) = -(\frac{1}{4} + \gamma^2)$, which is why q is real there and, by (6.4), nowhere else.

What this one orbit carries. By (9.8) the folded resolvent at the origin is $0.0230957\ldots$; the first orbit supplies $1/q_1 = 0.004998989\ldots$ of it, just under 22%. The second orbit sits at $q_2 = 442.1761\ldots$, so the ratio that governs the boundary of the whole ladder is

$$\frac{q_1}{q_2} = 0.4523999\ldots \tag{9.10}$$

Section R12 uses exactly this number.

On the prime side the same zero is the slowest wave. In Riemann's formula [74] each zero contributes an oscillation of period $2\pi/\gamma$ in $\log x$, so ρ_1 gives $2\pi/\gamma_1 = 0.4445212\ldots$ — the longest wavelength in the prime error, repeating every multiplicative factor $e^{2\pi/\gamma_1} = 1.5597432\ldots$ Everything faster comes from higher zeros. The rungs and the primes are reading the same list of numbers in two different coordinates.

Riemann's own count does not locate it. The smooth part of the zero-counting function is $N_0(T) = \frac{T}{2\pi}\log\frac{T}{2\pi} - \frac{T}{2\pi} + \frac{7}{8}$, which differs from $\theta(T)/\pi + 1$ by $1/(48\pi T) + O(T^{-3})$ (Stirling; this is the 0.0022 between the two heights below), so it first reaches 1 essentially where the Riemann–Siegel angle first vanishes: at $T = 17.8478\ldots$, against a first Gram point at $17.8456\ldots$ The first zero is at $14.1347\ldots$, lower by 3.71. At this height the smooth term is not in charge and the entire discrepancy is carried by the oscillating part $S(T)$ — the term every effective result in the subject has to bound, and the reason a *counting* statement and a *location* statement are different problems.

One constant, printed three times. The 7/8 above is not a third 7/8. It is the same number as the value $\mathfrak{Z}_\xi(0) = 7/8$ computed exactly at (TV.2), and as the coefficient of $1/x$ in the large-x expansion (OP.1) of S_ξ. The three agree for one reason: by the Mellin representation, the coefficient of x^{-1} in $\sum_{[\rho]} m_\rho (x + q_\rho)^{-1}$ is the value at $p = 0$ of $\sum_{[\rho]} m_\rho q_\rho^{-p}$, the regularized number of orbits; and for a spectrum whose counting function is a smooth main term plus 7/8 plus a mean-zero oscillation, the main term contributes to the *poles* of $\mathfrak{Z}_\xi$ and only the constant survives at the origin. So the constant in Riemann's counting formula, the regularized count of folded orbits, and the $1/x$ coefficient of the source expansion are one number.

The mechanism, displayed. From $(x + q)^{-1} = \frac{1}{2\pi i}\int_{(c)} \frac{\pi}{\sin \pi p} x^{-p} q^{p-1} dp$ $(0 < c < 1)$, summing over orbits for $0 < c < \frac{1}{2}$,

$$S_\xi(x) = \frac{1}{2\pi i}\int_{(c)} \frac{\pi}{\sin \pi p}\, \mathfrak{Z}_\xi(1-p)\, x^{-p}\, dp \tag{9.11}$$

Moving the contour right: the double pole of $\mathfrak{Z}_\xi(1-p)$ at $p = \frac{1}{2}$, inherited from the smooth count, gives the $x^{-1/2}\log x$ and $x^{-1/2}$ terms of (OP.1); the simple pole of $\pi/\sin \pi p$ at $p = 1$, where $\mathfrak{Z}_\xi$ is regular by (TV.2), gives $+\mathfrak{Z}_\xi(0)/x = \frac{7}{8}/x$. The oscillating part $S(T)$ contributes to no pole at $p \le 1$.

That identification is checked in the source package from the **source side alone**: computing S_ξ from (9.5), with Gamma and primes only and no zero used anywhere, $x\big(S_\xi(x) - \frac{\log x - 2\log 2\pi}{8\sqrt{x}}\big)$ takes the value $0.87495\ldots$ at $x = 10^7$; the limit as $x \to \infty$ is $7/8$. A finite evaluation is not the limit, and the two are printed separately.

Grade. The identities in (9.9) and (9.10) are exact; their printed decimals are approximations. The prime-side period is classical. The 7/8 identification is an identity among quantities the volume already carries, confirmed to four digits by an independent computation that uses no zero. **None of it is evidence for or against the hypothesis.** It is the scale of the objects, and it is here because a reader is entitled to see the coordinates carry a number at least once.

R10. Heat, Stieltjes, and complete Bernstein owners

The folded heat trace and its Laplace transform are

$$\Theta_\xi(u) = \sum_{[\rho]} m_\rho e^{-uq_\rho} \qquad S_\xi(x) = \int_0^\infty e^{-xu}\Theta_\xi(u)\, du \tag{10.1}$$

Three classes of function, and what each one contributes. The chain below uses them, and they are worth stating plainly.

- A **Stieltjes function** on $(0,\infty)$ is one of the form $a + \int_0^\infty (x+u)^{-1} d\mu(u)$ with $a \ge 0$ and μ a positive measure: exactly a nonnegative constant plus a superposition of simple poles on the negative axis, with positive weights. Comparing with (9.7), S_ξ is of that shape already — one pole per orbit — and **the whole content of the class membership is that the poles are real and the weights are positive**.
- A **complete Bernstein function** is one whose quotient by x is Stieltjes; equivalently it has an integral representation with the same positive measure, read one power lower. It is the form in which the criterion becomes a statement about $h(x) = xS_\xi(x)$ rather than about S_ξ.
- h is **operator monotone** on $(0,\infty)$ if $A \preceq B$ implies $h(A) \preceq h(B)$ for all positive operators. Among nonnegative functions, Löwner's theorem identifies this class with the complete Bernstein functions. Operator monotonicity alone is not sufficient for that class. The actual $h = xS_\xi$ is positive.

Widder's theorem is the discrete counterpart used from Part IV onward: it characterizes the same class by the sign of every derivative combination $(-1)^{k-1}D^{2k-1}[x^k f]$, which is precisely the family W_k. So the rungs of Part IV are not a new criterion. **They are this same equivalence, read one derivative at a time.**

The exact equivalence chain is

$$\boxed{\begin{aligned} \mathrm{RH} &\iff S_\xi \text{ is Stieltjes} \\ &\iff h(x) := xS_\xi(x) \text{ is complete Bernstein} \\ &\iff h \text{ is operator monotone on } (0,\infty) \end{aligned}} \tag{10.2}$$

For positive nodes $x_1, \ldots, x_N$, the Löwner matrix of h is

$$[\mathcal{L}_h]_{ij} = \begin{cases} \dfrac{h(x_i) - h(x_j)}{x_i - x_j}, & i \neq j \\ h'(x_i), & i = j \end{cases} \tag{10.3}$$

Löwner's theorem gives the all-node criterion

$$\boxed{\mathrm{RH} \iff \mathcal{L}_h(x_1, \ldots, x_N) \succeq 0 \quad \text{for every finite positive node set}} \tag{10.4}$$

This is one global matrix owner. The scalar Widder rungs of Part IV are local derivative shadows of it. In particular, its one-node entry is $h'(x) = W_1(x)$. Higher W_k are not additional diagonal entries of this same matrix: their exact connection uses the derivative array and boundary moment matrices developed in §§R12–R15.

R10A. Positive realizations: trace and finite-vector forms

An operator model must reproduce the particular scalar function S_ξ. Two compatible positive representations have different normalizations:

representation	scalar resolvent	Gram vector for $\mathcal{L}_h$
positive trace-class operator D	$\mathrm{Tr}[D(I+xD)^{-1}]$	$D^{1/2}(I+xD)^{-1}$ in Hilbert–Schmidt space
positive operator D and finite vector v	$\langle (I+xD)^{-1}v, v\rangle$	$(I+xD)^{-1}v$ in Hilbert space

In either row, equality with $S_\xi(x)$ for every $x > 0$ supplies a positive Löwner matrix. The proof is the elementary resolvent identity: the divided difference of $x/(1+xd)$ is $[(1+xd)(1+yd)]^{-1}$. The trace route has $\mathrm{Tr}\, D = \lambda_1$; the finite-vector route has $\|v\|^2 = \lambda_1$, where $S_\xi(0) = \lambda_1$ is the first of Li's coefficients, defined at (15.1a) and equal to the boundary moment μ_0.

The source itself fixes which normalization is possible. Expanding (9.5),

$$\boxed{S_\xi(x) = \frac{\log x - 2\log(2\pi)}{8\sqrt{x}} + \frac{7}{8x} + O\left(\frac{\log x}{x^{3/2}}\right)} \tag{OP.1}$$

Consequently $xS_\xi(x) \to \infty$. A proposed finite-vector formula $S_\xi = \langle D(I+xD)^{-1}v, v\rangle$ would instead imply $xS_\xi \le \|v\|^2$. It fails even under RH. The extra factor D is valid inside a trace, or for the different finite-vector function $[S_\xi(0) - S_\xi(x)]/x$; it cannot be silently moved between the two rows.

For the canonical folded diagonal C_ξ, the eigenvalues are $d_\rho = 1/q_\rho$, counted once per reflection orbit. It is a normal trace-class operator unconditionally. The classical zero-counting estimate gives

$$\boxed{C_\xi \in \mathcal{S}_p \iff p > \frac{1}{2}} \tag{OP.2}$$

Positivity of this diagonal is equivalent to RH. It is a useful exact spectral representation; an independent positivity theorem is still needed. In particular, an ordered model with $d_n = O(n^{-2})$ has a critical trace sum with at most a simple pole at $p = 1/2$. Section R17A will exhibit the double pole required by the completed source.

A fixed indefinite quartet metric has another limitation. Congruence preserves its inertia, so a matrix of signature $(2,2)$ cannot become a positive metric merely by changing coordinates. This says nothing against a different positive realization proved from the full source. Zero-indexed representations are not automatically circular; assuming their positivity would be the missing step.

R10B. What an off-line orbit leaves in the heat trace

The triangular imaginary part is an exact off-line marker. Write $q_\rho = a_\rho + ib_\rho$ in this section, with explicitly defined real coordinates

$$\boxed{a_\rho = \gamma^2 + \beta(1-\beta) > 0, \qquad b_\rho = \gamma(1-2\beta) = -2\Im T_{\rho-1}} \tag{HT.1}$$

Since $\gamma \neq 0$, $b_\rho = 0$ exactly on the critical line. A conjugate pair of folded orbits contributes

$$\underbrace{2me^{-ua}\cos(ub)}_{\text{heat contribution}} \qquad \text{against} \qquad \underbrace{2me^{-ua}}_{\text{phase removed}}, \qquad u > 0 \tag{HT.2}$$

Thus off-line geometry creates an oscillatory heat contribution. The total heat trace does not vanish under RH; it is then a positive sum of decaying exponentials. The meaningful absence statement concerns the off-line defect, not the whole trace.

Define the real-part envelope and its gap by

$$\Theta_{\text{env}}(u) = \sum_{[\rho]} m_\rho e^{-ua_\rho} \qquad \mathcal{D}_H(u) = \Theta_{\text{env}}(u) - \Theta_\xi(u) \tag{HT.3}$$

Conjugate pairing gives the nonnegative identity

$$\boxed{\mathcal{D}_H(u) = \sum_{[\rho]} m_\rho e^{-ua_\rho}[1 - \cos(ub_\rho)] \geq 0} \tag{HT.4}$$

All sums converge absolutely for $u > 0$. Therefore different orbits cannot cancel in this gap. A single orbit can still have a resonant zero at $ub \in 2\pi\mathbb{Z}$. Vanishing throughout any open interval of u excludes every nonzero b, whereas vanishing at one selected time alone does not supply that argument.

A resonance-free version uses the squared imaginary coordinate:

$$\boxed{\mathcal{E}_H(u) := \sum_{[\rho]} m_\rho b_\rho^2 e^{-ua_\rho} = 4\sum_{[\rho]} m_\rho (\Im T_{\rho-1})^2 e^{-ua_\rho}} \tag{HT.5}$$

For every fixed $u > 0$, each off-line orbit contributes strictly positively. The sum is finite, since $b_\rho^2 \leq \gamma^2$ and Gaussian decay dominates the zero count. Consequently

$$\boxed{\mathcal{E}_H(u) = 0 \iff \text{RH} \qquad \text{at any one prescribed } u > 0} \tag{HT.6}$$

This is an exact detector, not an independent source estimate. Its weights still use the unknown transverse zero coordinates. In the language of §R21, it has the regularized distributional representation $\mathcal{E}_H(u) = (4\pi)^{-1}\langle \Delta \log|\xi|, (\Im q)^2 e^{-u\Re q}\rangle$ over the critical strip. This supplies a source representation but leaves the zero-forcing bound unproved.

There is also a direct bridge back to resolvents. Put $S_{\text{env}}(x) = \sum_{[\rho]} m_\rho/(x + a_\rho)$. For $x > 0$,

$$\boxed{\begin{aligned} S_{\text{env}}(x) - S_\xi(x) &= \int_0^\infty e^{-xu}\mathcal{D}_H(u)du \\ &= \sum_{[\rho]} m_\rho \frac{b_\rho^2}{(x + a_\rho)[(x + a_\rho)^2 + b_\rho^2]} \geq 0 \end{aligned}} \tag{HT.7}$$

To prove the displayed fraction, integrate $e^{-(x+a)u}[1 - \cos(bu)]$, obtaining $1/(x + a) - (x + a)/[(x + a)^2 + b^2]$. Every nonzero b gives a strictly positive summand. Thus equality in (HT.7) at one prescribed x is again equivalent to RH. The missing step would be an independent source proof of the reverse inequality $S_{\text{env}}(x) \leq S_\xi(x)$, or a source proof that $\mathcal{E}_H(u) \leq 0$. The envelope itself is not presently recovered from an independently positive source model.

The established heat criterion remains

$$\boxed{\text{RH} \iff (-1)^k \Theta_\xi^{(k)}(u) \geq 0 \quad \text{for every } k \geq 0,\ u > 0} \tag{HT.8}$$

This is complete monotonicity, stronger than positivity of the total heat trace. For example, the synthetic folded spectrum with two atoms at 1 and one at each of $2 \pm i$ has $\Theta(u) = 2e^{-u} + 2e^{-2u}\cos u > 0$ for all $u > 0$, despite its nonreal pair. It is not asserted to be the Riemann spectrum.

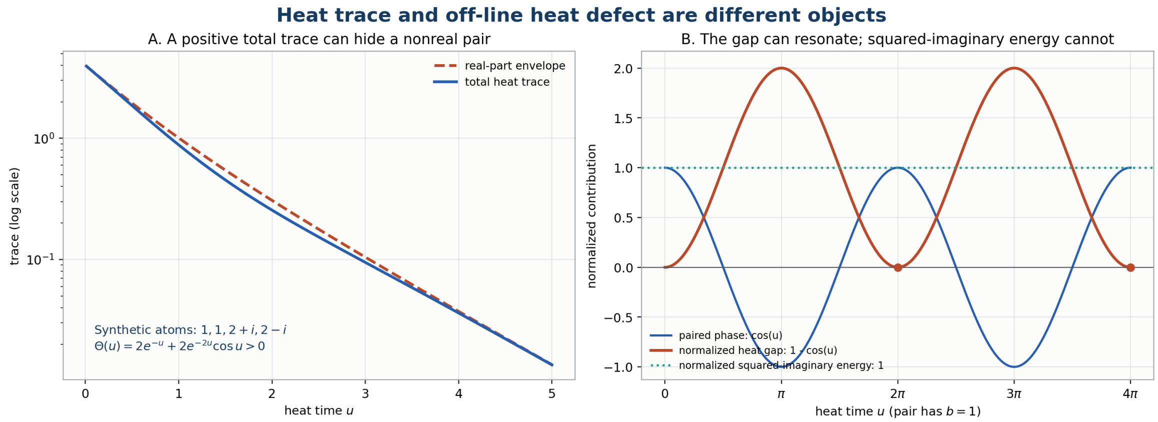

Figure 9: Synthetic heat traces: the total trace stays positive despite a nonreal pair, while the normalized off-line heat gap has isolated resonant zeros. The squared-imaginary-coordinate detector avoids those resonances.

Finally, the source already retains the prime heat term explicitly:

$$\Theta_\xi(u) = 1 + \Theta_\Gamma(u) - \Theta_P(u), \qquad \Theta_P(u) = \frac{e^{-u/4}}{2\sqrt{\pi u}} \sum_{n\geq 2} \frac{\Lambda_{\mathrm{vM}}(n)}{\sqrt{n}} e^{-(\log n)^2/(4u)} \tag{HT.9}$$

The prime term is beyond all algebraic orders as $u \downarrow 0$. This explains why matching the regularized fractions and the complete algebraic short-time expansion need not identify the heat trace itself. Conversely, a hypothetical off-line zero above the verified height contributes the factor e^{-ua_ρ} with $a_\rho > H^2$: at fixed time its signal can be extremely small. Proving its exact absence is a source theorem, not a numerical detection threshold.

Part IV. The Widder ladder and the sector geometry

This Part develops the reduced-Widder rung W_k of (R.3), and the criterion (R.4), proved by Stieltjes characterization in Dossier (33.1). **No finite prefix of this family is an RH statement.** Section R12 controls the status: $W_1 > 0$ is analytic and $W_2, \dots, W_6 > 0$ are source-certified A-CAT; a larger rectangle uses verified-height input. Section R11 fixes the carrier, R12A the shifted-resolvent basis, R13 the sector rectangle, and R14 one prescribed scale.

R11. Carrier, Cayley complement, and rungs

Everything in this Part is built from one identity of Part III: S_ξ is the sum of one simple pole per folded orbit, (9.7). Differentiating it produces the resolvents Z_r; combining those produces the rungs. The object that makes the combination work is the carrier.

For $x > 0$ define

$$\mathcal{F}_x(s) = \frac{1-s}{x+q(s)} \qquad u_x(q) = \mathcal{F}_x(s)\mathcal{F}_x(1-s) = \frac{q}{(x+q)^2} \tag{11.1}$$

On the critical line $s = 1/2 + it$,

$$\mathcal{F}_x\left(\frac{1}{2}+it\right) = \frac{\frac{1}{2}-it}{t^2+x+\frac{1}{4}} \qquad u_x(q) = \left|\mathcal{F}_x\left(\frac{1}{2}+it\right)\right|^2 \geq 0 \tag{11.2}$$

The reduced-Widder ladder is

$$\boxed{W_k(x) = j_{k-1}!\sum_{[\rho]} m_\rho \left(\frac{q_\rho}{(x+q_\rho)^2}\right)^k \qquad j_{k-1} = 2k-1} \tag{11.3}$$

Phase and the complete sum. For positive q, the carrier is positive and peaks at $q = x$. A nonreal conjugate pair contributes $2|u_x|^k \cos(k \arg u_x)$. For $q = |q|e^{i\theta}$ and $s_0 = \log(x/|q|)$, $4x|u_x(q)| = 2/(\cosh s_0 + \cos\theta) \leq \sec^2(\theta/2)$, with equality at $x = |q|$, where its phase vanishes. Also $\arg u_x(q) = \theta \tanh(s_0/2) + O(\theta^3)$. At a fixed nonzero phase ϕ, this individual pair first becomes strictly negative at $k = \lfloor \pi/(2|\phi|) \rfloor + 1$. This does not locate the first negative rung of the complete sum.

The correct all-zero evaluation retains the complex shifted ordinate:

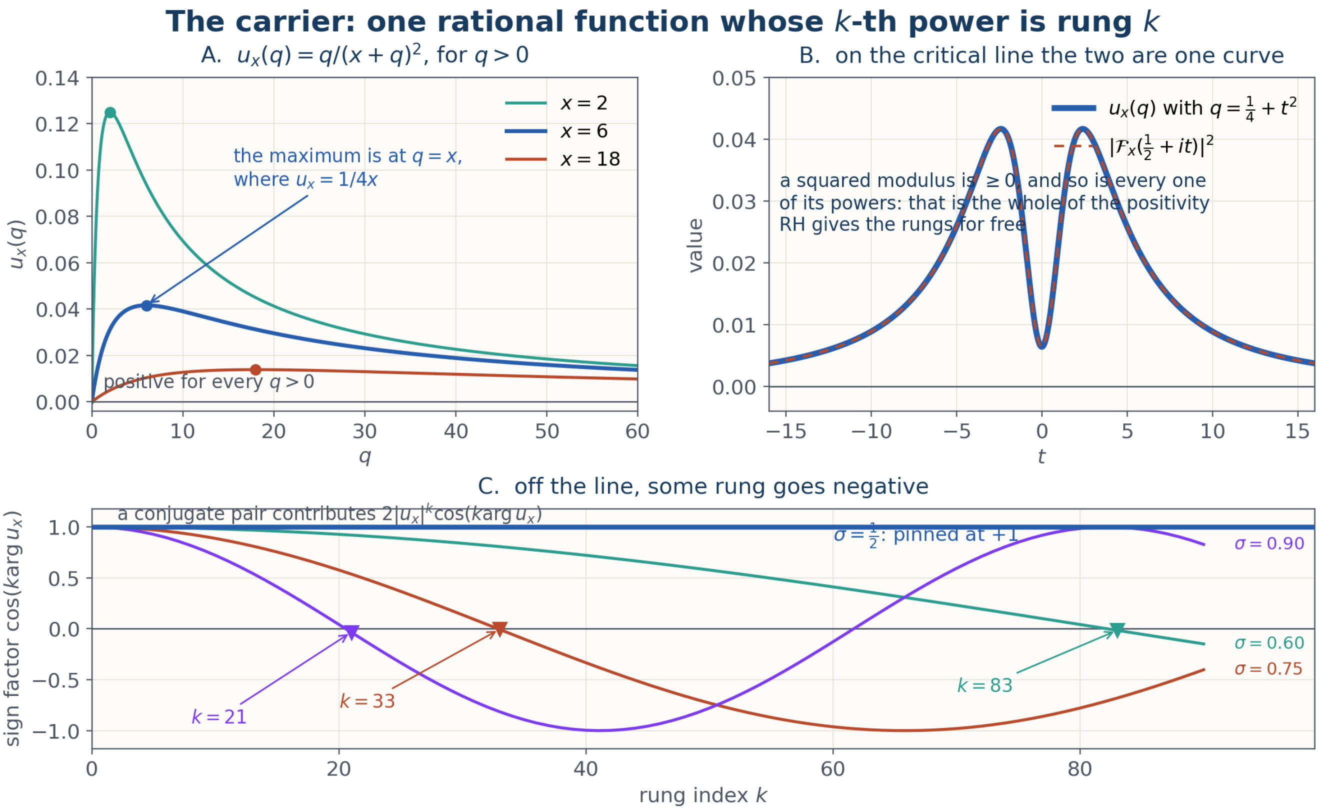

Figure 10: The carrier. **A:** $u_x(q) = q/(x+q)^2$ is positive for every $q > 0$ and peaks at $q = x$. **B:** on the critical line it coincides with $|\mathcal{F}_x(\frac{1}{2}+it)|^2$, so every power of it is nonnegative — that is the whole of the positivity the hypothesis gives the rungs for free. **C:** off the line a conjugate pair contributes $2|u_x|^k \cos(k \arg u_x)$, the sector theorem of §R13 excludes negative complete rungs through its stated finite order.

$$\tau_\rho = (\rho - 1/2)/i = \gamma + i(1/2 - \beta), \qquad q_\rho = 1/4 + \tau_\rho^2,$$
$$f_{k,x}(t) = \left[\frac{4x(t^2+1/4)}{(t^2+x+1/4)^2}\right]^k, \qquad W_k(x) = \frac{(2k-1)!}{2(4x)^k}\sum_{\rho \text{ all}} m_\rho f_{k,x}(\tau_\rho). \tag{11.3a}$$

The factor one-half converts all zeros to reflection orbits. Only on the line is τ_ρ the real ordinate γ. Theorem 22A.1 proves at least k Fourier sign changes on the positive axis. Its $k = 1$ transform is $\frac{\pi}{a}e^{-a|u|}[4x - \frac{2x^2}{a^2}(1+a|u|)]$, $a = \sqrt{x+1/4}$, negative beyond $(1+1/(2x))/a$ (below $\log 2$ when $x > 2.68$). The exponential-polynomial transform is not compactly supported. Scalar Fourier nonnegativity cannot prove the rung sign; a completed Weil-form or two-variable source argument is not excluded. The verified-height sector result gives a lower bound on the earliest possible negative rung, not an upper bound on how late it may occur.

The normalized Cayley complement

$$t_x(q) = 4xu_x(q) = \frac{4xq}{(x+q)^2} \tag{11.4}$$

lies in $(0, 1]$ for $q > 0$. Equivalently, with the scale-dependent coordinate

$$c_x(q) = \frac{q-x}{q+x} \tag{11.5}$$

one has

$$\boxed{u_x(q) = \frac{1-c_x(q)^2}{4x}, \qquad t_x(q) = 1 - c_x(q)^2} \tag{11.6}$$

In the log-scale variable $s = \log(q/x)$ these are hyperbolic functions:

$$\boxed{c_x(q) = \tanh\frac{s}{2}, \qquad u_x(q) = \frac{\operatorname{sech}^2(s/2)}{4x}, \qquad t_x(q) = \operatorname{sech}^2\frac{s}{2}} \tag{11.7}$$

and (11.6) is $1 - \tanh^2 = \operatorname{sech}^2$. So the rung (11.3) is a sum of sech^{2k} bumps centred on the orbits in log-scale. The half-maximum interval is exactly $|s| \le 2\,\operatorname{arcosh}(2^{1/2k})$, so the **half**-width is $\sim 1.665109/\sqrt{k}$ and the **full** width is $\approx 3.330218/\sqrt{k}$. Multiplying the full window by the smooth mean density gives a smoothed count $\approx 1.665\, k^{-1/2}\sqrt{x}\log(\sqrt{x}/2\pi)/2\pi$ of zeros a rung sees with weight above one half. That is a high-height smoothed estimate and not a bound on the actual count: at $x = q_1$ the first zero carries weight one for every k, so no literal count there is below one. This is the same quadratic complement that appears in the compact Hausdorff/Beta geometry. The disk fact $|c_x(q_\rho)| < 1$ follows already from $\Re q_\rho > 0$ and carries no RH content by itself.

R12. One ladder: explicit rungs, boundary moments, and proof channels

Write $S = S_\xi$. The differential and zero-side definitions are the same object:

$$\boxed{W_k(x) = (-1)^{k-1} D_x^{2k-1}[x^k S(x)] = (2k-1)! \sum_{[\rho]} m_\rho \frac{q_\rho^k}{(x+q_\rho)^{2k}}} \tag{12.1}$$

The first six rows are

$$
\begin{aligned}
W_1 &= S + xS' \\
W_2 &= -6S' - 6xS'' - x^2S''' \\
W_3 &= 60S'' + 60xS''' + 15x^2S^{(4)} + x^3S^{(5)} \\
W_4 &= -840S''' - 840xS^{(4)} - 252x^2S^{(5)} - 28x^3S^{(6)} - x^4S^{(7)} \\
W_5 &= 15120S^{(4)} + 15120xS^{(5)} + 5040x^2S^{(6)} \\
&\quad + 720x^3S^{(7)} + 45x^4S^{(8)} + x^5S^{(9)}
\end{aligned}
\tag{12.2}
$$

$$
\begin{aligned}
W_6 = &-332640S^{(5)} - 332640xS^{(6)} - 118800x^2S^{(7)} \\
&- 19800x^3S^{(8)} - 1650x^4S^{(9)} - 66x^5S^{(10)} - x^6S^{(11)}
\end{aligned}
\tag{12.2a}
$$

Leibniz's rule gives the coefficient of $x^jS^{(k+j-1)}$ as $(-1)^{k-1}(2k-1)!\binom{k}{j}/(k+j-1)!$ for $0 \le j \le k$. They are the factorially weighted rows of Figure 12; equation (SW.6) gives the exact conversion and the coefficient form of the recurrence.

Every next row is generated by the same centered odd coefficient:

$$
\boxed{W_{k+1} = -j_kW_k' - xW_k'' = -x^{-2k}D_x\left[x^{2k+1}W_k'\right] \qquad j_k = 2k+1}
\tag{12.3}
$$

The repeated $2k+1$ is therefore the rung version of the centered coordinate $j_n = 2n+1$; it is also the odd derivative/factorial index in the confluent Löwner hierarchy. For $k = 4$,

$$
\boxed{W_5 = -x^{-8}(x^9W_4')'}
\tag{12.4}
$$

Define the folded boundary moments $\mu_r = \sum_{[\rho]} m_\rho q_\rho^{-r-1}$, for $r \ge 0$. Then the exact comparison at every rung is

CLOSED FORM *boundary value of every rung*

$$
\boxed{\frac{W_k(0)}{(2k-1)!} = \mu_{k-1} = Z_k(0)}
\tag{12.4a}
$$

Here $Z_r(x) = \sum_{[\rho]} m_\rho(x+q_\rho)^{-r}$ is the r-th shifted resolvent, defined again with its derivative reading at (SW.2). Li's λ-coefficient expressions are printed in §R15.

Here $F(s) = (s-1)\zeta(s)$ is the regularized source, distinct from the two-index functional $F_{n,k}$ of (13.2).

rung	exact boundary value	is the sign true for all $x > 0$?	is there a source-side proof of it?
W_1	μ_0	PROVED analytic	PROVED analytic, through $F^{(2)}$
W_2	$3!\,\mu_1$	CERTIFIED	CERTIFIED through $F^{(4)}$
W_3	$5!\,\mu_2$	CERTIFIED	CERTIFIED through $F^{(6)}$
W_4	$7!\,\mu_3$	CERTIFIED	CERTIFIED through $F^{(8)}$
W_5	$9!\,\mu_4$	CERTIFIED verified-height theorem and source certificate	CERTIFIED source A-CAT through $F^{(10)}$
W_6	$11!\,\mu_5$	CERTIFIED verified-height theorem and source certificate	CERTIFIED source A-CAT through $F^{(12)}$
W_k, $7 \le k \le K_H$	$(2k-1)!\,\mu_{k-1}$	CERTIFIED same verified-height theorem, §R13	OPEN
W_k, $k > K_H$	$(2k-1)!\,\mu_{k-1}$	OPEN	OPEN

What a certified row asserts is stated with the status table in the front matter: the grade was established against the certificate of record and reviewed for this edition, not re-executed while this edition was produced.

Read the two right columns separately. The third column asks whether the inequality is *true*; the fourth asks whether *this program* has proved it from the Gamma–prime source without importing zero locations. In v4.6 those columns agree through W_6: the fifth and sixth signs have independent source-side continuum certificates joined to exact analytic tails, with no zero ordinates or RH assumption. The verified-height theorem remains a separate proof channel and continues much farther in rung index. From W_7 onward, the independent source column is open. Here $K_H = 4{,}712{,}664{,}392{,}502$ is the largest rung index admitted by that height, fixed exactly at (13.6).

This table is the controlling rung-status record for the whole volume; other sections point to it rather than restate what is open.

The boundary column does not need certifying. The second column is $W_k(0) = (2k-1)!\,\mu_{k-1}$, and those values are governed by one number.

CLOSED FORM *boundary dominance*

Order the folded orbits so that $q_1 < q_2 \le |q_\rho|$ for every other orbit. Then for every $k \ge 1$

$$\left|q_1^k \mu_{k-1} - 1\right| \le C \left(\frac{q_1}{q_2}\right)^k, \qquad C = q_2 \sum_{[\rho] \ne [\rho_1]} \frac{m_\rho}{|q_\rho|} < \infty \tag{12.7}$$

With the verified zero data $q_1/q_2 = 0.45240\ldots$ of (9.10) and $C = 8.0019\ldots$, so the right-hand side falls below 1 at $k = 3$ and

$$\boxed{W_k(0) > 0 \ \text{ for every } k \geq 3, \text{ with no hypothesis assumed}} \tag{12.8}$$

Proof. Multiply (12.4a) by q_1^k: the first orbit contributes 1 and each other contributes $m_\rho(q_1/q_\rho)^k$. For $k \geq 1$ and $|q_\rho| \geq q_2$, $|q_1/q_\rho|^k \leq (q_1/q_2)^k\, q_2/|q_\rho|$; summing gives (12.7). The series converges because $|q_\rho| \asymp \gamma^2$ while the zero count is $O(T \log T)$. When the bound is below 1 the left side cannot reach -1, so $q_1^k \mu_{k-1} > 0$. ☐

The constant C has an exact bound that needs no zero-counting tail estimate. Every orbit obeys $|\arg q| < \arctan(1/H)$ at the verified height H, so $1/|q| \leq \sqrt{1 + H^{-2}}\,\Re(1/q)$, and absolute convergence gives

$$\boxed{0 \leq C - C_0 \leq q_2\lambda_1\left(\sqrt{1+H^{-2}} - 1\right) \leq \frac{q_2\lambda_1}{2H^2}}, \qquad C_0 = q_2\Big(\lambda_1 - \frac{1}{q_1}\Big) \tag{12.7a}$$

using $\sqrt{1+h} - 1 \leq h/2$. The printed decimals of C retain the conditional scope of the carried enclosures for q_1, q_2 and λ_1; (12.7a) is what removes the unproved tail expression, not those enclosures.

What it says, and what it refuses to say. It says the boundary values are asymptotically a single real number, $\mu_{k-1} \sim q_1^{-k}$, with a geometric error fixed by the first two zeros: the constant in (12.7) is $C = q_2(\lambda_1 - 1/q_1)$ up to 1.4×10^{-9} from orbits above the verified height, $C \leq 8.001938048$ with no hypothesis, and $C(q_1/q_2)^3 = 0.741 < 1$ while $C(q_1/q_2)^2 = 1.64$, so $k \geq 3$ in (12.8) is where this argument starts. It also says that positivity **at the boundary is free**: for $k \geq 3$ it follows from the lowest zero being real, and would survive almost any rearrangement of the zeros above the verified height.

So the boundary column of this table is not where the hypothesis lives. The criterion (R.4) quantifies over every k **and every** $x > 0$, and $x = 0$ is the one place where the family is positive for reasons that have nothing to do with the question. **A verification of boundary positivity, finite or infinite, is not evidence for RH.** Positive boundary values do not control interference between all orbits at positive scales. The single-orbit carrier identities do not confine the complete sum to half-gap windows.

The boundary, in the classical literature. The boundary column is the power-sum side of Newton's identities. With e_n the Taylor coefficients of

$$\frac{\xi\big(\frac{1}{2} + \sqrt{\frac{1}{4} + x}\big)}{\xi(1)} = \prod_{[\rho]}\Big(1 + \frac{x}{q_\rho}\Big)^{m_\rho} = \sum_{n \geq 0} e_n x^n, \qquad n\, e_n = \sum_{i=1}^{n} (-1)^{i-1} e_{n-i}\, \frac{W_i(0)}{(2i-1)!} \tag{12.9}$$

The ordinary coefficients e_n in (12.9), normalized at $x = 0$, form a PF_∞ sequence exactly when the completed genus-zero function has only negative real zeros, hence exactly under RH [75]. This criterion concerns every Toeplitz minor of this specified ordinary sequence. The cited Turan and Jensen results [7,76–78] concern their own coefficient normalizations and

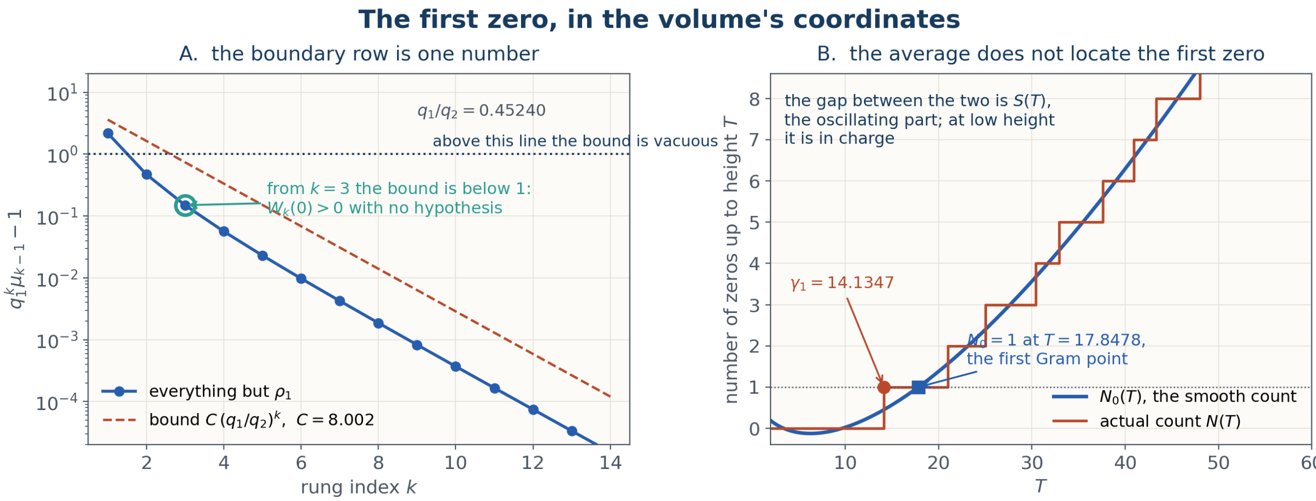

Figure 11: The first zero, in the volume's coordinates. **A:** the deviation $q_1^k\mu_{k-1} - 1$ against the bound of (12.7); from $k = 3$ the bound is below one, which is (12.8). **B:** Riemann's smooth count reaches one at the first Gram point, while the first zero sits well below it; the gap is the oscillating part $S(T)$, and at this height it is in charge.

polynomial families. No transfer to these e_n and all these minors is proved here, so those finite-minor statuses are not assigned to (12.9). The boundary power sums and the complete PF hierarchy are different sign questions.

Thus

$$\boxed{W_1(x), W_2(x), W_3(x), W_4(x), W_5(x), W_6(x) > 0 \quad (x > 0)} \tag{12.5}$$

The source certificate now closes the derivative sign

$$\boxed{(x^9 W_4')' < 0 \quad\Longleftrightarrow\quad W_5 > 0} \tag{12.6}$$

without importing zero data, and the same source method also proves $W_6 > 0$. Thus the independent Gamma–prime source prefix is now $W_1, \ldots, W_6$. The next scalar source task is $W_7 = -x^{-12}(x^{13}W_6')' > 0$, equivalently $(x^{13}W_6')' < 0$, whose owner reaches $F^{(14)}$. The recurrence remains non-raising: two new certified rungs do not supply an all-order induction. The zero-assisted theorem in §R13 still extends much farther, to $W_j > 0$ for $1 \le j \le K_H$.

One grid, several bases. The coefficient-shape crosswalk in Section R12A distinguishes row k, a segment of row $2k$, reflected positions, the central column and Pascal anti-diagonals. The conversions are exact, but the lists are not literally one row. Section R15 displays the worked W_6 triple.

family	one entry is	how it meets the grid	defined at
$c_{k,j}$	the grid entry itself	$(-1)^j\binom{k}{j}$	(R.1b)
$u_x(q)$	the carrier at one orbit	its k-th power expands using row k	(11.1)
$Z_r(x)$	the r-th shifted resolvent	the objects a row multiplies	(R.1c), (SW.2)
$W_k(x)$	rung k	row k against $Z_k, \ldots, Z_{2k}$	(R.3), (SW.4b)
$A_{k,j}$	the coefficient of $x^j S^{(k+j-1)}$	row k, factorially weighted	(SW.6)
$F_{n,k}(x)$	the full Widder functional	row k, resolvent index shifted by n	(13.2)
μ_r	the boundary moment $W_{r+1}(0)/(2r+1)!$	row k read at $x = 0$	§R12, (12.4a)
$h_n(x_0)$	a Hausdorff entry at one scale	row r is difference order r	(14.1), (14.3a)
λ_n	Li's coefficient	row $2k$ converts λ to μ_{k-1}	(15.1a), (15.3a)
$B_{N,j}(a)$	a completed Bernstein coefficient	row $N - j$	§R17F

Implication lattice: direct arrows only. Pairwise equivalence through RH is mathematically true for the equivalent criteria but does not compare their source difficulty, so those vacuous edges are not drawn. A displayed arrow below is included only when the paper proves it without assuming RH.

target	logical status	direct information retained here
all Widder signs (R.4)	**equivalent**	implies the necessary W_7 sign immediately
one-scale Hausdorff condition (14.2)	**equivalent**	no independent arrow to another source target is used
row-variation bound (BR.4)	**equivalent**	$\iff$ (BE.3) by $\sqrt{\mathscr{E}_N} \leq \mathcal{V}_N \leq \sqrt{N+1}\sqrt{\mathscr{E}_N}$
Laguerre-energy bound (BE.3)	**equivalent**	same direct row/energy equivalence as above
all-node Löwner sign (23.1)	**equivalent**	$\Longrightarrow$ the Stieltjes/Widder condition (R.4) by the Löwner–Pick/Stieltjes chain of §§R16–R17E
fixed taper $U_N = O_\epsilon(N^\epsilon)$, (155J.5)	**equivalent for that specified family**	no direct arrow to the matrix/source targets is proved
either curvature/boundary bound in (23.4)	**sufficient**	each $\Longrightarrow$ RH; no converse claimed
exact-prefix norm bound (155H.6)	**sufficient for the specified family**	no converse for arbitrary extensions
$W_7 > 0$ from the independent source	**necessary under RH; not sufficient**	next scalar source task only

The only nontrivial arrows used by the program are therefore sparse. All other connections either pass through RH itself or remain unknown. Part VIII records ruled-out arrows and shortcuts; blanks are intentional information, not missing editorial work.

R12A. The same rungs in the shifted-zeta basis

The differential coefficients in (12.2) become ordinary Pascal coefficients in a shifted resolvent basis. Define

$$\mathcal{Z}(p;v) = \sum_{[\rho]} m_\rho (\tau_\rho^2 + v)^{-p} \qquad \tau_\rho = \frac{\rho - 1/2}{i}, \qquad q_\rho = \tau_\rho^2 + \frac{1}{4} \tag{SW.1}$$

Here τ_ρ need not be real: this notation does not assume RH. For $v = x + 1/4$, $x \geq 0$, the principal-power series is absolutely convergent when $\Re p > 1/2$. Conjugate folded orbits are retained together. For positive integers r, write

$$\boxed{Z_r(x) := \mathcal{Z}(r; x + 1/4) = \sum_{[\rho]} \frac{m_\rho}{(x + q_\rho)^r} = \frac{(-1)^{r-1}}{(r-1)!} S_\xi^{(r-1)}(x)} \tag{SW.2}$$

For integers $n, k \geq 0$, define the full Widder functional

$$F_{n,k}[S_\xi](x) = (-1)^n D_x^{n+k}[x^k S_\xi(x)] = (n+k)! \sum_{[\rho]} m_\rho \frac{q_\rho^k}{(x + q_\rho)^{n+k+1}} \tag{13.2}$$

Voros's shift identity [56, §6.1] reads $\partial_v \mathcal{Z}(p;v) = -p\mathcal{Z}(p+1;v)$. The elementary expansion $q = (x+q) - x$ now gives the full array:

$$\boxed{\frac{F_{n,k}(x)}{(n+k)!} = \sum_{j=0}^{k} (-1)^j \binom{k}{j} x^j Z_{n+j+1}(x)} \tag{SW.3}$$

For fixed k, every value of n uses the same signed row k of Figure 12; only the resolvent index shifts. Its seed row is valid in this full array: $F_{n,0}/n! = Z_{n+1}$ for $n \geq 0$, and $F_{0,0} = Z_1 = S_\xi$. The reduced ladder instead selects $n = k - 1$, which requires $k \geq 1$.

In particular, with the odd factorial $(2k-1)!$ always in the denominator,

$$\begin{aligned}
&\tfrac{W_1}{1!} = Z_1 - xZ_2, \quad \tfrac{W_2}{3!} = Z_2 - 2xZ_3 + x^2 Z_4, \quad \tfrac{W_3}{5!} = Z_3 - 3xZ_4 + 3x^2 Z_5 - x^3 Z_6,\\
&\tfrac{W_4}{7!} = Z_4 - 4xZ_5 + 6x^2 Z_6 - 4x^3 Z_7 + x^4 Z_8,\\
&\tfrac{W_5}{9!} = Z_5 - 5xZ_6 + 10x^2 Z_7 - 10x^3 Z_8 + 5x^4 Z_9 - x^5 Z_{10}
\end{aligned} \tag{SW.4}$$

$$\boxed{\tfrac{W_6}{11!} = Z_6 - 6xZ_7 + 15x^2 Z_8 - 20x^3 Z_9 + 15x^4 Z_{10} - 6x^5 Z_{11} + x^6 Z_{12}} \tag{SW.4a}$$

For all $k \geq 1$, the diagonal $n = k - 1$ of (SW.3) is

CLOSED FORM *rung k in $k+1$ terms, for every $k \geq 1$*

$$\frac{W_k}{(2k-1)!} = \sum_{j=0}^{k}(-1)^j\binom{k}{j}x^j Z_{k+j} = \sum_{j=0}^{k} c_{k,j}\, x^j Z_{k+j} \tag{SW.4b}$$

No row of this identity is a truncation, an asymptotic, or a numerical fit. Row k of the grid is the complete answer for rung k, and the grid's own recurrence writes any row directly. What the closed form does **not** supply is the sign: knowing every coefficient of W_k exactly says nothing on its own about whether the sum is nonnegative, and that sign is the whole of the open problem.

At $x = 0$, (SW.4b) reduces to $W_k(0) = (2k-1)!Z_k(0) = (2k-1)!\mu_{k-1}$, joining the Li dictionary in §R15.

One grid, several coefficient chains. With the convention $c_{k,j} = 0$ outside $0 \leq j \leq k$, the signed Pascal array starts at

$$\begin{gathered} c_{k,j} = (-1)^j\binom{k}{j}, \qquad c_{0,0} = +1, \\ c_{k+1,j} = c_{k,j} - c_{k,j-1}, \qquad \sum_{j=0}^{k} c_{k,j} z^j = (1-z)^k \quad (k \geq 0). \end{gathered} \tag{SW.5}$$

The row sum is 1 at $k = 0$ and 0 for $k \geq 1$, so the top-left $+1$ is the algebraic seed of every displayed row.

Raising the carrier to a power is the same act as taking a row. Write $q = (x+q) - x$ and expand:

CLOSED FORM *the carrier and the grid are one object*

$$u_x(q)^k = \frac{q^k}{(x+q)^{2k}} = \sum_{j=0}^{k} c_{k,j}\,\frac{x^j}{(x+q)^{k+j}} \tag{SW.5a}$$

Summing (SW.5a) over the folded zeros with multiplicity gives (SW.4b) immediately.

Not every family occupies a whole row. The table in §R12 gave the chains and the identity that defines each; this one gives the shapes the remaining families occupy. All index formulas continue beyond the finite rows printed in Figure 12.

family and location	shape in the grid	reading Figure 12
Li boundary rows, §R15	**row segment**	Row $2k$, columns $k-1$ down to 0, with common sign $(-1)^{k+1}$.
Half-Gamma, inverse Jacobian and pole ladder, (PR.10b)–(PR.10c), §R17C	**centre column**	The central entries $c_{2m,m}$, with the displayed sign and scale.
Reciprocal polynomials, Dossier §171	**paired rows**	Two unsigned rows and the neighbouring-cell difference in (RP.3a).

family and location	shape in the grid	reading Figure 12
Bernstein rows and Laguerre, §§R17F–R17G	**rescaled rows**	Row $N-j$ for each Bernstein entry; row r divided by $j!$ for L_r.
Pascal energy matrix, §R17G	**anti-diagonals**	Entry (r,s) is $(-1)^r c_{r+s,r}$: its anti-diagonal $r+s=k$ is unsigned row k, and its row $r=2$ is the triangular track $M(2,s)=T_{s+1}$.
Triangular tracks, this section	**columns**	Column $j=2$ is T_{k-1}; column $j=3$ is the running sum of triangular numbers.

A shared shape is a shared coefficient list and nothing else. It transports identities, and it transports no inequality: two families can occupy the same row and still have unrelated signs, because the objects the coefficients multiply are different.

Two external instances, one each way. The arrangement is not peculiar to this volume. In a line running from Cloitre's tauberian approach of 2011 [67], through the floor-function characterization that introduces *regular arithmetic functions* [68], to the two-volume treatment of 2026 [69], a triangular two-index kernel $G(n,k)$ with $G(n,n) \neq 0$ is solved rank by rank and assigned a *regularity index*: the exponent at which its partial sums change behaviour. The Riemann hypothesis appears there as the statement that Ingham's kernel $G(n,k) = (k/n)\lfloor n/k \rfloor$ has index 1/2. The shared triangular shape and the shared rank-by-rank solve carry structure and an equivalence across, and carry no inequality: that index is a growth exponent, not a sign. Read the other way, Xu [70] obtains positivity in every degree for Chenevier's critical vectors by controlling the sign of every Verblunsky coefficient of an associated circle measure. There the inequality does transport, through a named mechanism rather than through a shared shape. The two together mark the gap in which this volume works. Both are recorded as read and are verified nowhere in this work.

On the k/n coordinate. The reduced rational address $z = a/q$ of Dossier §171 and the ratio k/n inside Ingham's kernel are the same coordinate, reached by different routes; the constructions raised on it are not the same object, and the two indices are not the same quantity. The present work reached its coordinate independently and without knowledge of [67]–[69], which have priority in the published record.

For the differential basis write $W_k = \sum_{j=0}^{k} A_{k,j} x^j S^{(k+j-1)}$, with $A_{k,j} = 0$ outside this range. Then

$$\begin{aligned} A_{k,j} &= (-1)^{k+j-1} \frac{(2k-1)!}{(k+j-1)!}\, c_{k,j}, \\ A_{k+1,j} &= -A_{k,j-1} - (2k+2j+1)A_{k,j} \\ &\quad - (j+1)(2k+j+1)A_{k,j+1}, \qquad k \geq 1. \end{aligned} \tag{SW.6}$$

The first line is the substitution (SW.2); the second follows by differentiating each term in (12.3). It generates the displayed arrays from $A_{1,0} = A_{1,1} = 1$. The polynomial source-jet arrays in Dossier §§34–38 add the Jacobian substitution $S = L/R$, $D_x = R^{-1}D_s$ to these same weighted rows; their additional factors are stated there.

FULL SIGNED WIDDER-PASCAL GRID

All 171 coefficients: rows k = 0 to 17, columns j = 0 to 17

k / j	0	1	2	3	4	5	6	7	8	9	10	11	12	13	14	15	16	17
0	+1																	
1	+1	-1																
2	+1	-2	+1															
3	+1	-3	+3	-1														
4	+1	-4	+6	-4	+1													
5	+1	-5	+10	-10	+5	-1												
6	+1	-6	+15	-20	+15	-6	+1											
7	+1	-7	+21	-35	+35	-21	+7	-1										
8	+1	-8	+28	-56	+70	-56	+28	-8	+1									
9	+1	-9	+36	-84	+126	-126	+84	-36	+9	-1								
10	+1	-10	+45	-120	+210	-252	+210	-120	+45	-10	+1							
11	+1	-11	+55	-165	+330	-462	+462	-330	+165	-55	+11	-1						
12	+1	-12	+66	-220	+495	-792	+924	-792	+495	-220	+66	-12	+1					
13	+1	-13	+78	-286	+715	-1287	+1716	-1716	+1287	-715	+286	-78	+13	-1				
14	+1	-14	+91	-364	+1001	-2002	**+3003**	-3432	**+3003**	-2002	+1001	-364	+91	-14	+1			
15	+1	-15	+105	-455	+1365	**-3003**	+5005	-6435	+6435	-5005	**+3003**	-1365	+455	-105	+15	-1		
16	+1	-16	+120	-560	+1820	-4368	+8008	-11440	+12870	-11440	+8008	-4368	+1820	-560	+120	-16	+1	
17	+1	-17	+136	-680	+2380	-6188	+12376	-19448	+24310	-24310	+19448	-12376	+6188	-2380	+680	-136	+17	-1

The shaded row is the coefficient seed. Even rows reverse unchanged; odd rows reverse sign.

Blank cells have j > k. Every nonblank cell is printed; no half-row convention is used.

Figure 12: The complete signed coefficient grid beside the W_k arrays (SW.4)–(SW.4a): all 171 entries $c_{k,j} = (-1)^j \binom{k}{j}$ for $0 \le k \le 17$, $0 \le j \le k$. The shaded seed is $c_{0,0} = +1$; in the full array it gives $F_{0,0} = S_\xi$, without defining a reduced W_0. For $k \ge 1$, row k multiplies $x^j Z_{k+j}$ in $W_k/(2k-1)!$. Both edges and both halves are printed.

The remaining finite arithmetic of the grid itself — how its columns read as tracks, the reflection identity, the interior triangular collisions including the eight positions of 3003, the $k = 0$ seed, and the odd factorial as an accumulated triangular product — is worked in Dossier §173. None of it is used below. The alternating rows encode cancellation, and neither they nor those collisions supply positivity: the proof channels and their current depth are exactly those tabled in §R12. Pearce-Crump [82] gives a recent external example in which Selberg's single mollifier square is replaced by a positive-semidefinite sum of three squared mollifiers and the resulting arithmetic quadratic form is optimized; this is a methodological analogy only, with no transfer asserted to the completed source here.

Dossier Theorem 32A.1 also represents every $F_{n,k}$ as a Laguerre transform of the heat trace. Its scalar kernel has exactly k simple sign changes for $k \geq 1$; an undifferentiated positive heat trace alone does not supply the required sign.

R13. Height-to-sector theorem and the full finite rectangle

For $q = a + ib$ with $a > 0$,

$$\arg u_x(q) = \arg q - 2\arg(x+q) \tag{13.1}$$

As x runs from 0 to ∞, this phase moves continuously from $-\arg q$ to $+\arg q$, crosses zero at $x = |q|$, and remains inside that closed angular band. Consequently a folded zero cannot rotate a fixed power outside the right half-plane once its height reaches the explicit threshold $H \geq \cot(\pi/2M)$ proved below.

The full functional $F_{n,k}$ is defined at (13.2) in §R12A; its reduced diagonal is $W_j = F_{j-1,j}$.

Full zero-assisted sector theorem. Suppose every nontrivial zero with $0 < |\Im\rho| \leq H$ lies on the critical line. Put $M = \max\{k, n+1\}$. Then

$$\boxed{H \geq \cot\left(\frac{\pi}{2M}\right) \Longrightarrow F_{n,k}[S_\xi](x) > 0 \quad (x > 0)} \tag{13.3}$$

To see the full two-index phase, put $\theta = \arg q$ and $\phi = \arg(x+q)$. A summand has phase

$$\alpha = k\theta - (n+k+1)\phi, \qquad |\alpha| < \max\{k, n+1\}|\theta| \quad (\theta \neq 0) \tag{13.3a}$$

For $x > 0$, ϕ lies strictly between 0 and θ when $\theta \neq 0$. If $\theta = 0$, the summand is positive real and the strict angular inequality is not needed. For an unverified zero above height H, $|\theta| < \arctan(1/H)$, since $\Re q = \gamma^2 + \beta(1-\beta) > \gamma^2$ and $|\Im q| = |\gamma(1-2\beta)| < |\gamma|$. Conjugate folded summands have opposite phases, so their real sum is strictly positive under (13.3).

Platt and Trudgian proved the verified height

$$H = 3{,}000{,}175{,}332{,}800 \tag{13.4}$$

and, in the same theorem, the full integer count: the lowest

$$\boxed{12{,}363{,}153{,}437{,}138} \tag{13.5}$$

nontrivial zeros lie on the critical line [42]. The largest integer admitted by the displayed height condition is now certified:

$$\boxed{K_H = \left\lfloor \frac{\pi}{2\arctan(1/H)} \right\rfloor = 4{,}712{,}664{,}392{,}502} \tag{13.6}$$

Exact rational enclosures prove that the number inside the floor lies strictly between 4,712,664,392,502 and 4,712,664,392,503. Thus (13.3) gives

$$\boxed{F_{n,k}[S_\xi](x) > 0 \quad (x > 0,\ 0 \le n \le K_H - 1,\ 0 \le k \le K_H)} \tag{13.7}$$

The exact lineage is

$$\boxed{\begin{aligned} W_j &= F_{j-1,j} \\ G_{n,k}(x) &= \frac{x^n}{(n+k+1)!} F_{n,k+1}[S_\xi](x) \\ G_{r-1,r-1} &= \frac{x^{r-1}}{(2r-1)!} W_r = \frac{x^{r-1}}{j_{r-1}!} W_r \end{aligned}} \tag{13.8}$$

Hence the same theorem gives $G_{n,k}(x) > 0$ for every $x > 0$ and $0 \le n, k \le K_H - 1$. The fixed-$x = 56$ theorem instead bounds n by 6,901,269,318 and permits every $k \ge 0$; the two rectangles are incomparable. On the reduced W_j diagonal, the height-to-sector rectangle is stronger.

Differentiating the summands also gives

$$\boxed{F'_{n,k} = -F_{n+1,k}, \qquad F_{n,k+1} = (n+k+1)F_{n,k} - xF_{n+1,k}} \tag{13.9}$$

Hence the certified rectangle includes finite strings of alternating derivative signs. In its interior, $0 \le n \le K_H - 2$ and $0 \le k \le K_H - 1$, one has

$$0 < -\frac{xF'_{n,k}}{F_{n,k}} < n + k + 1 \tag{13.10}$$

This is a finite zero-assisted A-CAT theorem. It does not prove the source-side $F^{(14)}$ inequality, and a finite rectangle—however large—does not replace the all-order quantifier in RH.

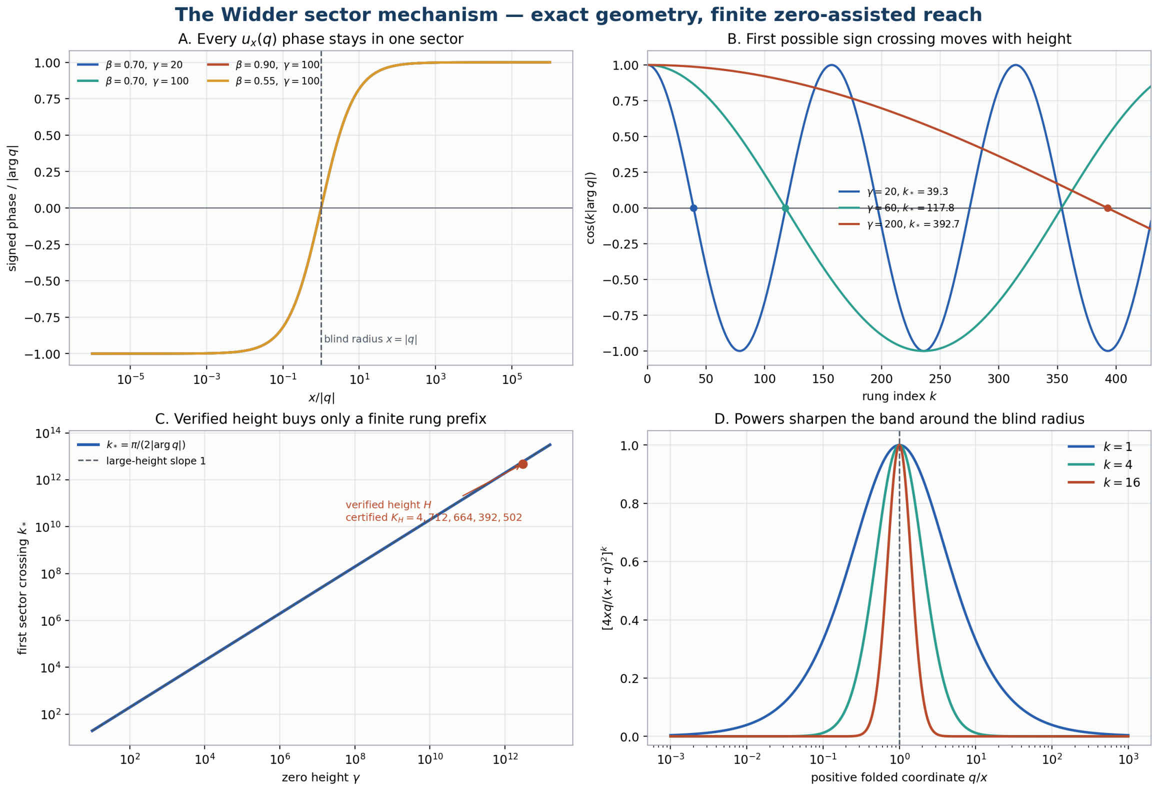

Figure 13: Four views of the sector mechanism: phase band, first cosine crossing, linear height-to-rung scale, and the blind-radius band pass.

R13A. How far the ladder is from the hypothesis, in one number

Dossier §48 writes the ladder at scale x as a power series $\mathcal{G}_x(z) = \sum_{k\ge1} W_k(x) z^{k-1}/(2k-1)!$ whose poles sit at $z_x(q_\rho) = (x+q_\rho)^2/q_\rho$, and Dossier §49 proves that its radius R_x satisfies $R_x \ge 4x$ for every x exactly when RH holds. Three facts locate the hypothesis inside that radius.

The deficit identity. For $q = |q|e^{i\theta}$ with $\Re q > 0$ and $x > 0$,

$$\boxed{4x - |z_x(q)| = 4x\sin^2\frac{\theta}{2} - \frac{(|q|-x)^2}{|q|}}, \qquad \max_{x>0}\bigl(4x - |z_x(q)|\bigr) = \frac{(|q|-\Re q)(3|q|-\Re q)}{|q|} \tag{13A.1}$$

the maximum at $x = 2|q| - \Re q$; at the blind radius $x = |q|$ the deficit is the strictly smaller $2(|q| - \Re q)$, which for a zero at abscissa β and ordinate γ is $(2\beta-1)^2(1+O(\gamma^{-2}))$. An off-line zero cuts the radius at its own scale by a **height-free** reading of its distance from the line.

The exact remainder. Write $d = 2\beta - 1$, $v = \gamma^2$, $c = \beta(1-\beta)$, $A = \Re q = v + c$ and $w = |q| - A \ge 0$, so that $w(2A+w) = vd^2$. The gap between the deficit and the squared transverse displacement is not an estimate but an identity, every factor positive off the line:

$$\boxed{d^2 - \max_{x>0}(4x - |z_x(q)|) = \frac{w\,[w^2 + c(3|q| - A)]}{v\,|q|} > 0} \tag{13A.1a}$$

together with the two-sided chain

$$\frac{4\gamma^2}{4\gamma^2+1}\,d^2 \;<\; 2w \;<\; \max_{x>0}(4x - |z_x(q)|) \;<\; d^2 \tag{13A.1b}$$

Both are proved at Dossier (48.29)–(48.30); the lower bound reduces to $v < v + \frac{1}{4}$. This replaces the parabola estimate of earlier editions, which carried an unnecessary height factor. On-line orbits have deficit $-(q-x)^2/q \le 0$. Hence

CLOSED FORM *the last unit of radius*

$$\boxed{4x - 1 < R_x \quad \text{for every fixed } x > 0, \text{ with no hypothesis assumed}} \tag{13A.2}$$

Put $\Delta = \sup_{x>0}(4x - R_x)$ and $d_* = \sup_\rho |2\Re\rho - 1|$. The minimum defining R_x is attained at each x, so (13A.1a) gives $\Delta \le d_*^2 \le 1$. **The displayed theorem is pointwise in x and does not assert $\Delta < 1$.** A uniform restriction $\delta \le \Re\rho \le 1-\delta$ gives $\Delta \le (1-2\delta)^2 < 1$; conversely $d_* = 1$ forces $\Delta = 1$ by (13A.1b). Here $d_* = 1$ is not attained: $\zeta(1+it) \ne 0$ excludes a zero on $\Re s = 1$, so $d_* = 1$ forces a sequence with $|2\Re\rho_n - 1| \to 1$. Finiteness of the zero count below any fixed height then forces $|\Im\rho_n| \to \infty$, and the factor $4\gamma_n^2/(4\gamma_n^2+1) \to 1$ in (13A.1b), giving $\Delta = 1$. Thus $\Delta < 1$ is equivalent to a uniform zero-free strip of positive width along **both** boundaries of the critical strip — not to the one-sided $\Re s < 1 - \delta$ of earlier editions, which names the wrong region and, read literally, excludes the line the known zeros are on. No such strip is known. And $\Delta = 0$ is RH (Dossier §49). Proofs: (48.31)–(48.32).

Two consequences. The high-scale statistic is strictly weaker: (48.33) gives $\limsup_{x\to\infty}(4x - R_x) = \limsup_{|\gamma|\to\infty}(2\beta-1)^2$, and a zero value there leaves finitely many off-line exceptions, or displacements tending to zero, untouched. And at the verified height $H = 3{,}000{,}175{,}332{,}800$,

$$0 \le d_*^2 - \Delta \le \frac{1}{4H^2+1} = \frac{1}{36{,}004{,}208{,}110{,}166{,}363{,}023{,}360{,}001} < 2.8 \times 10^{-26} \tag{13A.2a}$$

Conditional on the carried height input, the displayed amount bounds the gap between the two suprema. It is an error estimate, not a lower bound on computational distinguishability or a numerical-impossibility theorem. A uniform source estimate is still required to force $\Delta = 0$.

So the Euler product, whose absolute convergence stops at the parabola, reaches the deficit 1 and not one digit further — 1 is the width of the critical strip in these units, $(2\beta-1)^2 \le 1$ — and **the whole of the hypothesis at scale x is the last unit of R_x.** The deficit records

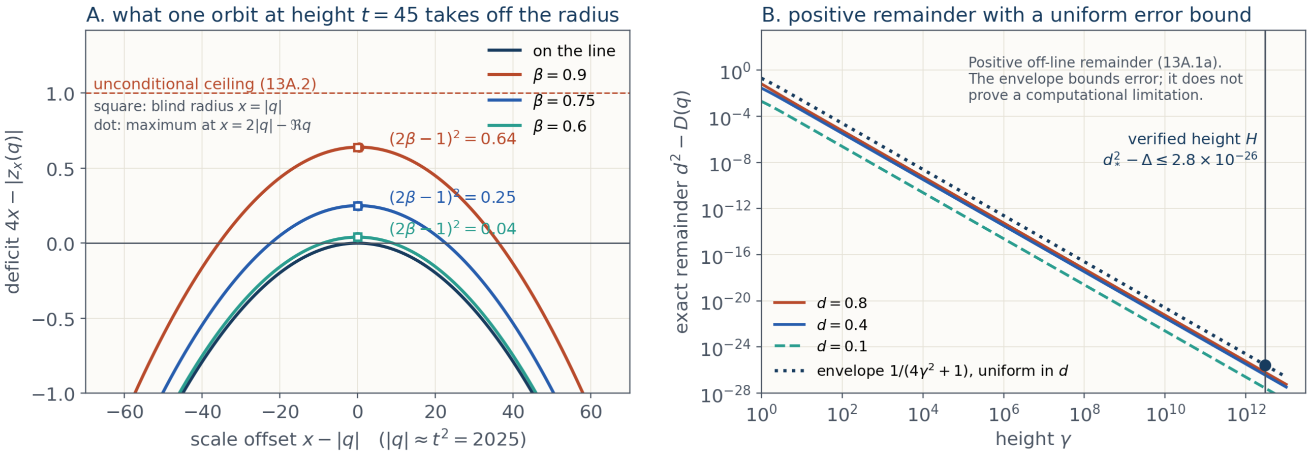

Figure 14: The last unit of radius. **A:** the deficit $4x - |z_x(q)|$ for one on-line orbit and three planted off-line orbits at height 45. The blind-radius value $2(|q| - \Re q)$ and the larger maximum at $x = 2|q| - \Re q$ approach $(2\beta - 1)^2$ as height tends to infinity. **B:** the strictly positive single-orbit remainder $d^2 - D(q)$, with envelope $1/(4\gamma^2 + 1)$ and the carried height marker. The weak global comparison $0 \leq d_*^2 - \Delta \leq (4H^2 + 1)^{-1}$ is an error bound, not a computational-impossibility statement. A uniform boundary strip would imply $\Delta < 1$; no such source estimate is proved.

extremal transverse displacement and nothing else; relating it to zero-density estimates or growth hypotheses needs a separate theorem with explicit quantifiers, which the radius identity does not supply. (23.1) is the statement that a source-side argument claims the whole unit.

Where the series comes from. With $a_k = (4x)^k W_k(x)/(2k-1)! = \sum_{[\rho]} m_\rho t_x(q_\rho)^k$ and $w = \sin^2(\varphi/2)$,

$$\boxed{\sum_{k\geq 1} a_k(x)\, w^k = 4xw\,\frac{h(xe^{-i\varphi}) - h(xe^{i\varphi})}{xe^{-i\varphi} - xe^{i\varphi}} = 2\tan\frac{\varphi}{2}\,\Im\, h(xe^{i\varphi})}, \qquad h = xS_\xi \tag{13A.3}$$

The factorization $1 - t_x(q)w = (q + xe^{i\varphi})(q + xe^{-i\varphi})/(x+q)^2$ and $\cos\varphi = 1 - 2w$ prove the identity in its Taylor convergence disk, with meromorphic continuation where defined. The rungs are its Taylor coefficients in w. Here h is the function whose Pick property is at issue, not an unconditionally known Pick function. The conjugate-node formula retains the reflection data that Section R20 requires. The Euler-source representation (9.5) applies where $\Re s_{xe^{i\varphi}} > 1$; its domain is not a proof of the full Pick sign.

R14. One prescribed scale and the Hausdorff theorem

Fix any $x_0 > 0$ and define

$$h_n(x_0) = (4x_0)^n \frac{W_{n+1}(x_0)}{(2n+1)!} \tag{14.1}$$

Then

$$\boxed{\text{RH} \iff (h_n(x_0))_{n\geq 0} \text{ is a Hausdorff moment sequence on } [0,1]} \tag{14.2}$$

Equivalently,

$$(-1)^r \Delta^r h_n(x_0) \geq 0 \qquad (n, r \geq 0) \tag{14.3}$$

With $\Delta h_n = h_{n+1} - h_n$, Figure 12 supplies the difference weights:

$$(-1)^r \Delta^r h_n(x_0) = \sum_{j=0}^{r} c_{r,j} h_{n+j}(x_0). \tag{14.3a}$$

Thus row r tests difference order r; the seed row $r = 0$ simply returns h_n. The weights alone do not determine the sign of the sum.

The theorem holds at any one scale chosen in advance, but it requires all orders at that scale. It is not a finite stopping rule.

Part V. Li data, Löwner matrices, and the source-energy construction

The boundary values $\mu_{k-1} = W_k(0)/(2k-1)!$ connect the rungs to Li's coefficients through (15.2). Section R15 gives that dictionary and the positive reserve with its explicit arithmetic defect. Sections R16–R17E separate the completed Gamma–prime matrix from its comparison models. Sections R17F–R17H construct the fixed-scale energy and its cutoffs. Section R17I connects an exact-divisor error to the same zeta denominator. The source upper bounds remain unproved.

R15. The central-Pascal boundary dictionary

Write ξ for the completed function of §R9 and let ρ run over its zeros with multiplicity, folded as in §R9 so that ρ and $1-\rho$ share the single point $q_\rho = \rho(1-\rho)$. **Li's coefficients** are

$$\boxed{\lambda_n = \sum_{\rho} \left[1 - \left(1 - \frac{1}{\rho}\right)^n\right] = \frac{1}{(n-1)!} \frac{d^n}{ds^n} \Big[s^{\,n-1} \log \xi(s)\Big]_{s=1}} \tag{15.1a}$$

the symmetrically grouped zero sum agreeing with the derivative definition [5]. The normalization is Li's: λ_n is n times Keiper's coefficient [57–58]. The first is the one this volume uses, because it is a sum over the very orbits that carry the rungs: pairing each zero with its mirror gives $\rho^{-1} + (1-\rho)^{-1} = q_\rho^{-1}$, so at $n = 1$

$$\lambda_1 = \sum_{[\rho]} \frac{m_\rho}{q_\rho} = S_\xi(0) = \mu_0, \tag{15.1b}$$

which is the value already used in §R10A. The rung chain and the Li chain are therefore two readings of one set of folded data, and (15.2) below is the conversion between them.

Li's coefficients satisfy

$$\text{RH} \iff \lambda_n \geq 0 \quad (n \geq 1) \tag{15.1}$$

The two chains are related by a single alternating transform on a doubled row index. It is an identity, proved from (15.1a) and the folded resolvent, and it is insensitive to where the zeros lie: the folded moments μ_{k-1} satisfy

$$\boxed{\mu_{k-1} = \sum_{j=1}^{k} (-1)^{j+1} \binom{2k}{k-j} \lambda_j \qquad W_k(0) = (2k-1)!\mu_{k-1}} \tag{15.2}$$

The first six rows are printed because the indexing matters:

$$\begin{aligned}
\mu_0 &= \lambda_1 \\
\mu_1 &= 4\lambda_1 - \lambda_2 \\
\mu_2 &= 15\lambda_1 - 6\lambda_2 + \lambda_3 \\
\mu_3 &= 56\lambda_1 - 28\lambda_2 + 8\lambda_3 - \lambda_4 \\
\mu_4 &= 210\lambda_1 - 120\lambda_2 + 45\lambda_3 - 10\lambda_4 + \lambda_5 \\
\mu_5 &= 792\lambda_1 - 495\lambda_2 + 220\lambda_3 - 66\lambda_4 + 12\lambda_5 - \lambda_6
\end{aligned} \tag{15.3}$$

These are exact segments of Figure 12, with a doubled row index:

$$\mu_{k-1} = (-1)^{k+1} \sum_{j=1}^{k} c_{2k,k-j} \lambda_j. \tag{15.3a}$$

Read columns $k-1, k-2, \ldots, 0$ of row $2k$, then apply the common sign $(-1)^{k+1}$. For $k = 6$, row 12 contributes $(-792, 495, -220, 66, -12, 1)$; reversing the common sign gives $(792, -495, 220, -66, 12, -1)$ in the μ_5 line. The -220 at column 3 equals the reflected entry at column 9 in (SW.4h), Dossier §173, and becomes $+220\lambda_3$ here. The seven-term resolvent row for W_6 is row 6; its six-term Li boundary row is this segment of row 12.

Thus $W_5(0) \leftrightarrow \mu_4$; the row ending $+12\lambda_5 - \lambda_6$ is $\mu_5 = W_6(0)/11!$, not the W_5 row. This alternating transform is exact but increasingly ill-conditioned, so it is a dictionary rather than a stable numerical inversion method.

One row, three readings. At $k = 6$, the signed grid Figure 12 gives these linked but distinct expressions:

$$\frac{W_6}{11!} = Z_6 - 6xZ_7 + 15x^2Z_8 - 20x^3Z_9 + 15x^4Z_{10} - 6x^5Z_{11} + x^6Z_{12} \quad \text{(SW.4a)}$$
$$W_6 = -332640S^{(5)} - 332640xS^{(6)} - 118800x^2S^{(7)} - \cdots - x^6S^{(11)} \quad \text{(12.2a)}$$
$$\mu_5 = 792\lambda_1 - 495\lambda_2 + 220\lambda_3 - 66\lambda_4 + 12\lambda_5 - \lambda_6 \quad \text{(15.3)}$$

The first two use row 6, $1, -6, 15, -20, 15, -6, 1$; the last uses row **12**, columns 5 down to 0. In the differential row, the factorial weights $11!/(5+j)!$ are $332640, 55440, 7920, 990, 110, 11, 1$. The derivative conversion $Z_{6+j} = (-1)^{5+j}S^{(5+j)}/(5+j)!$ cancels the column alternation and leaves the common negative sign; a global sign alone cannot cancel alternating columns. The first expression is the scalar rung, the second is the source-derivative basis, and the third is their Li boundary dictionary. A coefficient conversion does not introduce an evaluated-source sign.

The same boundary moments occupy the confluent matrix; this is the precise connection between the triangular coefficient image and the matrix image. Locally at the origin,

$$S_\xi(x) = \sum_{r\geq 0}(-1)^r\mu_r x^r, \qquad \frac{h^{(i+j+1)}(0)}{(i+j+1)!} = (-1)^{i+j}\mu_{i+j} \quad (15.4)$$

With indices $i, j = 0, \ldots, N-1$, set $H_N = [\mu_{i+j}]$ and $D_N = \operatorname{diag}((-1)^i)$. The normalized confluent matrix is $C_N(0) = D_N H_N D_N$, so it has the same inertia as H_N. For example,

$$\boxed{H_3 = \begin{pmatrix} \mu_0 & \mu_1 & \mu_2 \\ \mu_1 & \mu_2 & \mu_3 \\ \mu_2 & \mu_3 & \mu_4 \end{pmatrix}, \qquad (H_3)_{ii} = \frac{W_{2i+1}(0)}{(4i+1)!}, \quad i = 0, 1, 2} \quad (15.5)$$

Thus the first five boundary rungs determine every entry of H_3. Positive entries alone do not prove its principal minors positive; for example, the first 2×2 condition is $\mu_0\mu_2 - \mu_1^2 \geq 0$. At positive nodes the owner is the Löwner divided-difference matrix $\mathcal{L}_h$ of (10.3), with diagonal $W_1(x_i)$; its off-diagonal compatibility is the source comparison in §R16. The all-size Hankel condition and the all-node Löwner condition are RH-equivalent, whereas the finite scalar table in §R12 is already proved.

The reflected odd form. Define $\mathcal{P}_0 = 1$, $\mathcal{P}_1 = 3 - y$, and $\mathcal{P}_{m+1} = (2-y)\mathcal{P}_m - \mathcal{P}_{m-1}$, with $\mathcal{P}_m(y) = \sum_j d_{m,j}y^j$ and $d_{m,j} = (-1)^j(2m+1)(m+j)!/((m-j)!(2j+1)!)$. Dossier Section 155A proves

$$\boxed{K_N = \mathsf{C}_N H_N \mathsf{C}_N^{\mathsf{T}}, \qquad K_{r,s} = \lambda_{r+s+1} - \lambda_{|r-s|}, \qquad K_{m,m} = \lambda_{2m+1},} \quad (15.6)$$

where $\mathsf{C}_N = [d_{r,j}]$ and $\lambda_0 = 0$. Its determinant is ± 1, so the two matrices have identical inertia. For example, $\lambda_3 = 9\mu_0 - 6\mu_1 + \mu_2$: an odd Li diagonal already tests original off-diagonal information. For the actual ξ, all odd Li signs, even eventual ones, are RH-equivalent (Theorem 155A.2). They are not the already positive boundary rung values.

Beta filtering $\mu_j \mapsto b_j^k \mu_j$ makes every fixed block with positive diagonal positive at sufficiently large depth. Only one depth fixed before all ranks retains the criterion (Section 104A). Signed recovery uses $2m+1$ observations for λ_{2m+1}; positive outputs alone need not give a positive value. Section 166E controls common-source error at positive scale, not the regularized boundary of Section 155B.

An explicit positive comparison. Section 155C now constructs

$$\boxed{K_N = \mathsf{R}_N - \mathsf{D}_N, \qquad \mathsf{R}_N \succ 0, \qquad c_* = \frac{\pi}{4} + \frac{\log 2}{2} - 1.} \tag{15.7}$$

The reserve is a Catalan-density Gram form weighted by a resolvent trace of the even triangular sine modes. Its linear anchor is c_* rather than λ_1; the full cost $(c_* - \lambda_1)(2\min(r,s)+1)$ stays in the arithmetic defect. The original positive scalar reserve is indefinite as a matrix already at rank two. All-rank domination $\mathsf{D}_N \preceq \mathsf{R}_N$ remains unproved. Section 155D proves that any finite, polynomial, or all-rate subexponential upper relative bound would suffice. Under RH the upper extreme tends to one and the absolute norm grows linearly; a nonreal folded point forces both signs at an exponential rate. Only a constant absolute bound is ruled out. Section 155E's cosine basis makes the compensation δI and the remaining matrix explicit in one curvature sequence.

The recurring diagonal pictures now have a precise crosswalk:

construction	diagonal operation	exact value or owner
factorial extension (§R3)	identify the two input coordinates	the triangular value T_x
Widder array (§R13)	select $(n,k) = (j-1, j)$	$F_{j-1,j} = W_j$
boundary Hankel matrix	set $i = j$	$\mu_{2i} = W_{2i+1}(0)/(4i+1)!$
positive-node Löwner matrix	coalesce the two nodes	$h'(x_i) = W_1(x_i)$

Each picture records its own exact specialization. The derivative and moment identities above supply the links between them; matching diagonal values alone does not settle the off-diagonal source comparison.

R16. What L_Γ and L_P actually mean

Split the safe-axis formula (9.5) as

$$S_\xi(x) = \frac{1}{x} + G(x) - P(x) \tag{16.1}$$

where

$$G(x) = \frac{\psi((1+R)/4) - \log \pi}{2R} \qquad P(x) = \frac{1}{R}\sum_{n\geq 2} \frac{\Lambda_{\mathrm{vM}}(n)}{n^{s_x}} \qquad R = \sqrt{1+4x} \tag{16.2}$$

Define the scalar channel owners

$$h_\Gamma(x) = xG(x) \qquad h_P(x) = xP(x) \qquad h(x) = 1 + h_\Gamma(x) - h_P(x) \tag{16.3}$$

L_Γ and L_P are the ordinary Löwner divided-difference matrices of the Gamma owner and the prime owner. Explicitly,

$$[L_\Gamma]_{ij} = \begin{cases} \dfrac{h_\Gamma(x_i) - h_\Gamma(x_j)}{x_i - x_j}, & i \neq j \\ h'_\Gamma(x_i), & i = j \end{cases} \tag{16.4}$$

and the same formula with h_P gives L_P. Since the constant 1 drops out of divided differences,

$$\boxed{\mathcal{L}_h = L_\Gamma - L_P} \tag{16.5}$$

The open statement is therefore a comparison:

$$\boxed{c^*(L_\Gamma - L_P)c \geq 0 \quad \text{for every finite positive node set and every } c} \tag{16.6}$$

Neither channel is asserted positive separately. In fact L_Γ already has a negative 1×1 value near $x = 0$:

$$\lim_{x \downarrow 0} h'_\Gamma(x) = -\frac{\gamma_E + \log(4\pi)}{2} < 0 \tag{16.7}$$

Completion is therefore cancellation-first. The theorem, if proved, must control the difference rather than dominate a negative prime matrix by an independently positive Gamma matrix.

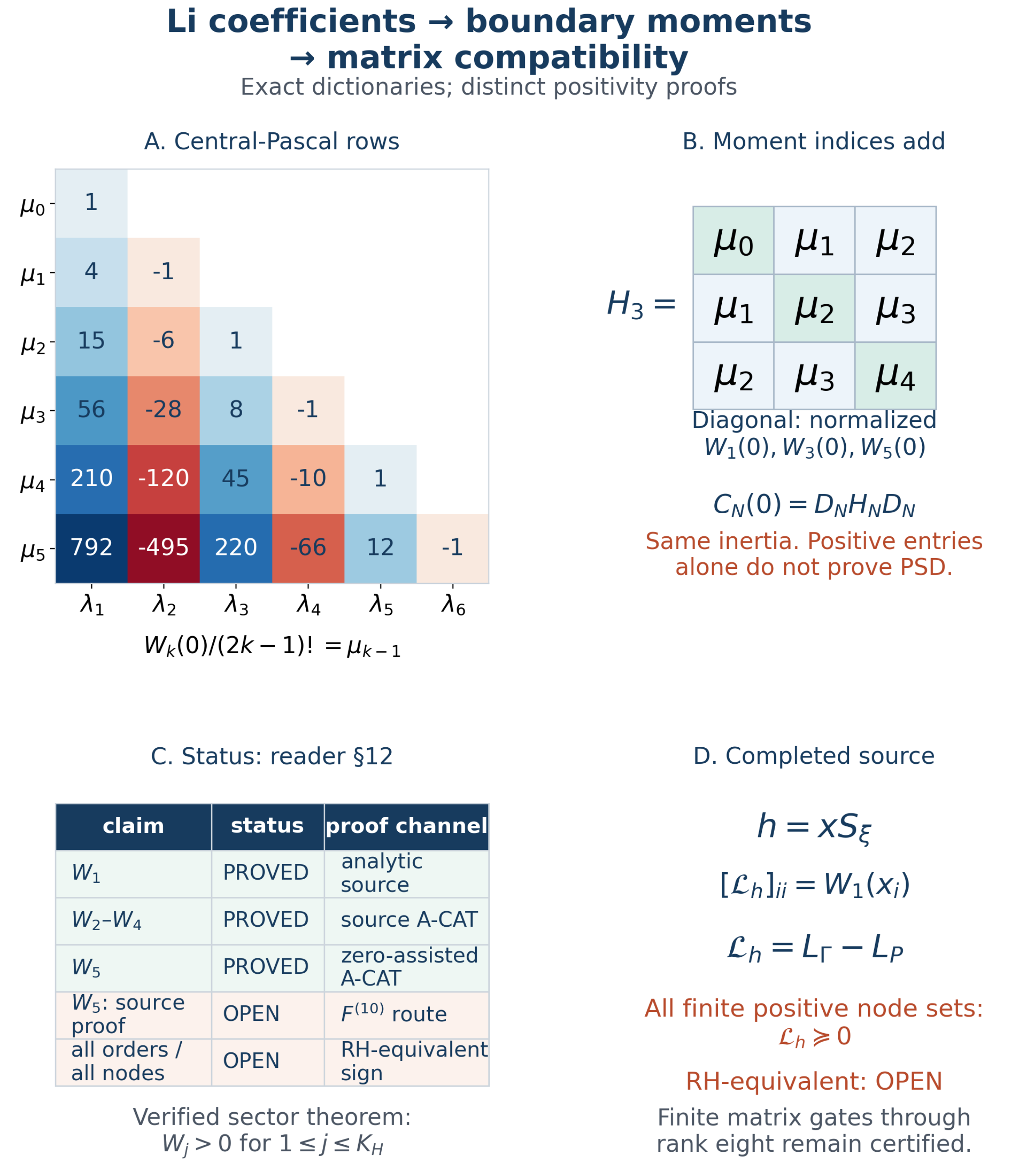

Figure 15: One dictionary, two levels of positivity: the central-Pascal rows identify the boundary moments, and the Hankel and Löwner matrices test their compatibility. The rung status is controlled by §R12; the completed all-node sign remains open.

R17. The Gamma triangular scaffold—and why it is not L_Γ

Antisymmetrize the Gamma logarithmic derivative across the two reflection sheets. The result is the exact Cauchy transform

$$\boxed{\mathfrak{G}_\triangle(q) = \frac{1}{2}\sum_{m=0}^{\infty} \frac{1}{q + 2T_{2m}}} \tag{17.1}$$

Its poles are

$$q = -2T_{2m} = 0, -6, -20, -42, -72, \ldots \tag{17.2}$$

and its normalized owner has an all-order positive Löwner Gram representation. This is a genuine triangular theorem. It is nevertheless a different object from the one-sheet safe-axis h_Γ in (16.3). In the completed function, the elementary and zeta terms cancel every pole of (17.1). Substituting the positive scaffold for L_Γ would therefore discard the very completion coupling that the source problem requires.

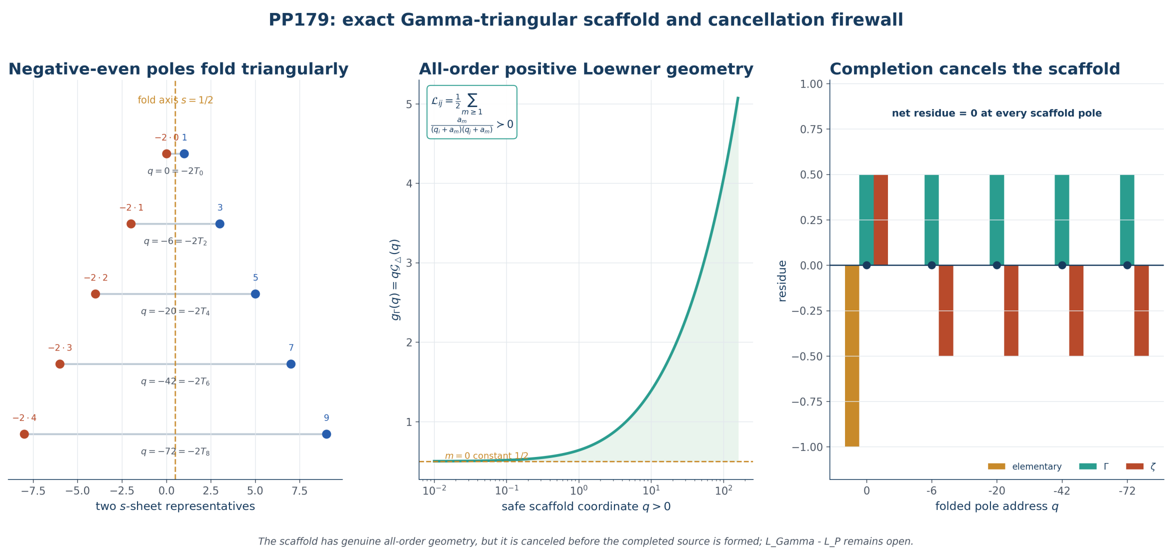

Figure 16: The Gamma triangular scaffold is positive before completion; completion cancels its apparent triangular poles.

The quarter shift makes this normalization explicit: $C(q) = \Gamma(s/2)\Gamma((1-s)/2)$, $q = s(1-s)$, satisfies $-(\log C)' = 2G_\triangle$. Dossier Section 133A derives its even-triangular product and a positive Li comparison model; neither replaces the completed source.

R17A. The completed spectral zeta and its source signature

The sequence $A_n = 1/(2T_{2n})$ of (TR.2) and the folded Riemann sequence define two different spectral zeta functions:

$$\boxed{Z_A(p) = \sum_{n\geq 1} (2T_{2n})^{-p}, \qquad \mathfrak{Z}_\xi(p) = \sum_{[\rho]} m_\rho q_\rho^{-p} = \mathcal{Z}(p; 1/4)} \tag{VZ.1}$$

Both series converge absolutely for $\Re p > 1/2$. The first is built from positive triangular numbers. The second uses the principal powers of possibly complex, conjugate-paired q_ρ; positivity of those locations is exactly the RH question. Their common critical exponent does not identify their spectra.

For $1/2 < \Re p < 1$, the scalar Mellin resolvent identity gives

$$\boxed{\mathfrak{Z}_\xi(p) = \frac{\sin \pi p}{\pi} \int_0^\infty x^{-p} S_\xi(x)\, dx = \frac{\sin \pi p}{\pi} \int_1^\infty [s(s-1)]^{-p} \frac{\xi'(s)}{\xi(s)}\, ds} \tag{VZ.2}$$

In the second integral $x = s(s-1) = 2T_{s-1}$ and $dx = (2s-1)ds$: the source Jacobian cancels exactly. Completion must be combined before integration near $s = 1$; its separate elementary and prime poles cancel there.

Subtracting the large-x terms of (OP.1) continues this expression across the critical exponent. With $p = 1/2 + \varepsilon$,

$$\boxed{\mathfrak{Z}_\xi(1/2 + \varepsilon) = \frac{1}{8\pi\varepsilon^2} - \frac{\log(2\pi)}{4\pi\varepsilon} + O(1), \qquad \mathfrak{Z}_\xi(0) = \frac{7}{8}} \tag{VZ.3}$$

These are classical formulas of Voros [56, equations (40)–(41)], recovered here from the completed source. The value at zero is an analytic continuation value, not the ordinary trace of an infinite identity operator. The two Laurent coefficients test more than the exponent 1/2 alone.

Voros normalizes his completed function as $\Xi_V = 2\xi$, so $\Xi_V(0) = \Xi_V(1) = 1$. This normalization leaves logarithmic derivatives unchanged but matters when comparing determinants.

R17B. Regularized triangular values: the fraction sequence

The continuation of (VZ.1) has a particularly simple triangular relation at nonpositive integers. Let the signed Euler numbers be defined by

$$\operatorname{sech} t = \sum_{j\geq 0} E_{2j} \frac{t^{2j}}{(2j)!} \qquad E_0, E_2, E_4, E_6, E_8 = 1, -1, 5, -61, 1385 \tag{TV.1}$$

Triangular trace identity. For every integer $m \geq 0$, the analytic continuations satisfy

$$\boxed{\mathfrak{Z}_\xi(-m) = \frac{1}{2}\delta_{m0} + \frac{(-1)^{m+1}}{2} Z_A(-m)} \tag{TV.2}$$

The first values make both the sign pattern and the factor of two visible:

m	completed value $\mathfrak{Z}_\xi(-m)$	triangular value $Z_A(-m)$
0	$7/8$	$-3/4$
1	$-1/16$	$-1/8$
2	$-1/16$	$1/8$
3	$-5/32$	$-5/16$
4	$-13/16$	$13/8$
5	$-227/32$	$-227/16$

These are finite regularized values of divergent power sums. The negative signs do not contradict positivity of an ordinary positive spectrum: analytic continuation is not a positive summation operation.

Proof. The centered triangular identity gives

$$2T_{2n} = 4\left[\left(n + \frac{1}{4}\right)^2 - \frac{1}{16}\right] \tag{TV.3}$$

Expanding in the constant shift and continuing by the Hurwitz zeta function yields, at $p = -m$,

$$Z_A(-m) = 4^m \sum_{j=0}^{m} \binom{m}{j} \left(-\frac{1}{16}\right)^j \zeta\left(-2(m-j), \frac{5}{4}\right) \tag{TV.4}$$

Here the Hurwitz series is being continued as a family before the integer is substituted. The Bernoulli-polynomial and Hurwitz identities [2, §25.11]

$$\begin{aligned} \zeta(-2r, a) &= -\frac{B_{2r+1}(a)}{2r+1} \\ B_{2r+1}(1/4) &= -\frac{(2r+1)E_{2r}}{4^{2r+1}} \\ \zeta(-2r, 5/4) &= \frac{E_{2r} - 4}{4^{2r+1}} \end{aligned} \tag{TV.5}$$

reduce (TV.4) to a finite rational sum. Independently, the completed Stirling expansion in (VZ.2), or Voros's trace formula [56, §6.1 and Table 1], gives

$$\boxed{\mathfrak{Z}_\xi(-m) = \delta_{m0} - \frac{1}{2\,4^{m+1}} \sum_{j=0}^{m} (-1)^j \binom{m}{j} E_{2j}} \tag{TV.6}$$

Substitution proves (TV.2), including the separate constant term at $m = 0$. Thus the result is an exact cross-identification of classical continuation formulas with our triangular scaffold, with no claim of literature priority.

Replacing p by -1 before continuing would suggest $4\zeta(-2)+2\zeta(-1) = -1/6$. The continuation of $Z_A(p)$ instead gives $Z_A(-1) = -1/8$. In an uncentered binomial continuation a coefficient vanishing at $p = -1$ multiplies a zeta pole and leaves $+1/24$. Equation (TV.4) keeps this contribution correctly. Formal linearity between different regularization families would lose it.

The value $\zeta(-1) = -1/12$ of Dossier §172 reappears in that tempting calculation; it does not by itself define the continuation of a quadratic triangular family.

The identity at integers does not assert $\mathfrak{Z}_\xi(p) = \frac{1}{2}(-1)^{p+1}Z_A(p)$ as a function of p. In fact their poles at $p = 1/2$ have different orders. It also does not assert that a completed zero equals a triangular scaffold pole.

R17C. The odd-coordinate pole ladder and the determinant

The shifted family makes another coefficient sequence visible. At $p = 1/2 - m$, the coefficient of the double pole of $\mathcal{Z}(p; v)$ is

$$C_m(v) = \frac{1}{8\pi}\frac{\Gamma(m+1/2)}{m!\Gamma(1/2)}v^m = \frac{1}{8\pi}\binom{2m}{m}\left(\frac{v}{4}\right)^m \tag{PC.1}$$

This follows by shifting the leading double pole of the centered family [56, equations (91)–(94)]. At $v = 1/4$, write $C_m(1/4) = c_m/(8\pi)$. Then

$$\boxed{c_m = \frac{\binom{2m}{m}}{16^m}, \qquad c_0, c_1, c_2, c_3, c_4 = 1, \frac{1}{8}, \frac{3}{128}, \frac{5}{1024}, \frac{35}{32768}} \tag{PC.2}$$

Figure 12 makes this pole chain explicit: $c_m = (-1)^m c_{2m,m}/16^m$, and $C_m(v) = (-1)^m c_{2m,m}(v/4)^m/(8\pi)$. Here the one-index c_m denotes the scaled pole coefficient, while the two-index $c_{k,j}$ denotes a signed grid entry. In particular, the value $c_0 = 1$ uses the newly printed grid seed $c_{0,0} = +1$.

The recurring odd index has a direct coefficient role:

$$\boxed{\frac{c_{m+1}}{c_m} = \frac{2m+1}{8(m+1)} = \frac{j_m}{8(m+1)}} \tag{PC.3}$$

Compare the two recurrences horizontally, with $m \geq 1$ in the Widder row:

$$\underbrace{W_{m+1} = -j_m W'_m - xW''_m}_{\text{Widder differential ladder}} \qquad \underbrace{c_{m+1} = \frac{j_m}{8(m+1)}c_m}_{\text{central-binomial pole ladder}} \tag{PC.4}$$

They expose the same odd integer $2m+1$, through different operations. One recurrence does not prove positivity of the other. A related determinant count is exact rather than heuristic: a Vandermonde on n nodes scales with degree T_{n-1}, and for confluent multiplicities m_i the surviving degree is $T_{n-1} - \sum_i T_{m_i-1} = \sum_{i<j} m_i m_j$. Raw derivative columns also carry $\prod_i \prod_{j=0}^{m_i-1} j!$; Taylor-normalized jets remove that factor. This is a bookkeeping check for confluent determinants, not a source sign. At the first lower pole, for example,

$$\mathfrak{Z}_\xi(-1/2+\varepsilon) = \frac{1}{64\pi\varepsilon^2} - \frac{3\log(2\pi)+4}{96\pi\varepsilon} + O(1) \tag{PC.5}$$

There is also a logarithmic companion to (TV.2):

$$\boxed{Z_A'(0) = -\frac{1}{2}\log(2\pi), \qquad \mathfrak{Z}_\xi'(0) = \frac{1}{4}\log(8\pi) = \frac{1}{2}\log 2 - \frac{1}{2}Z_A'(0)} \tag{PC.6}$$

For completeness, differentiating the centered Hurwitz expansion of Z_A at zero gives

$$\begin{aligned} Z_A'(0) &= \frac{3}{4}\log 4 + 2\zeta'(0,5/4) + \sum_{r\geq 1} \frac{\zeta(2r,5/4)}{r16^r} \\ &= \frac{3}{4}\log 4 - \log(2\pi) + \log\Gamma(3/2) + \log\Gamma(1) \\ &= -\frac{1}{2}\log(2\pi) \end{aligned} \tag{PC.7}$$

The Gamma product identity sums the absolutely convergent series in the first line, using $\zeta'(0,a) = \log\Gamma(a) - \frac{1}{2}\log(2\pi)$ [2, equation 25.11.18]. Voros gives the completed value in (PC.6) [56, equation (41)]. Both statements concern specified regularized determinants, not ordinary products of infinitely many positive numbers.

More strongly, the full shifted derivative is

$$\boxed{\partial_p \mathcal{Z}(p; x+1/4)|_{p=0} = \frac{1}{4}\log(8\pi) - \log\frac{\xi(s_x)}{\xi(1)}} \tag{PC.8}$$

Indeed, differentiating the left side in x gives $-S_\xi(x)$; its value at $x=0$ is (PC.6). Thus a proposed positive model must match the full x-dependent function on the safe axis, or its logarithmic derivative together with the normalization at $x=0$. The determinant $\xi(s_x)/\xi(1)$ is entire in x; its logarithm is not entire. Matching a finite list of regularized constants does not establish this identity.

R17D. What the triangular–Volterra benchmark establishes

The scaffold can be enlarged to have the correct critical pole order. Let A be the diagonal with entries $A_n = 1/(2T_{2n})$ from (TR.2), and let B_a have eigenvalues $[\pi^2(n+a)^2]^{-1}$, $n \geq 0$, $a > 0$. Then

$$Z_{A\otimes B_a}(p) = Z_A(p)\pi^{-2p}\zeta(2p,a) \tag{BM.1}$$

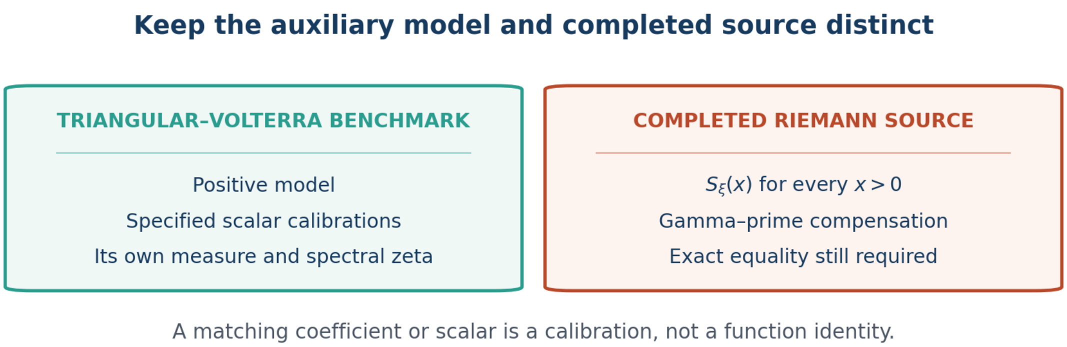

Figure 17: Two spectral objects: the triangular–Volterra benchmark can match specified scalar data, whereas an exact realization of S_ξ must match the whole function and its completed source. Calibration does not supply that equality.

Define the convergent constant

$$\kappa_\triangle = \frac{\gamma_E - \log 2}{2} + \sum_{n\geq 1}\left(\frac{1}{\sqrt{2T_{2n}}} - \frac{1}{2n}\right) \tag{BM.2}$$

The double-pole coefficient of (BM.1) agrees with (VZ.3). Its simple-pole coefficient agrees exactly when

$$\boxed{\psi(a_*) = \log 2 + 2\kappa_\triangle, \qquad \frac{7}{4} < a_* < 2} \tag{BM.3}$$

Strict monotonicity of ψ gives uniqueness. The bracket is supported by an exact rational interval certificate; $a_* \approx 1.75164355$ is only a numerical orientation. It is not the exact quarter-step $7/4$.

At zero, however,

$$Z_{A\otimes B_{a_*}}(0) = \frac{3}{4}(a_* - 1/2), \qquad Z_{A\otimes B_{a_*}}(0) - \frac{7}{8} = \delta := \frac{3a_* - 5}{4} \in (1/16, 1/4) \tag{BM.4}$$

An exact infinite-row adjustment matches this coefficient: replace the first row $A_1B_{a_*}$ by A_1B_b, where $b = a_* + \delta = (7a_* - 5)/4$. Its zeta correction is

$$A_1^p\pi^{-2p}\left[\zeta(2p,b) - \zeta(2p,a_*)\right] \tag{BM.5}$$

The correction is regular at $p = 1/2$ and equals $-\delta$ at $p = 0$. The row perturbation has entries $O(n^{-3})$ and belongs to $\mathcal{S}_p$ for $p > 1/3$; it is infinite rank. Replacing a finite list of positive entries by another list of the same length leaves all three regularized data unchanged. By choosing a sufficiently long list, its sum can also be adjusted to λ_1 while the untouched tail stays fixed.

Consequently positive models can match the two critical Laurent coefficients, the value 7/8, and the trace λ_1. The benchmark is exact; it does not select the source: redistributing two positive replacement entries at fixed sum changes $\operatorname{Tr} D^2$ and therefore changes the resolvent. The derivative (PC.6), lower poles such as (PC.5), and the exact fractions in (TV.2) are additional tests. The decisive target remains (PC.8) for every x, together with an independent proof of positivity.

The raw triangular–Volterra tensor is still easier to exclude. For $(Vf)(u) = \int_0^u f(t)dt$ on $L^2[0,1]$, V^*V has kernel $1 - \max(u,v)$ and trace $1/2$. Thus

$$\operatorname{Tr}(A \otimes V^*V) = \frac{1 - \log 2}{2} \neq \lambda_1 \tag{BM.6}$$

Its positivity is exact; its scalar source is different. No inference here requires the particular tensor architecture to be unique.

R17E. What the continuation retains about primes

The regularized fractions and polar coefficients are unusually explicit because $\log \zeta(s)$ is exponentially small as real $s \to +\infty$. It contributes no term to the algebraic Stirling expansion used in (TV.6). Therefore even an entire ladder of those asymptotic coefficients does not determine the prime-dependent remainder of the source.

Voros supplies a complementary integral that retains that remainder. Let $\mathscr{Z}_c(p) = \mathscr{Z}(p;0)$ and distinguish the linear half-step zeta function

$$\mathcal{S}_{1/2}(z) = \sum_{n \geq 1} (2n + 1/2)^{-z} = 2^{-z}\zeta(z, 5/4) \tag{VP.1}$$

For $0 < \Re p < 1/2$, his regular-integrand continuation is

$$\begin{aligned} \mathscr{Z}_c(p) = &- \frac{\mathcal{S}_{1/2}(2p)}{2\cos \pi p} \\ &+ \frac{\sin \pi p}{\pi} \int_0^\infty t^{-2p} \left[\frac{\zeta'}{\zeta}(1/2 + t) + \frac{1}{t - 1/2} \right] dt \end{aligned} \tag{VP.2}$$

The apparent singularity of the bracket at $t = 1/2$ is removable: the zeta logarithmic derivative has residue -1 at its pole. Keep the two terms inside the bracket combined. This is an unconditional continuation formula [56, equation (74)], with a different centered parameter from $\mathfrak{Z}_\xi(p) = \mathscr{Z}(p; 1/4)$.

Equation (VP.2) is useful for deriving a completed source remainder before seeking a sign. It does not display a positive kernel. The prime series for $\zeta'/\zeta(1/2 + t)$ converges only when $t > 1/2$, so termwise use of that series throughout the integral is invalid. Voros's separate raw prime-cutoff resummation in equation (79) explicitly invokes RH; it cannot serve as an unconditional forcing step here.

The same center gives another odd-index sequence [56, equation (81)]:

$$\boxed{(\log|\zeta|)^{(2m+1)}(1/2) = \frac{(2m)!}{2}(2^{2m+1}-1)\zeta(2m+1) + \frac{\pi^{2m+1}}{4}|E_{2m}|, \quad m \geq 1} \tag{VP.3}$$

For example, the third and fifth derivatives are $7\zeta(3) + \pi^3/4$ and $372\zeta(5) + 5\pi^5/4$. These are derivatives in the real s direction at $1/2$. They express the vanishing odd derivatives of $\log\xi$ at its reflection center. They do not fix the even derivatives or the all-node Löwner sign.

The first Stieltjes cumulant is $\gamma_1^c = \gamma_1 + \gamma_E^2/2 \approx 0.093773116$ [56–57]. The normalization is Li's. These conventions govern the sequence tables.

R17F. The completed Bernstein row

Fix one prescribed scale $a > 0$ and define the completed derivative row

$$\boxed{B_{N,j}(a) = \frac{a^j}{j!(N-j)!}F_{j,N-j}(a), \qquad 0 \leq j \leq N.} \tag{BR.1}$$

With $\theta = a/(a+q)$, each folded zero contributes a Bernstein row,

$$B_{N,j}(a) = \sum_{[\rho]} \frac{m_\rho}{a+q_\rho}\binom{N}{j}\theta_\rho^j(1-\theta_\rho)^{N-j}. \tag{BR.2}$$

The scalar Widder carrier is the fold $t_a(q) = 4\theta(1-\theta)$; the full row retains θ and $1-\theta$ separately. Its signed mass is exactly conserved,

$$\sum_{j=0}^{N} B_{N,j}(a) = S_\xi(a), \qquad \mathcal{V}_N(a) = \sum_j |B_{N,j}(a)| \geq S_\xi(a). \tag{BR.3}$$

The existing scalar ladder sits on the central entries: $B_{2k-1,k-1} = a^{k-1}W_k/[(k-1)!k!]$. Thus the source-certified $W_1, \ldots, W_6$ are visible inside the row, but no finite set of central entries controls its total variation.

Section 164 proves the ordinary root-growth limit. Consequently RH is equivalent, at one fixed $a > 0$, to the still-open source estimate

$$\boxed{\forall\varepsilon > 0\ \exists C_{a,\varepsilon} < \infty\ \forall N: \quad \mathcal{V}_N(a) \leq C_{a,\varepsilon}(1+\varepsilon)^N.} \tag{BR.4}$$

The verified-height theorem makes the row positive over an enormous finite prefix; (BR.4) is an all-degree statement and is not supplied by that prefix.

R17G. The same row as a positive energy

The Bernstein coefficients have an exact Laguerre realization

$$\mathcal{Q}_N(t;a) = \sum_{j=0}^{N} B_{N,j}(a) L_j^{(0)}(t), \qquad \mathscr{E}_N(a) = \int_0^\infty e^{-t} |\mathcal{Q}_N(t;a)|^2 dt = \sum_{j=0}^{N} B_{N,j}(a)^2. \quad \text{(BE.2)}$$

Hence $\sqrt{\mathscr{E}_N} \le \mathcal{V}_N \le \sqrt{N+1}\sqrt{\mathscr{E}_N}$. Theorem 164.2 gives $\mathscr{E}_N(a) \sim \mathcal{K}(a)\mathcal{R}(a)^{2N}/\sqrt{N}$, where $\mathcal{R}(a) = \sup_q (a + |q|)/|a+q|$. Under RH the energy decays like $N^{-1/2}$; any off-line folded pair forces exponential growth. The source obligation is therefore equivalently

$$\boxed{\forall \varepsilon > 0\ \exists C_{a,\varepsilon} < \infty\ \forall N : \quad \mathscr{E}_N(a) \le C_{a,\varepsilon}(1+\varepsilon)^{2N}.} \quad \text{(BE.3)}$$

The Gamma channel has a finite signed Stieltjes variation, so §166B isolates the same open condition in the full prime source. At the concrete scale $a = 2$ it becomes

$$\boxed{\forall N \ge 0 : \quad \mathscr{E}_N[P](2) \le \left(1 + \log 2 + \frac{\pi}{6}\right)^2.} \quad \text{(BE.5)}$$

Theorem 166B.1 proves that this all-degree cap is RH-equivalent; it does not prove the cap. The full v4.5 derivations of the Bernstein involution, Pascal Gram matrix and energy asymptotics remain in the source provenance; this Reader keeps the objects and the exact unsupported line.

R17H. What the prime-cutoff attack proves

The cap in (BE.5) is a statement about the full prime source at every degree. Dossier §166C examines the natural attempt to pass to it from finite Euler sums P_X. The sums include prime powers $n \le X$. For each fixed degree their derivatives converge to those of P. That convergence is not uniform over all degrees.

The sharp distinction appears in the last Bernstein coefficient:

$$\boxed{B_{N,N}[P](a) \to \frac{1}{a}, \qquad B_{N,N}[P_X](a) \to 0 \quad (X \text{ fixed})} \quad \text{(CUT.1)}$$

Both statements are unconditional. The full endpoint comes from the pole $1/x$ after completion; the finite sum has only its signed continuous cut measure. Their energy-norm distance therefore has lower limit at least $1/a$. A fixed cutoff cannot approximate all degrees, even if RH is true.

The positive contributions to this endpoint define an exact probability distribution on prime powers. Theorem 166C.3 proves that their logarithms have center $(N+1)/a$, variance $(N+1)(2/a + 1/a^2)$, and a normal limit. At $a = 2$, half the endpoint mass is asymptotically captured near $X = \exp((N+1)/2)$; fixed normal quantiles occur at

$$\boxed{\log X_N = \frac{N+1}{2} + v\sqrt{\frac{5(N+1)}{4}}, \qquad B_{N,N}[P_{X_N}](2) \to \frac{\Phi(v)}{2}} \tag{CUT.2}$$

Here Φ is the standard normal distribution function. This theorem comes from the moving pole at $x = \omega(1+\omega) = 2T_\omega$ of the shifted source $-\zeta'/\zeta(s_x - \omega)/R_x$. It needs neither RH nor the prime number theorem. The triangular coordinate is part of the residue calculation.

There is a second, stronger restriction on the cutoff strategy:

$$\boxed{\sup_{X\geq 2,\ N\geq 0} \frac{\mathscr{E}_N[P_X](2)}{(1.01)^{2N}} = \infty} \tag{CUT.3}$$

Theorem 166C.4 proves this by the exact row generating function and the pole of zeta at one. A uniform bound over all raw cutoffs would force bounded Euler partial sums at $s = 3/4 + i/4$, contradicting that pole by Abel summation. The obstruction is independent of zero locations.

Theorem 166D.1 now proves the full-row error bound for the prescribed schedule $X_N = 20^{N+1}$ at $a = 2$, with an explicit remainder tending to zero. Endpoint recovery alone is insufficient, but this entire-row approximation is proved. What remains open is the RH-equivalent bound $\sup_N \|\mathcal{Q}_N[P_{20^{N+1}}](\cdot;2)\|_{L^2(e^{-t}dt)} < \infty$ of (166D.2). Section 166E transfers the same error to fixed-degree filtered outputs at a positive scale, not to unregularized boundary data.

Growing approximations at one fixed scale. Section 166D also proves whole-row convergence for $X_N = 13^{N+1}$. Direct Cauchy estimates in Section 166E control every recovered degree $2m \leq N$ at 5^{N+1}. These are different bounds. For the full degree-below-d mixed jet block, Section 166F uses the sharper constant $\Sigma_d = 9(9^d - 9^{-d})/128 + 3d/8$ and cutoff $X_d = 5^{2d-1}$. Its reserve-normalized common error tends to zero. The target there is a separately defined completed matrix at $a = 2$, not a boundary Li matrix. A polynomial upper bound on its largest normalized cutoff-defect eigenvalue would imply RH; that bound remains unproved. Neither convergence nor a finite computed prefix supplies it.

A separate route to the actual boundary. Section 166G forms the finite Taylor polynomial

$$\widehat{S}_d(z) = \sum_{\ell=0}^{15d-1} \frac{S^{(\ell)}_{8^{15d}}(2)}{\ell!}(z-2)^\ell. \tag{CUT.4}$$

It evaluates this polynomial at zero, never the raw cutoff. Both the completed Taylor remainder and the finite prime-tail error are controlled; the full boundary rank-d error, normalized by the same reserve, is $O(d\Theta^d)$ with $\Theta = 36(18/23)^{15} < 1$. The boundary defect's polynomial upper bound remains unproved. Independent coefficient rounding has an additional error budget.

R17I. Exact divisors and one denominator residual

Accurate boundary reconstruction leaves an arithmetic question: why should the actual signed source remain bounded? Sections 155F–155G test what information a proof must use. The regularized direct curvature formula keeps a polynomial counterterm and a finite endpoint. A PNT-size envelope alone, even with nonnegative integer weights, admits a fixed countermodel with superexponential positive even curvature. A second model retains actual prime-power support, any fixed exact prime prefix, positive Euler coefficients and the same envelope, yet has exponentially growing curvature on every fixed progression. Neither model retains the actual completed source or all its divisor identities.

The actual denominator is $\mathcal{B}(z) = z\zeta(1/(1-z))$, with its removable value $\mathcal{B}(0) = 1$. Its Taylor coefficients b_n^{den} obey the signed convolution (155G.3); they are not the Beta weights of Section 104A. The directed enclosure $b_{17}^{\mathrm{den}} < 0$ refutes coefficient positivity, while their square sum $\log(2\pi) - \gamma_E$ does not supply a lower bound for the denominator. Section 155I connects this denominator to a different use of the exact arithmetic, rather than inferring positivity from its coefficients.

Write $\mu(d)$ for the Möbius function. The actual laws $\Lambda * 1 = \log$ and $\mu * 1 = \delta_1$ imply, for $N = \lfloor X \rfloor$,

$$\sum_{k=1}^{N} M\left(\log \frac{X}{k}\right) = \log(N!) - XH_N + N, \qquad H_N = \sum_{k=1}^{N} \frac{1}{k}. \tag{DIV.1}$$

Now take finitely supported real coefficients c_d with $\sum c_d/d = 0$ and set $D_c(s) = \sum c_d d^{-s}$, $h_c(x) = 1 - \sum c_d \lfloor x/d \rfloor$. Balance cancels the linear term in the floors. The resulting squared error is

$$\boxed{\mathscr{N}(c) = \int_1^\infty h_c(x)^2 \frac{dx}{x^2} = \sum_{n \geq 1} \frac{h_c(n)^2}{n(n+1)}.} \tag{DIV.2}$$

Here $1/[n(n+1)] = 1/(2T_n)$ is the integral over one unit interval. The square follows the signed arithmetic sum; it does not replace each term by an independent absolute budget. If $c_d = \mu(d)$ for $d \leq K$, then $h_c = 0$ on $[1, K+1)$. Every zero $\rho = \sigma + i\gamma$ with $\sigma > 1/2$ would force

$$\boxed{\mathscr{N}(c) \geq \frac{2\sigma - 1}{|\rho|^2} (K+1)^{2\sigma - 1}.} \tag{DIV.3}$$

Section 155H proves this by Mellin evaluation at the zero and Cauchy–Schwarz on the remaining tail. Section 155J now fixes one explicit linear-taper family $V_N(s) = \sum_{d \leq N} \mu(d)(1 - d/N)d^{-s}$ and proves

$$\boxed{\lim_{N \to \infty} \frac{\log(1 + U_N)}{\log N} = 2\Theta_\zeta - 1}, \qquad \Theta_\zeta = \sup_\rho \Re\rho. \tag{DIV.3a}$$

Its balanced dyadic plateau has the same exponent. Hence RH is equivalent, for this specified family, to $U_N = O_\epsilon(N^\epsilon)$ for every $\epsilon > 0$; one fixed unbounded index set is enough. The proof uses the classical zero-free-half-plane estimate quoted in [25] and the exact-prefix lower bound above. It does not prove boundedness or convergence under RH.

The same section also records a distinct scalar target $B_{\log}(x) = 1 - \sum_{d\le x}(\mu(d)/d)\log(x/d)$. RH is equivalent to $B_{\log}(n) \le C_\epsilon n^{-1/2+\epsilon}$ on the eventual integer tail. Section 155J now proves a logarithmic-chord interpolation theorem: it is enough to verify the corresponding bound at all sufficiently large fourth powers k^4, or at the squared triangular samples T_k^2. This is structured sampling, not permission to use an arbitrary sparse set. The canonical prefix family is also shown to have exact power exponent $2\Theta_\zeta - 1$, while the fixed taper has the unconditional bound $U_N \ll N\exp(-c\sqrt{\log N})$ for some $c > 0$. None is yet subpower unconditionally.

The two approaches meet in one exact identity. Put $\mathcal{C}_c(z) = D_c(1/(1-z))/z$, filling its removable value. Then

$$\boxed{\begin{aligned} 1 - \mathcal{B}(z)\mathcal{C}_c(z) &= \sum_{n\ge 0} r_n(c) z^n, \\ r_n(c) &= \int_0^\infty e^{-u} h_c(e^u) L_n^{(0)}(u)\,du, \\ \mathscr{N}(c) &= \sum_{n\ge 0} |r_n(c)|^2. \end{aligned}} \tag{DIV.4}$$

This is the normalized Hardy coefficient norm, proved by the complete Laguerre expansion in Section 155I. It is not the finite row energy $\mathscr{E}_N$ or the curvature sequence I_n. Section 155J further writes the same norm as a weighted sine integral and isolates the signed mixed Möbius sum $\mathcal{X}_N$, with $U_N - \mathcal{X}_N = \kappa \log N + \kappa_0 + o(1)$. Thus the closing arithmetic task may be stated as a one-sided subpower bound for $\mathcal{X}_N$, or as the scalar $B_{\log}$ decay above. Neither bound is established. A finite coefficient prefix still gives only a lower bound on the full norm.

Part VI. Translation defects and reflection contours

The defects record what an off-line zero would leave behind. Sections R18–R18B compare the translation, Beta and varying-endpoint forms; R19 gives stationary-symbol blindness; R20 gives the reflection contour and the missing conjugation. Sections R21–R21B connect strict one-node defects, heat and signed-row growth. The completed detectors vanish under RH, but none has been forced to vanish from the source.

R18. Positive defects with a negative scalar anchor

On the resolvent test span, the archimedean channel admits the exact translation-defect form

$$\boxed{Q_\Gamma(F) = a_\Gamma \|F\|_2^2 + \frac{1}{2}\int_0^\infty \|(I-\tau_v)F\|_2^2 \, \frac{e^{v/2}}{2\sinh v}\, dv} \tag{18.1}$$

with

$$a_\Gamma = \frac{1}{2}\left(\psi\left(\frac{1}{4}\right) - \log \pi\right) = -\frac{\zeta'}{\zeta}\left(\frac{1}{2}\right) < 0 \tag{18.2}$$

The identity is exact; the right side is not manifestly nonnegative because the scalar anchor is negative. The equality in (18.2) uses analytic continuation at the functional-equation center. It is not the divergent prime mass $\sum \Lambda(n)/\sqrt{n}$.

The compact Beta measure $2(1-u)\,du$ of (4.5) and the Gamma defect density in (18.1) are different measures with different supports, total masses, and moment growth. Their shared triangular language does not make them interchangeable.

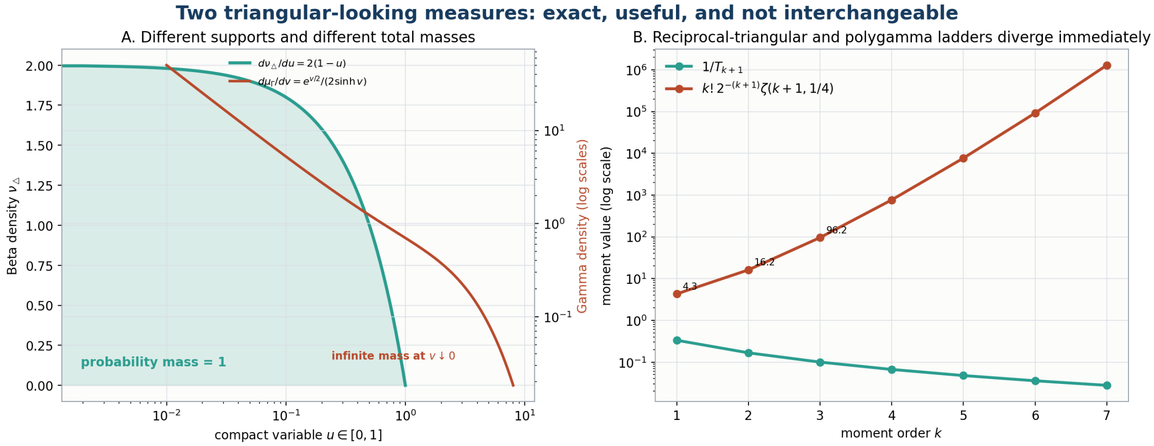

Figure 18: Compact Beta moments and the infinite Gamma translation-defect measure must remain separate.

R18A. Beta and Volterra forms side by side

The compact triangular moment measure and the Volterra operator are both positive, but they produce different quadratic forms. For $F \in L^2[0,1]$, put

$$\mathcal{B}[F] = 2\int_0^1 (1-u)|F(u)|^2 du \qquad \mathcal{Q}[F] = 2\|VF\|_2^2 \tag{VG.1}$$

With $K(u,v) = 1 - \max(u,v)$, their exact difference is

$$\boxed{\begin{aligned}\mathcal{B}[F] - \mathcal{Q}[F] = &\int_0^1 (1-u)^2 |F(u)|^2 du \\ &+ \int_0^1\int_0^1 K(u,v)|F(u)-F(v)|^2 du\, dv > 0\end{aligned}} \tag{VG.2}$$

for nonzero F. To check the coefficients, use $\int_0^1 K(u,v)dv = (1-u^2)/2$ and expand the square. The strict difference supplies an exact comparison, not an equality with the completed Gamma–prime form.

For logarithmic characters $e_L(u) = e^{2\pi i L u}$, use the inner product conjugate-linear in its first slot, and set $E(t) = \int_0^1 e^{2\pi i t u} du$. The Volterra Gram entries are

$$\boxed{Q(L,M) := 2\langle Ve_L, Ve_M\rangle = \frac{E(M-L) - E(-L) - E(M) + 1}{2\pi^2 LM}} \tag{VG.3}$$

The values at $L = 0$ or $M = 0$ are defined by continuous extension. In particular,

$$Q(L,L) = \frac{1 - \sin(2\pi L)/(2\pi L)}{\pi^2 L^2} \qquad Q(0,0) = \frac{2}{3} \tag{VG.4}$$

The negative phases in (VG.3) are the conjugates of the positive phases; $Q(M,L) = \overline{Q(L,M)}$. Positivity follows from its Gram definition. Nevertheless, normalized adjacent entries satisfy

$$\frac{Q(\log n, \log(n+1))}{\sqrt{Q(\log n, \log n) Q(\log(n+1), \log(n+1))}} \longrightarrow 1 \tag{VG.5}$$

The fixed interval therefore leaves neighboring logarithmic frequencies strongly coherent. Positivity alone does not give the cancellation required by the completed source.

R18B. A varying-endpoint Gram candidate

One way to change that coherence is to let the interval length vary with the integer label. Define

$$\phi_n(u) = n^{-1/2}\mathbf{1}_{[0,n]}(u) e^{2\pi i (\log n) u} \qquad J_L(a) = \int_0^L e^{2\pi i a u} du \tag{EG.1}$$

Its exact Gram matrix is

$$K_{mn} = \langle \phi_m, \phi_n \rangle = \frac{J_{\min(m,n)}(\log(n/m))}{\sqrt{mn}} \qquad K_{nn} = 1, \quad K_{nm} = \overline{K_{mn}} \tag{EG.2}$$

For every fixed positive integer k,

$$\boxed{K_{n+k,n} = -\frac{k}{2n} + O_k(n^{-2})} \tag{EG.3}$$

Indeed, $n \log(1 + k/n) = k - k^2/(2n) + O_k(n^{-2})$; the leading phase is an integer multiple of 2π. This gives a contrasting pair of adjacent limits: fixed-interval Volterra coherence tends to 1, whereas the varying-endpoint Gram entry tends to 0.

The estimate is for fixed k and is not a uniform bound on growing matrices. For any fixed signed nonzero integer k, its leading term is $-|k|/(2n)$; (EG.3) uses $k > 0$. Also, the 2π frequency scale and endpoint length must be transported together: removing 2π while leaving the endpoints unchanged destroys the integer-phase cancellation.

Candidate boundary. The Gram positivity in (EG.2) is proved. Section 161 now excludes its fixed ordinary tensor-norm translation lift as the completed owner, for finite sums and strongly convergent series. Singular form limits or a different source-defined realization remain open and must match the complete source, with a specified domain and topology.

For example, expanding a candidate norm involving $\phi_n \otimes (I - \tau_{\log n})F$ introduces mixed translations $\log(n/m)$. Equal reduced ratios must be grouped before a coefficient is declared noncancellable. The stronger obstruction in §161 uses the absolutely continuous Fourier density of the regular lift; mixed shifts alone do not prove a no-go theorem.

R19. Why stationary symbols are blind

Put

$$\Phi(s) = \frac{\xi'(s)}{\xi(s)}, \qquad s = \sigma + it \tag{19.1}$$

Away from zero ordinates, $\xi(1/2 + it)$ is real, so

$$\Re\Phi\left(\frac{1}{2} + it\right) = 0 \tag{19.2}$$

In the distributional boundary value, a functional-equation pair at $\beta = 1/2 \pm \delta$ cancels exactly. The surviving stationary symbol is

$$\Omega(t) = \pi \sum_{\rho:\, \Re\rho = 1/2} m_\rho \delta_{\Im\rho}(t) \geq 0 \tag{19.3}$$

unconditionally. Thus a construction that collapses internally to this scalar multiplier has erased the off-line information. The no-go is scoped: it rejects premature stationary compression, not the translation covariance of the final Weil form.

The scalar-weight class is closed too, and by an inequality rather than a cancellation. For real $\alpha \neq 0$, $-\alpha g_F(v) = \frac{1}{2}\|(I - \alpha\tau_v)F\|_2^2 - \frac{1+\alpha^2}{2}\|F\|_2^2$, so rewriting the prime channel with per-frequency scalar weights $\alpha_m > 0$ forces a coefficient of $\|F\|^2$ equal to $\sum_m \lambda_m(\alpha_m + \alpha_m^{-1})/2 \geq \sum_m \lambda_m = +\infty$, with $\lambda_m = \Lambda(m)/\sqrt{m}$, because $\alpha + \alpha^{-1} \geq 2$. The divergence of the scalar defect is therefore not an artifact of the unit weight; it is forced by the arithmetic–geometric mean. The surviving class is the *operator*-weighted one, and it is open.

R20. Reflection contour and the missing conjugation

For a finite positive node set and real coefficients define

$$\Psi_X(q) = \sum_{i=1}^{N} \frac{c_i}{x_i + q} \qquad \mathscr{L}_F(s) = q(s)\Psi_X(q(s))^2 \tag{20.1}$$

Use the explicitly meromorphic carrier $\mathcal{F}_X(s) = (1-s)\Psi_X(q(s))$, so $\mathscr{L}_F(s) = \mathcal{F}_X(s)\mathcal{F}_X(1-s)$. The real-frequency symbol is its boundary restriction $\widehat{F}(t) = \mathcal{F}_X(1/2+it)$. Here the convention is $\widehat{F}(t) = \int_{\mathbb{R}} F(u)e^{-itu}\, du$ for the real resolvent combination $F = \sum_i c_i f_{x_i}$ defined in (153.5). The positive-sign transform is $\overline{\widehat{F}(t)}$ and has numerator $1/2 + it$ in each summand. Only the meromorphic carrier is evaluated at complex zeros; a real-frequency Fourier formula is not silently continued there.

The test symbol is reflection-even, while Φ is reflection-odd:

$$\mathscr{L}_F(1-s) = \mathscr{L}_F(s) \qquad \Phi(1-s) = -\Phi(s) \tag{20.2}$$

For

$$1 < \sigma_0 < \min_i \frac{1 + \sqrt{1 + 4x_i}}{2} \tag{20.3}$$

the exact folded zero form is

$$\boxed{Q_X(c) = \sum_{[\rho]} m_\rho \mathscr{L}_F(\rho) = \frac{1}{2\pi i} \int_{(\sigma_0)} \mathscr{L}_F(s)\Phi(s)\, ds} \tag{20.4}$$

At $s = 1/2 + it$,

$$\mathscr{L}_F\left(\frac{1}{2} + it\right) = |\widehat{F}(t)|^2 \geq 0 \qquad \Phi\left(\frac{1}{2} + it\right) \in i\mathbb{R} \tag{20.5}$$

The positive terminal object and the pairing are orthogonal. The critical-line integral is zero only as a symmetrically indented principal value; the integrand is not zero. The RH content lies in shifting the contour and collecting residues.

The type mismatch can now be stated without shorthand:

$$\underbrace{\mathcal{F}_X(\rho)\mathcal{F}_X(1-\rho)}_{\text{reflection; bilinear}} \quad \text{versus} \quad \underbrace{\mathcal{F}_X(\rho)\overline{\mathcal{F}_X(\rho)}}_{\text{conjugation; Hermitian}} \tag{20.6}$$

For a fixed real-coefficient test and $0 < \Re s < 1$, away from the test poles, their pointwise agreement is exactly

$$\mathcal{F}_X(s)\mathcal{F}_X(1-s) = |\mathcal{F}_X(s)|^2 \iff \sigma = 1/2 \text{ or } \Psi_X(q(s)) = 0 \tag{20.6a}$$

For example, nodes $(1, 2, 3)$ and coefficients $(1289, -5330, 4553)$ give

$$\Psi_X(q) = \frac{512[(q - 19/16)^2 + 1/4]}{(q+1)(q+2)(q+3)} \tag{20.6b}$$

which annihilates the synthetic off-line point $s = 1/4 + i$. This point is not asserted to be a zeta zero. A single multinode test can therefore hide an off-line orbit. The RH equivalence requires a separating family; a nonzero one-node carrier has no such accidental zero. A successful source construction must create the identification

$$\boxed{s \mapsto 1 - s \quad \text{with} \quad s \mapsto \bar{s}} \tag{20.7}$$

without assuming RH.

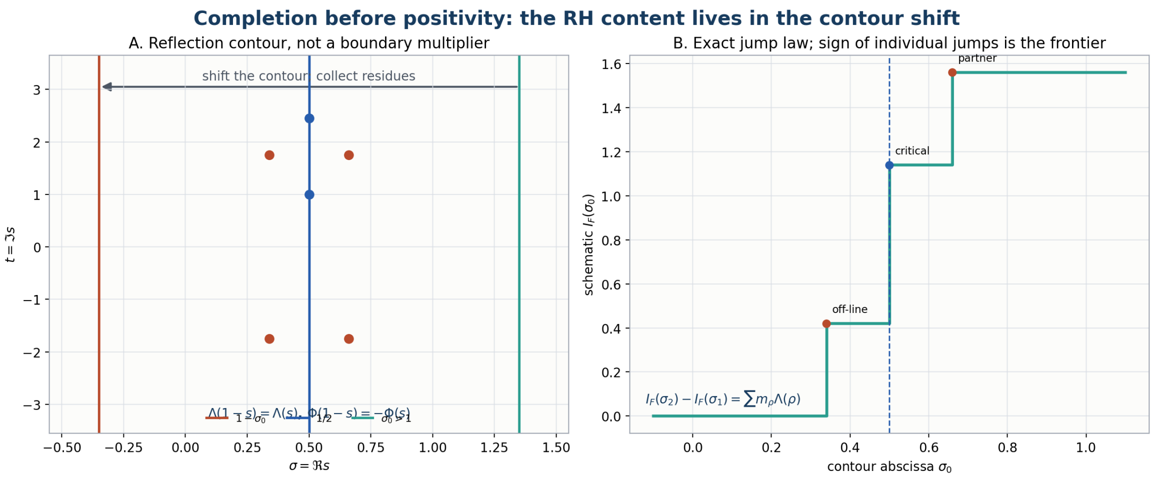

Figure 19: The reflection contour, principal-value center, and jump law. The plotted jump profile is schematic; the identity is exact.

R21. The one-node strict defect

For the one-node carrier $u_x(q) = q/(x+q)^2$ of (11.1), define the Hermitian comparison

$$\mathscr{H}_x = \frac{1}{2} \sum_{\rho \text{ all}} m_\rho |\mathcal{F}_x(\rho)|^2 \tag{21.1}$$

Pairing every zero with its reflected-conjugate partner gives the exact global square

$$\boxed{\mathscr{H}_x - W_1(x) = \frac{1}{4} \sum_{\rho \text{ all}} m_\rho \left| \mathcal{F}_x(\rho) - \overline{\mathcal{F}_x(1-\rho)} \right|^2 \geq 0} \tag{21.2}$$

For this carrier the defect is individually strict for every off-line quartet, so equality is equivalent to RH. For a general multinode test, accidental agreement is possible (§R20).

The same one-node carrier produces a positive measure on zero abscissae. Put

$$w_x(s) = \frac{q(s)}{[x+q(s)]^2} \tag{21.3}$$

and group conjugate ordinates at each real part:

$$d\nu_x(\sigma) = \sum_\beta \left(\sum_{\Re\rho = \beta} m_\rho w_x(\rho) \right) \delta_\beta(d\sigma) \tag{21.4}$$

Then

$$d\nu_x \geq 0, \qquad \nu_x(\mathbb{R}) = 2W_1(x) \tag{21.5}$$

The positivity is termwise after conjugate pairing. If $q = a + ib$, $a > 0$,

$$2\Re\frac{q}{(x+q)^2} = \frac{2[a(x+a)^2 + (a+2x)b^2]}{[(x+a)^2 + b^2]^2} > 0 \tag{21.5a}$$

The weights are absolutely summable: they are $O(\gamma^{-2})$ at large height and the zero-counting function is $O(T \log T)$. Thus grouping conjugate ordinates does not depend on a conditional ordering.

The topology must be stated with its closure:

$$\boxed{\mathrm{Atoms}(\nu_x) = \{\Re\rho\} \qquad \operatorname{supp}\nu_x = \overline{\{\Re\rho : \xi(\rho) = 0\}}} \tag{21.6}$$

Reflection centers this measure at $1/2$. Its unnormalized centered second moment is

$$\boxed{M_{2,x} := \int \left(\sigma - \frac{1}{2}\right)^2 d\nu_x(\sigma) \geq 0 \qquad M_{2,x} = 0 \iff \mathrm{RH}} \tag{21.7}$$

The probability measure $\nu_x/[2W_1(x)]$ has variance $M_{2,x}/[2W_1(x)]$. Nonnegativity is automatic on the zero side; forcing this moment to vanish from the source is the hard direction.

Exact regularized Riesz/Green representations are available. With

$$U = \log|\xi| \qquad d_x(s) = \left|\mathcal{F}_x(s) - \overline{\mathcal{F}_x(1-s)}\right|^2 \tag{21.8}$$

one has, as improper distributional pairings over admissibly truncated strips,

$$\boxed{\mathscr{H}_x = \frac{1}{4\pi}\left\langle \Delta U, |\mathcal{F}_x|^2 \right\rangle \qquad \mathscr{H}_x - W_1(x) = \frac{1}{8\pi}\langle \Delta U, d_x \rangle} \tag{21.9}$$

Also, for

$$h_x^{\perp}(s) = \left(\Re s - \frac{1}{2}\right)^2 \Re\left(\frac{s(1-s)}{[x + s(1-s)]^2}\right) \tag{21.10}$$

$$\boxed{M_{2,x} = \frac{1}{2\pi}\left\langle \Delta U, h_x^{\perp} \right\rangle} \tag{21.11}$$

These are source representations; they do not provide the missing reverse sign. No one-variable meromorphic function can equal $|\mathcal{F}_x(s)|^2$ on an open set, since $\partial_{\bar{s}}|\mathcal{F}_x|^2$ is generically nonzero. The surviving source owner must therefore remain two-variable, nonlocal, distributional, or discrete.

For the one-dimensional source contour, begin with the meromorphic weight w_x in (21.3) and define, on zero-free vertical lines,

$$I_x(\sigma) = \frac{1}{2\pi} \lim_{T_j \to \infty} \int_{-T_j}^{T_j} w_x(\sigma + it)\Phi(\sigma + it)\, dt \tag{21.12a}$$

The heights T_j avoid zero ordinates and make the horizontal contour remainders vanish. On lines through zeros, symmetric indentation and midpoint boundary values specify the principal-value representative. The residue theorem then identifies that source contour with

$$I_x(\sigma) = -W_1(x) + \nu_x((0, \sigma)) + \frac{1}{2}\nu_x(\{\sigma\}) \tag{21.12}$$

Then

$$\boxed{M_{2,x} = \frac{W_1(x)}{2} - 4\int_{1/2}^{1} \left(\sigma - \frac{1}{2}\right) I_x(\sigma)\, d\sigma} \tag{21.13}$$

The first unsupported reverse forcing line is

$$\boxed{\int_{1/2}^{1} \left(\sigma - \frac{1}{2}\right) I_x(\sigma)\, d\sigma \geq \frac{W_1(x)}{8}} \tag{21.14}$$

The positive zero measure gives the opposite inequality. An independent source proof of (21.14) would force equality and RH.

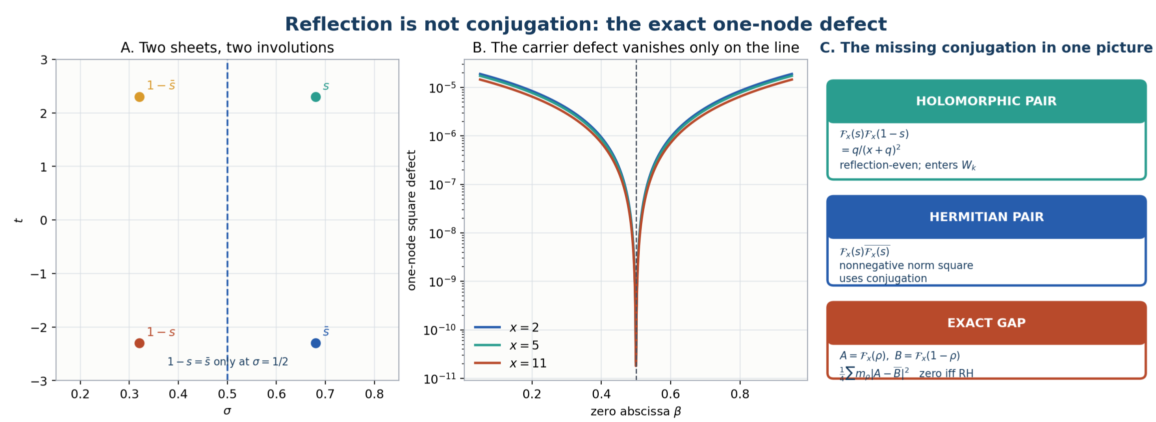

Figure 20: The two reflection sheets, the strict one-node defect, and the bilinear versus Hermitian pairings.

R21A. Strict defects and the Green boundary

The one-node reflection defect factors exactly:

$$d_x(s) = |f(s) - \overline{g(s)}|^2 = (1-2\sigma)^2 \frac{|x+(1-s)\bar{s}|^2}{|x+q(s)|^4} \geq 0, \tag{GM.1}$$

and vanishes precisely on $\sigma = 1/2$. Its Laplacian is strictly positive away from carrier poles. Therefore the Green identity for $U = \log|\xi|$ necessarily contains both bulk and boundary terms; adding a constant to U transfers mass between them while leaving the zero sum unchanged. A bulk sign alone cannot force the defect to vanish.

The heat-resolvent version is even shorter. For $q = A + ib$,

$$r_x = \frac{1}{x+A} - \Re\frac{1}{x+q} = \frac{b^2}{(x+A)|x+q|^2} \geq 0. \tag{GM.3a}$$

The same transverse coordinate controls the higher moment sequence. If $M_{2m,x}$ is the $2m$th centered abscissa moment, then $[M_{2m,x}/(2W_1(x))]^{1/(2m)}$ tends to the support radius $\sup_\rho |\Re\rho - 1/2|$. This is an exact support diagnostic, not a source-side upper bound.

R21B. Heat, transverse distance, and source-energy growth

For a nontrivial zero $\rho = \beta + i\gamma$ write $q = A + ib$. Then

$$b = \gamma(1-2\beta), \qquad b^2 = 4\gamma^2(\beta - 1/2)^2. \tag{HG.1}$$

The off-line heat defect $\mathcal{E}_H(h) = \sum m_\rho b_\rho^2 e^{-hA_\rho}$ vanishes for one (hence every) $h > 0$ exactly under RH. At fixed source scale $a > 0$, the Bernstein row sees the same transverse quantity through

$$\boxed{R_q(a)^2 - 1 = \frac{2ab^2}{(|q|+A)|a+q|^2} = \frac{2a(a+A)}{|q|+A}\, d_a(q).} \tag{HG.4}$$

Thus the heat defect, the row-growth factor and the distance from the critical line are three readings of the same b^2. Theorem 164.2 converts that geometry into the ordinary energy-growth limit. None of these exact detectors supplies the remaining source estimate; they identify what an off-line zero would force if it existed.

Part VII. Results and the research boundary

Section R22 records results with their quantifiers; R23 states the first unsupported source inequality; R24 maps the reading routes. Comparison positivity and finite certificates remain distinct from the all-order completed-source assertion.

R22. Results and their quantifiers

mathematical layer	established result	status, and what is still required
Triangular arithmetic	primitive, factorial, reciprocal, cyclic and Pell identities	**PROVED** Reader §§R1–R5E and the Dossier arithmetic chapters. **EVIDENCE** empirical spacing comparisons remain separate (§168).
Completion and exact criteria	heat, Stieltjes, Widder, Hausdorff, Li and Loewner criteria; scalar curvature and admissible progressions	**RH-EQUIVALENT** Each retains its stated full quantifier; Sections 155D–155E and 166F–166G add growth targets, not their source bounds.
Source rungs	W_1–$W_6 > 0$ globally from the source	**PROVED** analytic W_1; **CERTIFIED** A-CAT W_2–W_6; status table in §R12 and Dossier §74A. **OPEN** the independent $W_7 \rightsquigarrow F^{(14)}$ proof.
Verified-height rectangle	$F_{n,k} > 0$ for all $x > 0$, $n \leq K_H - 1$, $k \leq K_H$	**CERTIFIED** $K_H = 4{,}712{,}664{,}392{,}502$; includes $W_5, W_6 > 0$ with zero-assisted input (§R13).
Finite matrices	global order eight; rank twelve at $x = 56$	**CERTIFIED** with different quantifiers. **OPEN** global order nine and the all-node sign (§§92–93, 138).
Positive comparison and reserve growth	triangular sine projection, compensated Catalan reserve, exact linear/exponential defect alternatives	**PROVED** Sections 12A–12B, 61A, 95A, 155C–155D. **OPEN** the one-sided arithmetic upper bound.
Reflection and heat defects	exact nonnegative detectors; vanishing is RH-equivalent	**RH-EQUIVALENT** **OPEN** contour and Green representations exist; the reverse forcing signs do not (§§R20–R21B).
Completed and prime energy	exact rows, Pascal/Laguerre norm, boundedness equivalence and prime plateau	**PROVED** signed Gamma measure. **RH-EQUIVALENT** **OPEN** the full-prime all-degree cap (BE.5), §§163–166B.
Prime cutoffs and boundary reconstruction	whole rows at 20^{N+1} and 13^{N+1}; shifted block at 5^{2d-1}; actual boundary from degree $15d - 1$ and cutoff 8^{15d}	**PROVED** Sections 166C–166G. **OPEN** the uniform or polynomial source bounds; convergence alone supplies no sign.

mathematical layer	established result	status, and what is still required
Exact-divisor residual	Mellin/Hardy/Laguerre/sine norm, plateau/canonical exponents, scalar transfer and structured sampling	PROVED Sections 155H–155J. The fixed taper and canonical family have exponent $2\Theta_\zeta - 1$; fourth powers and T_k^2 suffice for the scalar criterion. OPEN the subpower mixed-sum bound or the required scalar upper decay.
Radius deficit	exact single-orbit remainder, two-sided chain, and the separation of Δ from its high-scale limsup	PROVED §§R13A, 48A. OPEN $\Delta < 1$, equivalently a uniform zero-free boundary strip.
NO-GO ledger	scalar-Fourier, Gamma-sublattice, tensor-lift, large-sieve, cutoff-envelope and finite-prefix shortcuts	PROVED unconditional limitations collected once in §R25; proofs remain at their Dossier homes.

One entry in the second row now has a machine-checkable statement of record: the Li criterion has been formalized in Lean against the ambient library's own Riemann-hypothesis predicate, stated without hypothesis binders and reporting only the three standard axioms [71]. It is recorded here as read and not built: the project was not compiled in the course of this work, so this is a report of someone else's certificate and not a certificate of this volume. It formalizes the equivalence, and it asserts nothing about the sign of the coefficients.

A finite certificate proves its stated finite region. None replaces the all-order quantifier in an RH criterion. The table separates an open statement from an open independent proof of an already established sign.

R23. The first unsupported lines, by route

There is no proved reduction of all surviving routes to one source inequality. The matrix route begins with:

OPEN *equivalent to RH; not proved here or anywhere in the Dossier*

$$\boxed{\begin{gathered}\text{No source-side argument presently proves}\\ L_\Gamma - L_P \succeq 0\\ \text{for every finite positive node set}\end{gathered}} \tag{23.1}$$

Equivalently, no source-side argument proves

$$\sum_{[\rho]} m_\rho \mathscr{L}_F(\rho) \geq 0 \tag{23.2}$$

for every rational-resolvent test. The surviving design target is a positive two-sheet form before compression that preserves reflection information, whose final compression recovers the reflection contour and the translation covariance of the Weil functional.

A distinct compact-window problem. Zhu [72] reports half-width 0.8; Liu [81] reports

1 and 17/16 plus a localization NO-GO beyond $\log 8/2$. Liu's manuscript is submitted, not peer-reviewed or on arXiv, and not yet externally reproduced. These are comparison results only: the rung transforms here are noncompact, so the fixed-window bounds do not transfer as stated.

At one node the same boundary is (21.14), or equivalently the missing independent upper sign in the Green identity for d_x. The source-rung prefix now reaches W_6 independently. The first scalar rung not yet owned directly by the Gamma–prime source is $W_7 = -x^{-12}(x^{13}W_6')' > 0$, requiring the $F^{(14)}$ owner. These are different compressions of the frontier; no finite source prefix replaces the all-order condition.

For a positive trace-class model D, the corresponding concrete target is

$$\boxed{\det(I + xD) = \frac{\xi(s_x)}{\xi(1)} \quad (x \geq 0)} \tag{23.3}$$

Differentiation would identify its resolvent with S_ξ and yield the positive Gram form in §R10A. The continued zeta identities and the triangular–Volterra benchmark constrain this target; they do not establish it. The ordinary strongly convergent tensor lift is ruled out in §161 and listed with the other finished limitations in §R25; singular-form and source-defined discrete realizations remain candidates.

Section R17F now supplies a specific source-defined discrete sequence. Its next source target is (BR.4): for one fixed $a > 0$, bound the completed row variation by $C_{a,\varepsilon}(1+\varepsilon)^N$ for every $\varepsilon > 0$ and every N. By the growth criterion of §164, quoted above, that bound at one prescribed $a > 0$ is not merely sufficient for RH but equivalent to it. Equivalently one may bound the exact Laguerre energy in (BE.3). Lemma 166A.1 supplies the elementary/Gamma growth estimate. The signed measure in §166B further reduces the question to the explicit bounded full-prime criterion (BE.5). That all-degree source inequality remains open. The heat identity (HG.4) shows that the excess growth detects the same squared imaginary folded coordinate as the off-line heat defect. This gives a common coordinate for two distinct source obligations.

A proposed transfer, not an identified theorem. The growth exponent of Theorem 164.1 invites comparison with the regular-arithmetic-function framework [67–69] and its Tauberian/Volterra methods [73]. The differential rung recurrence $W_{k+1} = -j_k W_k' - xW_k''$ does not by itself verify the hypotheses of a rank-by-rank arithmetic transfer theorem. Applicability to (BR.4) is open. It is not claimed here in either direction; these external statements were read, not verified.

Two concrete source targets. The curvature already defined in Section 155B is $I_n = \int_0^\infty e^{-u} M(u) L_{n+1}^{(0)}(u)du$, with $M(u) = \Psi(e^u) - e^u + 1$. Section 155E proves that a one-sided polynomial upper bound on either parity separately would suffice. Its progression argument uses an explicit pole-angle condition to prevent cancellation; it does not license arbitrary sparse scalar sampling. Independently, Section 166F defines the cutoff defect at fixed scale $a = 2$ and proves its growing-block error tends to zero. The remaining alternatives are

$$\boxed{\begin{array}{lll} & I_{2m} \le C(m+1)^{A} & (m \text{ sufficiently large}), \\ \text{or} & \widehat{\beta}^{+}_{2,d} \le C'(1+d)^{A'} & (d \ge 1). \end{array}} \tag{23.4}$$

Each alternative requires fixed finite constants; each would imply RH. Neither is established. The odd-curvature alternative uses I_{2m+1}. Section 166G now gives a separate controlled boundary reconstruction; a polynomial upper bound on $\widehat{\beta}^{\partial,+}_{d}$ would also suffice. Section R17I gives a fixed exact-divisor alternative: for the linear taper V_N, RH is equivalent to $U_N = O_\epsilon(N^\epsilon)$ for every $\epsilon > 0$ (even on one fixed unbounded index set). Equivalently one may attack the signed mixed sum $\mathcal{X}_N$. For the scalar $B_{\log}$ route, Section 155J proves that the eventual-integer premise may be replaced by all sufficiently large fourth powers, or by the squared triangular mesh T_k^2, with the stated endpoint decay. Neither required arithmetic estimate is proved. The original full-row cap (BE.5), the bounded cutoff norms in (166D.2)/(166D.4), and the one-sided reserve growth theorem remain valid routes to the same obligation. The compensation, complete prime-error kernel and its regularization stay present throughout. A smaller cutoff, a positive comparison model, or a finite sign list does not supply the missing uniform source estimate.

R24. Proof map and reading routes

The Dossier chapters follow mathematical dependencies: triangular arithmetic and geometry, completion, flux and source rungs, moment and matrix criteria, arithmetic cancellation, and the completed discrete energy. Reader sections carry an **R** prefix and Dossier sections keep their existing identifiers, so section numbers need not increase at every chapter boundary; the convention is stated in full in the notation table of the study spine.

question	reader entry	full proof or comparison
What does the triangular primitive generate?	§§R1–R1A, R3–R5E	Dossier §§5–14, 76–78, 94–98 (including 95A), 156, 162, 167–168
How do reflection and the complex fold connect?	§§R6–R10	§§12A, 16–18, 20–31, 61A, 152–153
Which scalar signs are proved from the source?	§§R11–R13	§§32–38, 74–75, 55; §49 supplies the general negative-rung converse
Why do moments become matrices?	§§R14–R16	§§48–54, 104, 136, 145; finite gates in §§85–93 and 138
Which positive Gamma models match the source?	§§R17–R17E	§§131–133; compare the source split in §54 and the reserve/defect in §155C
What remains in prime oscillation?	§R13 and the source split	§§56–61, 105–113, 118, 129; each route states its own limit and uniformity
What do finite Weil models establish?	§§R10A, R18–R18B	§§19, 44, 123–125; cutoff, band and prime limits remain separate
Where does conjugation enter?	§§R18–R21B	§§103, 137, 148–149, 154, 157–161
What is the fixed-scale source-energy task?	§§R17F–R17H, R21B	§§163–166E; the all-degree full-prime cap (166B.11) is open
What degree growth would force the source sign?	Sections R15, R23	Sections 155D–155E: reserve growth, curvature and progression proofs

question	reader entry	full proof or comparison
Which cutoff approximates its own matrix target?	Sections R17H, R23	Sections 166D–166G: whole row, shifted block, and actual boundary reconstruction

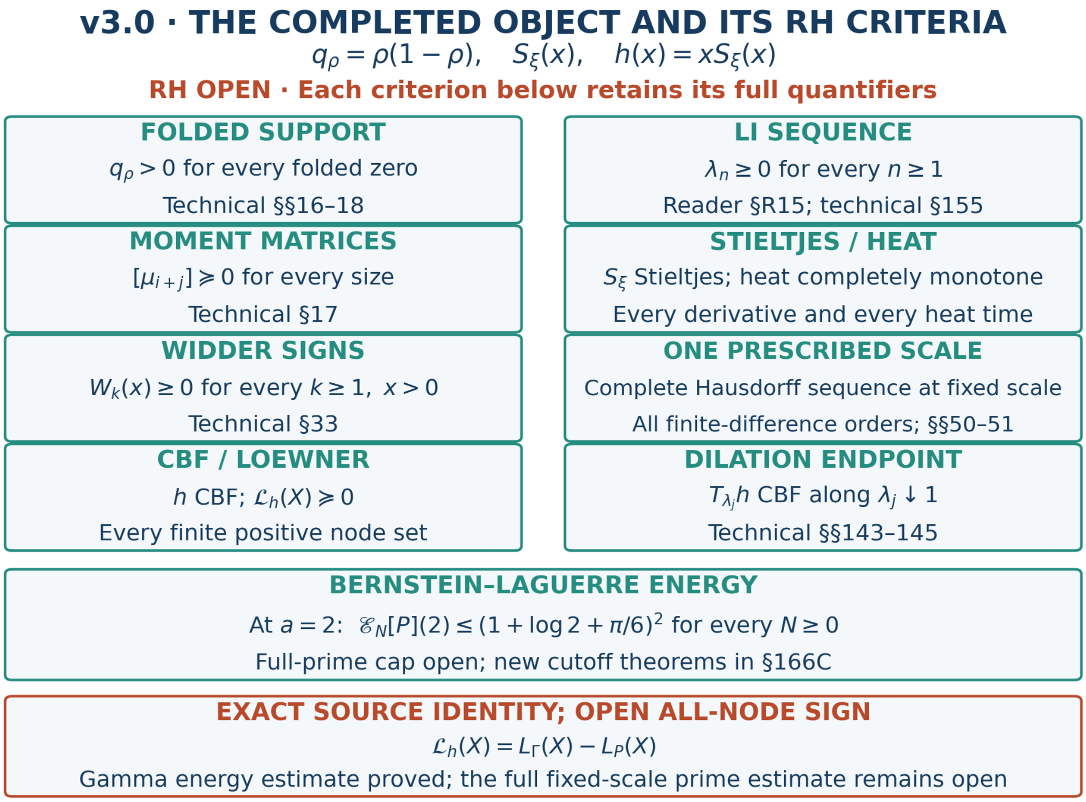

Figure 21: The proof map for this volume. Each criterion retains its full quantifiers. The source identities are exact; the surviving all-order source bounds are listed by route in §R23.

For the new boundary reconstruction, read R17H with Dossier Section 166G. For exact-divisor cancellation and its denominator residual, read R17I with Sections 155H–155J; Sections 155F–155G explain the countermodels that motivate this use of actual arithmetic.

The map uses the same completed object S_ξ, with $h = xS_\xi$. Auxiliary Gamma and triangular models retain their own measures. Reproducibility details and the section review are in the source package.

Part VIII. What this approach cannot do

The proofs stay at their original Dossier locations; this Part is the single NO-GO ledger. Each row names the shortcut killed and the corridor left open.

R25. No-go ledger and the surviving corridor

exact limitation	what it kills	what survives
Theorem 22A.1: every scalar rung test has at least k Fourier sign changes and is not positive definite	scalar Fourier positivity as a rung proof	completed/two-variable Weil forms and the arithmetic source
§48C: centered Gamma-pole terms have a universal rank-two negative direction, and neither pole-index sublattice absorbs the prime channel with a finite baseline	"unused Gamma poles" as a positive Löwner reserve	the repaired reserve and the full signed prime-error estimate
§49 and §69: a fixed positive rung/Li/Hankel prefix can coexist with later failure	any finite certificate as an infinite stopping rule	the full quantifiers in §§R12, R14, R23
§161: ordinary strongly convergent tensor/vector-multiplier realizations cannot own the completed meromorphic Stieltjes target	the regular translation-energy tensor lift	singular-form, atomic/discrete, or different source-norm owners
Theorems 107.1 and 112.1: the loose diagonal is exponent-self-limiting, and the classical blockwise large sieve misses the short-shift target by at least $X^{1/2+o(1)}$	those two coarse analytic closures	the exact-diagonal/interior-saddle route or a stronger arithmetic mechanism
§§155F–155G and (H07): PNT-quality envelopes, positive prime-power support, sparse support counts, long prefixes and meromorphic Euler products do not force the needed curvature/source sign	replacing the actual signed arithmetic remainder by support or envelope domination	exact divisor arithmetic and the weighted completed prime error

These are unconditional theorems about what this approach cannot do. They are finished and explain the surviving corridor; none is evidence for RH or against it.

References

1. E. Bombieri, *The Riemann Hypothesis - official problem description*, Clay Mathematics Institute, Millennium Prize Problems, Clay problem description.
2. NIST Digital Library of Mathematical Functions, Sections 5.5, 5.7–5.9, 5.11, 24.4, 25.4, 25.10, 25.11, and 25.16; in particular Hurwitz special values and derivatives, zero counting, and Gamma and digamma asymptotics.
3. E. C. Titchmarsh, revised by D. R. Heath-Brown, *The Theory of the Riemann Zeta-Function*, 2nd ed., Oxford University Press, 1986.
4. X.-J. Li, "The positivity of a sequence of numbers and the Riemann hypothesis," *Journal of Number Theory* 65 (1997), 325-333.
5. E. Bombieri and J. C. Lagarias, "Complements to Li's criterion for the Riemann hypothesis," *Journal of Number Theory* 77 (1999), 274-287.
6. L. de Branges, *Hilbert Spaces of Entire Functions*, Prentice-Hall, 1968.
7. G. Csordas, T. S. Norfolk, and R. S. Varga, "The Riemann hypothesis and the Turan inequalities," *Transactions of the American Mathematical Society* 296 (1986), 521-541.
8. J. Huckstead, *Divisor-Band Bijections and Totient Shells in the Triangular-Fractional Grid*, version 5, Zenodo (2026), DOI 10.5281/zenodo.21440877.
9. J. Huckstead, *Triangular Addressing, Null Coordinates, and Reciprocal-Metallic Locks in a Scale-Covariant Plane Geometry*, Working Draft III, Zenodo (2026), DOI 10.5281/zenodo.21444929.
10. J. Huckstead, *From Measure to Flux: Energy-Conjugate Bookkeeping and Exact Semidiscrete Scattering in Finite Radial Wave Models*, publication layer v0.6.13, Zenodo (2026), DOI 10.5281/zenodo.21444339.
11. J. Huckstead, *Two-Term Asymptotics for the Total Variation of Exponentially Weighted Laguerre Polynomials*, v0.1, Zenodo (2026), DOI 10.5281/zenodo.21861619.
12. J. Sondow and C. Dumitrescu, "A monotonicity property of Riemann's xi function and a reformulation of the Riemann hypothesis," *Periodica Mathematica Hungarica* 60 (2010), 37-40, DOI 10.1007/s10998-010-1037-3; arXiv:1005.1104.
13. Y. Matiyasevich, F. Saidak, and P. Zvengrowski, "Horizontal monotonicity of the modulus of the Riemann zeta function and related functions," arXiv:1205.2773 (2012).
14. J. C. Lagarias, "On a positivity property of the Riemann xi-function," *Acta Arithmetica* 89 (1999), 217-234.
15. A. D. Sokal, "Real-variables characterization of generalized Stieltjes functions," *Expositiones Mathematicae* 28 (2010), 179-185; arXiv:0902.0065.
16. D. V. Widder, "The Stieltjes transform," *Transactions of the American Mathematical Society* 43 (1938), 7-60.
17. F. Johansson, "Rigorous high-precision computation of the Hurwitz zeta function and its derivatives," arXiv:1309.2877 (2013).

18. GNU MPFR Project, *GNU MPFR 4.2.2 Manual*, https://www.mpfr.org/mpfr-current/mpfr.html.
19. F. Hausdorff, "Summationsmethoden und Momentfolgen. I," *Mathematische Zeitschrift* 9 (1921), 74-109, DOI 10.1007/BF01378337.
20. F. Hausdorff, "Summationsmethoden und Momentfolgen. II," *Mathematische Zeitschrift* 9 (1921), 280-299, DOI 10.1007/BF01279032.
21. A. Pringsheim, "Ueber Functionen, welche in gewissen Punkten endliche Differentialquotienten jeder endlichen Ordnung, aber keine Taylor'sche Reihenentwickelung besitzen," *Mathematische Annalen* 44 (1894), 41-56, EuDML 157700.
22. K. Löwner, "Über monotone Matrixfunktionen," *Mathematische Zeitschrift* 38 (1934), 177-216, DOI 10.1007/BF01170633.
23. R. L. Schilling, R. Song, and Z. Vondraček, *Bernstein Functions: Theory and Applications*, 2nd ed., De Gruyter, 2012, DOI 10.1515/9783110269338.
24. M. Riesz, "Sur l'hypothèse de Riemann," *Acta Mathematica* 40 (1916), 185-190, DOI 10.1007/BF02418544.
25. L. Báez-Duarte, "A sequential Riesz-like criterion for the Riemann hypothesis," *International Journal of Mathematics and Mathematical Sciences* 2005, 3527-3537, DOI 10.1155/IJMMS.2005.3527.
26. A. Agarwal, M. Garg, and B. Maji, "Riesz-type criteria for the Riemann hypothesis," *Proceedings of the American Mathematical Society* 150 (2022), DOI 10.1090/proc/16064.
27. H. L. Montgomery and R. C. Vaughan, "Hilbert's inequality," *Journal of the London Mathematical Society* (2) 8 (1974), 73–82.
28. H. L. Montgomery, *Ten Lectures on the Interface Between Analytic Number Theory and Harmonic Analysis*, CBMS Regional Conference Series in Mathematics 84, American Mathematical Society, 1994.
29. H. Iwaniec and E. Kowalski, *Analytic Number Theory*, American Mathematical Society Colloquium Publications 53, 2004.
30. J. B. Conrey and A. Gamburd, "Pseudomoments of the Riemann zeta-function and pseudomagic squares," arXiv:math/0307213v2; *Journal of Number Theory* 117 (2006).
31. M. Wahl, "On the mod-Gaussian convergence of a sum over primes," arXiv:1201.5295v3 (2013), especially equation (1.4).
32. M. Gerspach and Y. Lamzouri, "Low pseudomoments of Euler products," arXiv:2103.03870 (2021).
33. A. Connes, "The Riemann Hypothesis: Past, Present and a Letter Through Time," arXiv:2602.04022v1 (2026).
34. D. S. P. Salazar, "Order-Moment Transport and Hankel Determinants in Special-Function Inequalities," arXiv:2606.31647v2 (2026).
35. M. Bhowmik, A. Chatterjee, and M. Putinar, "Holomorphic Interpolation of Multivariate Completely Monotone Functions," arXiv:2606.12102 (2026).
36. L. Guth and J. Maynard, "New large value estimates for Dirichlet polynomials," *Annals of Mathematics* 203 (2026), no. 2, 623–675, DOI 10.4007/annals.2026.203.2.6; arXiv:2405.20552v2.
37. B. Chen, V. Gupta, and Y. C. Li, "Large Value Estimates for Dirichlet Polynomials with Characters and Zero Density of Dirichlet L-Functions," arXiv:2507.08296v2 (2026).

38. A. Bondarenko, O. F. Brevig, E. Saksman, K. Seip, and J. Zhao, "Pseudomoments of the Riemann zeta function," *Bulletin of the London Mathematical Society* 50 (2018), no. 4, 709–724, DOI 10.1112/blms.12183; arXiv:1701.06842v3.

39. E. Lill, "Résolution graphique des équations numériques de tous les degrés à une seule inconnue, et description d'un instrument inventé dans ce but," *Nouvelles Annales de Mathématiques*, 2e série, 6 (1867), 359–362.

40. E. Lill, "Résolution graphique des équations algébriques qui ont des racines imaginaires," *Nouvelles Annales de Mathématiques*, 2e série, 7 (1868), 363–367.

41. B. Bellotti and P.-J. Wong, "Improved estimates for the argument and zero-counting function of the Riemann zeta-function," arXiv:2412.15470v2 (2025), accepted by *Mathematics of Computation*.

42. D. J. Platt and T. S. Trudgian, "The Riemann hypothesis is true up to $3 \cdot 10^{12}$," *Bulletin of the London Mathematical Society* 53 (2021), 792–797; arXiv:2004.09765.

43. O. Dobsch, "Matrixfunktionen beschränkter Schwankung," *Mathematische Zeitschrift* 43 (1938), 353–388.

44. W. F. Donoghue, Jr., *Monotone Matrix Functions and Analytic Continuation*, Grundlehren der mathematischen Wissenschaften 207, Springer, 1974.

45. Euclid, *The Thirteen Books of The Elements*, translated with introduction and commentary by T. L. Heath, 2nd ed., Dover, 1956, Book VII, Definition 22, and Book IX, Proposition 36.

46. L. E. Dickson, *History of the Theory of Numbers*, Volume I: Divisibility and Primality, Carnegie Institution of Washington, 1919, Chapter I.

47. A. Groskin, "A finite Guinand–Weil dictionary and archimedean tail order for the truncated Weil quadratic form," arXiv:2607.02828v3 (2026), archival DOI 10.5281/zenodo.21124802.

48. A. Connes, C. Consani, and H. Moscovici, "Zeta Spectral Triples," arXiv:2511.22755v1 (2025), forthcoming in the EMS Lecture Notes in Mathematics volume *Applications of Noncommutative Geometry to Gauge Theories, Field Theories, and Quantum Space-Time*.

49. A. Connes and W. D. van Suijlekom, "Quadratic Forms, Real Zeros and Echoes of the Spectral Action," arXiv:2511.23257v1 (2025).

50. A. Connes, C. Consani, and H. Moscovici, "Zeta zeros and prolate wave operators," arXiv:2310.18423v2 (2024).

51. M. Suzuki, "Weil's quadratic form via the screw function," arXiv:2606.09096v2 (2026).

52. A. Groskin, "High-Precision Approximation of Riemann Zeros via the Truncated Weil Form," arXiv:2605.20224v4 (2026), archival DOI 10.5281/zenodo.19546514.

53. E. W. Weisstein, "Gamma Function," *MathWorld–A Wolfram Web Resource*, MathWorld entry, page captured 27 August 2026.

54. *Hermitian Spaces*, Chapter 12 lecture slides, CIS 5150, University of Pennsylvania, Sections 12.1–12.2, especially the definitions of sesquilinear/Hermitian forms and the complex polarization identities, https://www.cis.upenn.edu/~cis5150/cis515-20-sl9.pdf.

55. J. Huckstead, *The Polar Shell Renderer: A Lens, Not a Law*, revised 9 July 2026, Zenodo, DOI 10.5281/zenodo.21280464.

56. A. Voros, "Zeta functions for the Riemann zeros," *Annales de l'Institut Fourier* 53 (2003), no. 3, 665–699; first preprint 2001, arXiv:math/0104051v4. Equations (40)–(41), (59), (74), (81), and (91)–(95), and Table 1 supply the classical spectral-zeta formulas used here.

57. A. Voros, "Erratum - Zeta functions for the Riemann zeros," *Annales de l'Institut Fourier* 54 (2004), no. 4, 1139, DOI 10.5802/aif.2046.

58. J. B. Keiper, "Power series expansions of Riemann's ξ function," *Mathematics of Computation* 58 (1992), no. 198, 765–773.

59. NIST, *Digital Library of Mathematical Functions*, §§5.4–5.5, Gamma special values, recurrence, reflection, and duplication. Official formulas.

60. S. M. Eisenberg, "Moment Sequences and the Bernstein Polynomials," *Canadian Mathematical Bulletin* 12 (1969), no. 4, 401–411. DOI 10.4153/CMB-1969-050-8. Classical background; the source-specific growth argument is printed independently in §164, without a claim of literature novelty.

61. *A Search-Adjusted Audit of Row-Sector Modulus Signals in Terminal Zeta-Zero Spacing Residuals*, user-supplied historical report, 10 pages, supplied as Orthogonal_Followup. Reported tables only; raw arrays and permutation replay were not supplied.

62. *A Finite-Count Search for Localized Enrichment Near 2.75 in Unfolded Riemann Zeta-Zero Gap Coordinates*, user-supplied historical report, May 2026, 24 pages, supplied as Zeta_Zeros_2. The reported counts and stated design are compared in §168.

63. NIST, *Digital Library of Mathematical Functions*, sine Maclaurin series and Euler infinite product, and the fourth-kind Chebyshev representation. The triangular factorization in (PR.6) is a direct regrouping of the factorial coefficients; Gamma reflection is covered by [59].

64. L. Euler, *De formulis exponentialibus replicatis*, E489 (1778), original paper in the Euler Archive. The fixed-point differentiation and stability calculation used here are displayed in §R5E.

65. A. Edelman and G. Strang, *Pascal Matrices*, MIT course essay. Classical symmetric Pascal matrix, Vandermonde factorization, and determinant one. Section 163A identifies this matrix inside the completed-source energy.

66. Y. Lamzouri, *A new proof that more than two thirds of the zeros of the Riemann zeta function are simple or on the critical line*, arXiv:2609.02882v2, 17 pages. Proposition 2.1, Lemma 3.1 and Theorem 1.1 are the statements compared in §159. Its notation is local to that paper; in particular its critical-line counting symbol is not the smooth approximation N_0 of §168.

Entries 67–73 are external work consulted while this edition was prepared. Each was read at the level its entry states and **none is verified anywhere in this work**; they are cited for what they say, not as support for anything claimed here.

67. B. Cloitre, *A tauberian approach to RH*, arXiv:1107.0812, submitted 5 July 2011. Introduces functions of good variation and the family approaching $x \mapsto x^{-1}\lfloor x \rfloor$, by the author's account inspired by the Ingham summation process. Cited in §R12A for the shared coordinate and in §R23 for the exponent route.

68. B. Cloitre, *A tauberian characterization of the Riemann hypothesis through the floor function*, arXiv:2407.18859, submitted 26 July 2024. The term *regular arithmetic function* and the floor-function characterization appear here.

69. B. Cloitre, *Regular arithmetic functions, Volume I: theory, applications, examples*, arXiv:2609.09366, submitted 8 September 2026, 374 pages. The kernel $G(n,k)$, the regularity index, and the statement that the hypothesis holds exactly when Ingham's kernel has index 1/2. Abstract read; the body is not read.

70. S. Xu, *Positivity and asymptotics for Chenevier's orthogonal polynomials*, arXiv:2609.10328, submitted 9 September

2026. Positivity in every degree from strict negativity of all Verblunsky coefficients of an associated circle measure. Cited in §R12A as the transporting case. Abstract read.

71. Lean formalization of the Li criterion against the ambient library's own Riemann-hypothesis predicate, public repository `li-criterion-rh-equivalence-lean`, registry entry `PALOMAR-2026-09-05-000005`. Statement and sources read at file level; the project was not compiled in the course of this work, and the axiom report quoted in §R22 is the one the sources declare.

72. X. Zhu, *Weil positivity in compact windows: a finite reduction, certified two-sided bounds, and a Landau–Widom decay law*, arXiv:2608.24827, submitted 25 August 2026, revised 2 September 2026, 34 pages. The certified window bound and the two-sided decay law quoted in §R23. Abstract, discussion and failed-route sections read; the body is not read.

73. B. Cloitre, *On the orthorecursive expansion of unity*, arXiv:2505.09645, submitted 11 May 2025. The tauberian transfer from a discrete recurrence to a Volterra integral equation referred to in §R23. Abstract read.

74. B. Riemann, *Ueber die Anzahl der Primzahlen unter einer gegebenen Grösse*, Monatsberichte der Königlich Preussischen Akademie der Wissenschaften zu Berlin, November 1859. The source of the hypothesis, of the explicit formula whose oscillation periods are quoted in §R9A, and of the counting statement completed by von Mangoldt.

75. M. Aissen, I. J. Schoenberg, and A. Whitney, "On the generating functions of totally positive sequences I," *Journal d'Analyse Mathématique* 2 (1952), 93–103; A. Edrei, "On the generating functions of totally positive sequences II," *ibid.*, 104–109. Announced in M. Aissen, A. Edrei, I. J. Schoenberg and A. Whitney, "On the generating functions of totally positive sequences," *Proceedings of the National Academy of Sciences* 37 (1951), 303–307, which carries all four names on one note; the 1952 sequel is the two-part paper cited first. The characterization of Pólya frequency sequences used at (12.9).

76. D. K. Dimitrov and F. R. Lucas, "Higher order Turán inequalities for the Riemann ξ-function," *Proceedings of the American Mathematical Society* 139 (2011), 1013–1022.

77. M. Griffin, K. Ono, L. Rolen, and D. Zagier, "Jensen polynomials for the Riemann zeta function and other sequences," *Proceedings of the National Academy of Sciences* 116 (2019), 11103–11110. Hyperbolicity of every fixed degree for all large n; all degrees for all n is the hypothesis.

78. J. Holland, *A new hyperbolicity wedge and a joint semicircle limit for Jensen polynomials of Riemann's ξ-function*, arXiv:2608.08682, submitted 9 August

2026. Reports the threshold $n^3 \log^2(n+2) \geq Kd^5$ for its own Jensen family; no transfer to the ordinary-coefficient minors in (12.9) is asserted. Abstract and statement of the wedge read; the body is not read.

79. H. L. Montgomery, "The pair correlation of zeros of the zeta function" (1973), pp.181–193. The historical theorem and conjectured density are distinguished in Section 61A; the comparison does not import the conjecture as an actual-source estimate.

80. Elaissaoui and Guennoun, arXiv:1809.02829v2, Theorem 1.1 and Corollary 2.4: the zeta Fourier-coefficient and Parseval identities. Attribution and normalization are retained from the supplied Orange source note; Section 155G reproduces the Mellin normalization.

81. V. Liu, *Certified Weil Positivity Beyond the Unit Window*, manuscript submitted to *Mathematics of Computation*, 14 September 2026; reproducible source repository `luciferyu666/certified-weil-positivity`. Fixed-window claims only; not peer-reviewed,

not on arXiv, and the repository states that external reproduction has not yet been completed. Cited in §R23 only as an external comparison and NO-GO for a specified localization.

82. A. Pearce-Crump, *Optimising Selberg's method for critical zeros*, arXiv:2609.15329v1, 14 September 2026. Theorem 1.1 proves $\kappa_0 > 0.0700162$ by a positive-semidefinite sum of three squared mollifiers; cited in §R12 only as a methodological comparison.